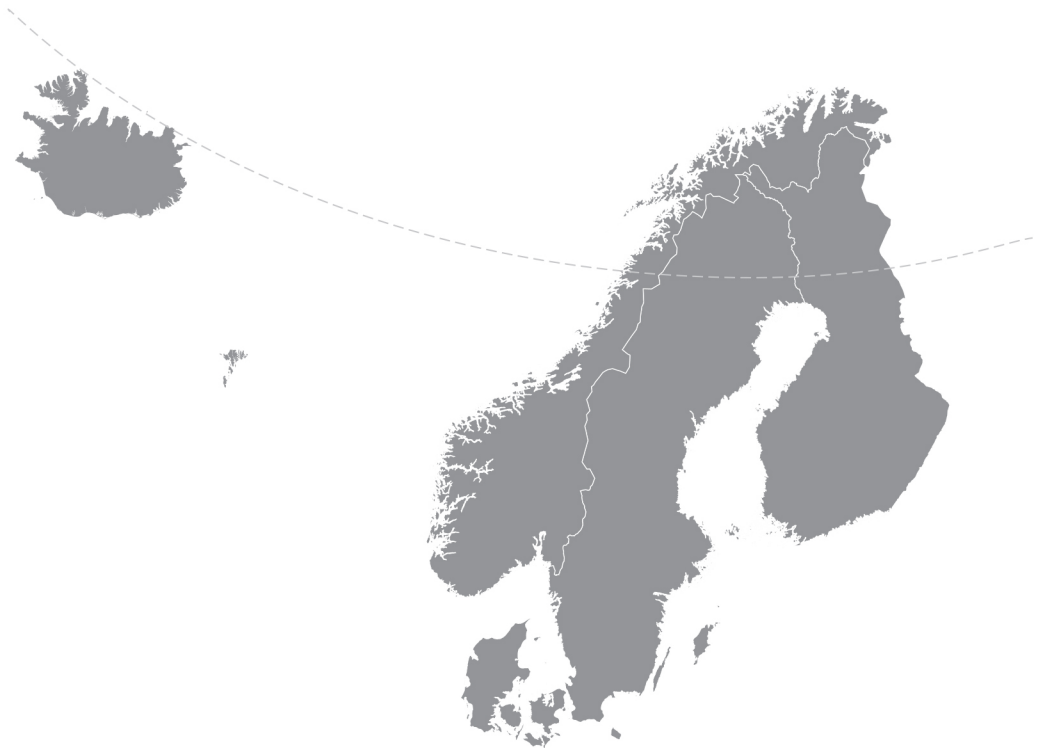


Nordic Concrete Research



Nordic
Concrete
Federation

PUBLICATION NO. 45 1/2012

NORDIC CONCRETE RESEARCH

**EDITED BY
THE NORDIC CONCRETE FEDERATION**

**CONCRETE ASSOCIATIONS OF: DENMARK
FINLAND
ICELAND
NORWAY
SWEDEN**

**PUBLISHER: NORSK BETONGFORENING
POSTBOKS 2312, SOLLI
N - 0201 OSLO
NORWAY**

VODSKOV, JUNE 2012

Preface

Nordic Concrete Research is since 1982 the leading scientific journal concerning concrete research in the five Nordic countries, e.g., Denmark, Finland, Iceland, Norway and Sweden. The content of *Nordic Concrete Research* reflects the major trends in the concrete research.

Nordic Concrete Research is published by the Nordic Concrete Federation that beside the publication activity also organizes the Nordic Concrete Research Symposia that have constituted a continuous series since 1953 in Stockholm. The Symposium circulates between the five countries and takes normally place every third year. The next symposium, no. XXII, will be held Reykjavik, Iceland 19 - 21 June 2013 only two years ahead, in parallel with the, ECO-CRETE conference.

Since 1982, 386 papers have been published in the journal. Since 1994 the abstracts and from 1998 both the abstracts and the full papers can be found on the Nordic Concrete Federation's homepage: www.nordicconcrete.org. The journal thus contributes to dissemination of Nordic concrete research, both within the Nordic countries and internationally. We are very pleased, that during the latest years, growing interests in participating in the Nordic Concrete Research symposia, as well as for publishing in NCR have been observed.

Since 1975, 75 Nordic Miniseminars have been held – it is the experience of the Research Council of the Nordic Concrete Federation, that these Miniseminars have a marked influence on concrete research in the Nordic countries. In some cases, the information gathered during such Miniseminars has been used as Nordic input to CEN activities.

Vodskov, June 2012

Dirch H. Bager

Editor, *Nordic Concrete Research*

CONTENTS

1. Olli Kerokoski, Antti Nurmikola & Tommi Rantala Loading Tests of Concrete Monoblock railway Sleepers	1
2. Knut O. Kjellsen & Sidney Diamond The Development of Microstructure of Portland cement Mortars from the Fresh to the Hardened State	15
3. Peter Fjellström, Jan-Erik Jonasson, Mats Emborg & Hans Hedlund Model for Concrete Strength Development Including Strength Reduction at Elevated Temperatures.	25
4. Tomas Sandström, Katja Fridh, Mats Emborg & Manouchehr Hassanzadeh The influence of temperature on water absorption in concrete during freezing. ..	45
5. Lamis Ahmed, Richard Malm & Anders Ansell Finite element simulation of shotcrete exposed to underground explosions	59
6. Jerry Hedebratt & Johan Silfwerbrand Lessons Learned – Swedish Design and Construction of Industrial Concrete Floors	75
7. Anders Lindvall, Oskar Esping, Ingemar Löfgren & Tang Luping Properties of concretes mixed with Pulverized Fly Ash	93
8. Nelson Silva, Dimitrios Boubitsas, Tang Luping & Jan Erik Lindquist Critical Conditions for Depassivation of Steel in Concrete: Interface Chloride Profiles and Steel Surface Condition	111
Research Council and Editorial Board of NCR.....	125
Review Group.....	126

Loading Tests of Concrete Monoblock Railway Sleepers



Olli Kerokoski
Dr.Tech.
Associate Professor
Department of Civil Engineering
Tampere University of Technology
P.O. Box 527
FI-33101 Tampere, Finland



Antti Nurmikolu
Dr.Tech.
Associate Professor
Department of Civil Engineering
Tampere University of Technology
P.O. Box 527
FI-33101 Tampere, Finland



Tommi Rantala
M.Sc.
Researcher
Department of Civil Engineering
Tampere University of Technology
P.O. Box 527
FI-33101 Tampere, Finland

ABSTRACT

Prestressed concrete monoblock sleepers have served Finnish railways well for several decades. The main reason to launch a comprehensive research project was to investigate the deterioration mechanisms that primarily determine the life cycle of the sleepers. The loading tests were a part of the study. This paper presents the results of static and dynamic loading tests on concrete sleepers. Several 30- to 40-year-old sleepers removed from Finnish railway lines were loaded. The behaviour of new sleepers was compared to the behaviour of used sleepers. All used sleepers had cracks underneath at the rail seat sections. These cracks did not affect ultimate bending moment capacities. An estimate of the structural performance of the sleepers was developed.

Key words: Concrete sleeper, loading test, damage, crack.

1. INTRODUCTION

Currently nearly 70% of the Finnish rail network is equipped with prestressed concrete monoblock sleepers. The sleeper is one of the most important components of a railway track because of its behaviour under loading. The most important functions of sleepers are to transfer rail forces to the ballast bed, to serve as a support and mount for the rail foot and fastenings, and to preserve track gauge.

Given the need to better understand the life cycle of sleepers installed during various decades, the Finnish Transport Agency (FTA) launched a comprehensive research programme at the Tampere University of Technology (TUT) Department of Civil Engineering. Before completing the tests presented here, the researchers at TUT performed field tests to determine longitudinal and transverse track resistances [1] and cyclic loading tests on concrete sleepers under varying ballast conditions [2] to estimate the soil-structure interaction of a railway track.

Loading tests on concrete sleepers have been reported, for example, by Thun [3] and Gustavson [4]. Departing from them and other available literary sources, the focus of this study was on structural behaviour during static and dynamic loading of different types of concrete sleepers with different service histories.

2. LOADING TEST ARRANGEMENTS AND TESTED SLEEPERS

2.1 Testing programme

Loading tests were performed both on unused and used railway sleepers according to European standard EN 13230 [5]. The used sleepers had been removed from the tracks for various reasons. The testing programme comprised static tests on the rail seat section and sleeper centre, as well as dynamic tests on the rail seat section. Despite not being specified in the EN standard, dynamic tests were also performed on the sleeper centre. The test programme is presented in Table 1. Besides the requirements set in the standard, vertical sleeper deflections and concrete strains were also measured during the tests.

Table 1 – Number of performed loading tests [6].

Test type	New sleeper (unused)	Used sleeper
Static, rail seat section	4	10
Static, sleeper centre	4	10
Dynamic, rail seat	2	2
Dynamic, sleeper centre	2	2

The aim of the loading tests was to compare differences in the behaviour of new (unused) and used sleepers.

2.2 Tested sleepers

Two new and unused sleeper types were tested: BP99 (date of manufacture 30.11.2009, depicted in Figure 1) and B97 (13.3.2009). The sleepers had 12 strands that were each 6.5 mm in diameter.

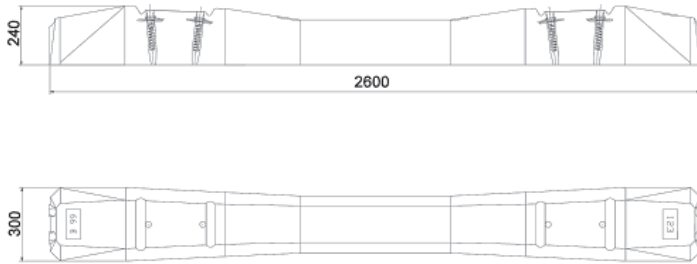


Figure 1 – Concrete sleeper type BP99. Height is 185 mm at the centre.

Three used sleeper types were tested: B63, B75, and BV75. Types B63 and B75 (Figure 2) have almost identical dimensions, where type B75 is only 5 mm higher at the rail seat section. These types were manufactured by the post-tensioning method using $\varnothing 9.4$ mm steel bars. Type BV75 was manufactured by the pre-tensioning method using 12 pieces of 7-wire strands that were each 6.4 mm in diameter. Both damaged and undamaged sleepers were tested. The BV75 sleepers were manufactured in 1977, the B75 sleepers in 1976, and the B63 sleepers in 1974. The number in the sleeper type names represents the year when the sleeper type was developed.

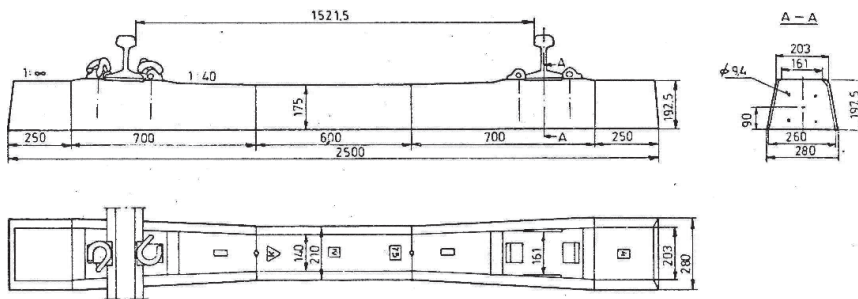


Figure 2 – Concrete sleeper type B75.

2.3 Loading apparatus

A loading frame (Figure 3) was constructed at TUT for both the static and the dynamic tests.

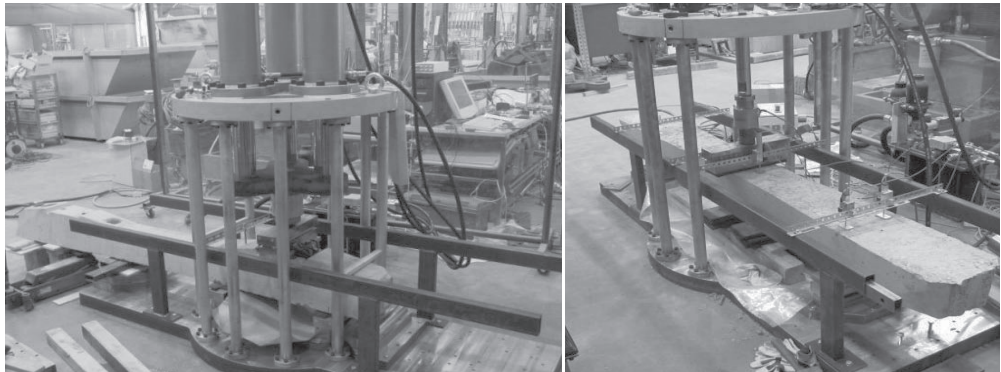


Figure 3 – Loading frame. Test on rail seat section (left) and test on sleeper centre (right) [6].

2.5 Measuring devices

A loop-shaped strain gauge model developed and calibrated at TUT was used to measure concrete strains during the loading tests. Four traditional strain gauges were glued on the inner surface of the loop. The gauge measures strain over a 100 mm distance. It was attached to the sleeper with two bolts as shown in Figure 4. The advantage of this measurement method is that the gauge is able to continue measuring after cracking has started. However, the result of measurement varies according to crack location, between the measuring points or just next to them. Strains were measured directly below the point of loading. Crack width was measured with a digital microscope.

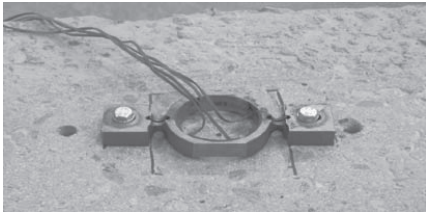


Figure 4 – Loop-shaped strain gauge [6].

As illustrated in Figures 5 and 6, four vertical displacement transducers were installed precisely in the middle of the two support lines, and an additional two displacement transducers were installed 105 mm from the point of the loading force.

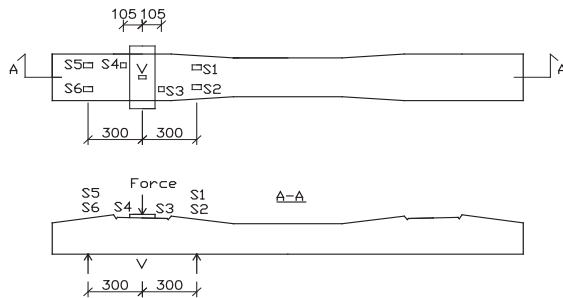


Figure 5 – Locations of sleeper strain gauge (V) and vertical displacement transducers (S) for the rail seat section tests.

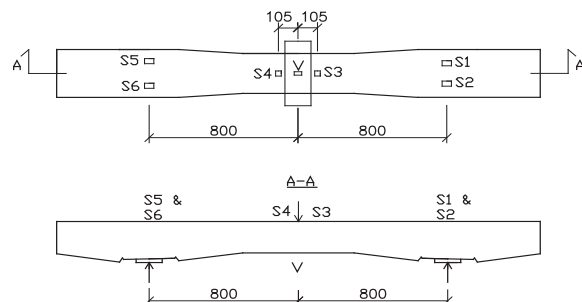


Figure 6 – Locations of sleeper strain gauge (V) and vertical displacement transducers (S) for the sleeper centre tests.

2.6 Loading tests

European standard EN 13230-2 [5] gives guidelines for calculating reference test loads for different concrete sleeper types. The reference loads are needed to determine the criteria of test loads. The first criterion to be considered is the test load that produces the first crack. In addition, the standard sets the criteria for the test load that produces a 0.05 mm crack that persists after removal of the load. Finally, the maximum test load is measured.

In the static load tests on the rail seat section, the sleeper has to withstand 1.8 times the reference test load Fr_0 before a permanent 0.05 mm wide crack forms, and the ultimate load has to be 2.5 times the reference test load. In the dynamic tests, the respective coefficients are 1.5 and 2.2. In this paper the criteria are presented in tabular form as in Table 2, for example, and they correspond to a 215 kN axle load when the train speed is over 200 km/h and to a 250 kN axle load when the train speed is less than 200 km/h.

All loading tests were load-controlled. The support arrangements for static and dynamic loading tests on rail seat sections were as shown in Figure 7, where the distance L_c between the support centrelines was 600 mm. The supports were 100 mm wide. Resilient pads (with thickness of 15 mm and Shore hardness of A65) required by the standard were placed between the supports under the sleepers and the undersides of sleepers. In dynamic loading tests, the sleepers were also provided with lateral and longitudinal supports that prevented lateral and longitudinal sleeper movement during the cycles.

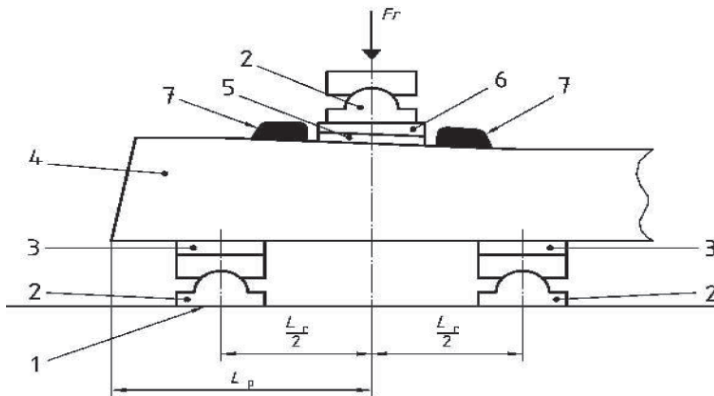


Figure 7 – Test arrangement of the rail seat section for the positive load test [5].

Descriptions of the labels in Figures 7 and 8 are as follows: 1. Rigid support, 2. Articulated support, 3. Resilient pad, 4. Prestressed monoblock sleeper, 5. Standard rail pad as defined by the purchaser, 6. Tapered packing, and 7. Lateral stop and base plate.

An attempt was made to adhere to the load curve set in the standard for loading sleepers. In loading tests on rail seat sections, the width of the permanent crack was measured between load steps while the sleeper was unloaded.

In static loading tests on sleeper centres, support was provided as shown in Figure 8, with the distance between supports L_c being 1600 mm.

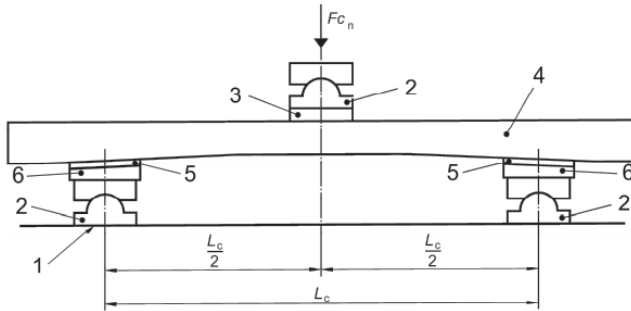


Figure 8 – Test arrangement of the centre section for the negative load test [5].

The minimum force always to be exceeded during dynamic loading tests on rail seat sections was 50 kN, and the first load step equalled the reference test load F_{r0} . Load step increments were 20 kN. The minimum force during tests on centre sections was 15 kN, and load step increments were 10 kN. At each step, 5000 loading cycles were applied at a frequency of 2 Hz.

3. RESULTS

3.1 Static loading test on rail seat sections

The general condition of the used sleepers was good. The sides of the sleepers had occasional 50-300 mm long longitudinal cracks, and small pieces of concrete had chipped off some sleepers. Only the B63 sleepers (Figure 9) appeared to be in poor condition visually.



Figure 9 – Cracks at the end of a B63 sleeper [6].

Each used sleeper subjected to loading already had a vertical crack in the rail seat section. The cracks were almost fully closed and could generally be noticed only when looking at the sleepers from the side during loading.

According to the criteria of Standard EN 13230-2 [5], a sleeper must be able to take the reference test load without cracking. The new sleepers clearly met this criterion. The standard also sets a criterion for a permanent crack that is 0.05 mm in width. Table 2 shows that sleepers BV75, B97, and BP99 meet the criterion well. The B75 sleepers only just meet the criterion, but the degraded B63 sleeper does not meet it at all. Moreover, the standard sets a criterion for the maximum load that a sleeper must be able to take. The various sleeper types clearly meet this criterion with the exception of the only tested B63 sleeper.

The bending moments corresponding to the formation of the first crack and to failure were added to the table. The bending moments for a 0.6 m span and a central force were calculated by the formula $M = FL/4 = 0,15m \cdot F$. The moment could have been calculated by taking into account the 140 mm wide steel plate on the sleeper acting as a short beam. Then, the moments would have been 20% smaller.

Table 2 – Results of static loading tests on rail seat sections [6].

Tested sleepers	First crack		Crack width $\geq 0,05$ mm when unloaded	Failure	
	Force [kN] (Criterion > 128 kN)	Moment [kNm]	Force [kN] (Criterion > 230 kN)	Force [kN] (Criterion > 320 kN)	Moment [kNm]
BV75 (test 3)	-	-	450	530	80
BV75 (test 6)	-	-	430	548	82
BV75 (test 7)	-	-	420	484	73
BV75 (test 8)	-	-	400	465	70
BV75 (test 9)	-	-	410	477	72
BV75 (test 10)	-	-	370	465	70
BV75 (test 11)	-	-	460	503	75
B97 (test 2)	170	26	310	565	85
B97 (test 12)	180	27	370	511	77
BP99 (test 4)	180	27	340	509	76
BP99 (test 13)	190	29	400	480	72
B63 (test 1)	-	-	200	300	45
B75 (test 14)	-	-	250	387	58
B75 (test 5)	-	-	250	397	60

Under loading the behaviour of sleepers B63 and B75 differed from the others. In the case of B63 and B75, crack widths increased steadily until about 300 kN. Thereafter, crack widths increased significantly when the load was increased. With the other tested sleeper types, crack widths increased steadily during almost the entire loading test while being clearly smaller compared to B63 and B75 sleepers when nearing the failure load. Figure 10 shows a B75 sleeper under about 360 kN loading. When loading ended, the crack width was about 2 mm.

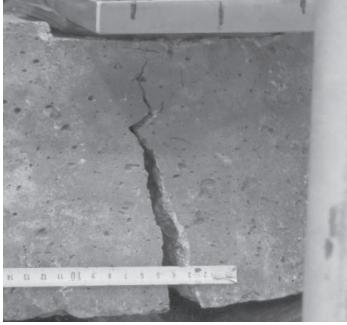


Figure 10 – B75 sleeper under 360 kN static loading of the rail seat section.

The failure mode of the loaded rail seat sections was most often bending failure or shear-bending failure where the prestressed reinforcement finally yielded to the tensile loads and broke. The exception was the degraded B63 sleeper where the failure mode was compression-bending failure. In the case of the BV75 sleepers, it should be noted that failure always occurred at the cross section of the sleeper where there was existing crack before loading.

No slipping of the strands was observed in the static loading tests except once during test 10 on BV75, where slipping produced a permanent 0.05 mm crack at the 370 kN loading level. The slip explains the earlier increase in permanent crack width in this sleeper than in other sleepers of the same type.

3.2 Dynamic loading tests on rail seat sections

The used sleepers appeared to be in good condition visually. Table 3 presents the results of the dynamic loading tests on rail seat sections.

Table 3 – Results of dynamic loading tests on rail seat sections.

Tested sleepers	First crack	Crack width $\geq 0,05$ mm when unloaded	Failure
	[kN] (Criterion > 128 kN)	[kN] (Criterion > 192 kN)	[kN] (Criterion > 282 kN)
BV75 (test 16)	-	230	310
BV75 (test 17)	-	270	390
B97 (test 15)	190	290	430
BP99 (test 18)	210	290	390

Comparison of new and used sleepers shows that a permanent 0.05 mm crack formed in the BV75 sleepers at a lower loading level than in the B97 and BP99 sleepers. In static loading tests, the opposite was true.

All criteria were met in all tests. While one BV75 sleeper clearly met the failure criterion, the other one only narrowly passed. A possible reason is the length of the pre-existing cracks of the sleepers. The sleeper that failed at 310 kN had a crack of about 110 mm in length before loading, while the sleeper that failed at 390 kN had a crack of only about 50 mm in length

before loading. The failure mode of dynamic loading tests on rail seat sections was bending failure. The prestressing strands broke starting from the lowest row.

3.3 Static loading tests on sleeper centres

As Table 4 shows, new sleepers of type B97 and BP99 clearly met the criteria set for formation of the first crack. All except three of the used sleepers had pre-existing vertical cracks.

Table 4 – Results of static loading tests on sleeper centres [6].

Tested sleepers	First crack		Failure	
	Force [kN] (Criterion > 25 kN)	Moment [kNm]	Force [kN]	Moment [kNm]
BV75 (test 19)	-	-	125	50
BV75 (test 20)	-	-	118	47
BV75 (test 21)	-	-	118	47
BV75 (test 22)	-	-	126	50
BV75 (test 23)	-	-	114	46
BV75 (test 24)	-	-	124	50
BV75 (test 25)	45	18	133	53
B75 (test 26)	-	-	81	32
B63 (test 27)	45	18	93	37
B63 (test 28)	35	14	88	35
B97 (test 29)	45	18	103	41
B97 (test 30)	50	20	109	44
BP99 (test 31)	45	18	100	40
BP99 (test 32)	50	20	102	41

The bending moments corresponding to the formation of the first crack and to failure for the 1.6 m span and a central force were calculated by the formula $M = FL/4 = 0,4m \cdot F$.

3.4 Dynamic loading tests on sleeper centres

Dynamic tests were performed on the sleeper centres despite not being specified in the EN standard. Tested BV75 sleepers appeared to be in good condition visually. Table 5 presents the results of the dynamic loading tests on sleeper centres.

Table 5 – Results of dynamic loading test on sleeper centres

Tested sleepers	First crack	Crack width $\geq 0,05$ mm when unloaded	Failure
	[kN]	[kN]	[kN]
BV75 (test 35)	-	85	105
BV75 (test 36)	35	95	115
B97 (test 33)	45	85	105
BP99 (test 34)	45	85	105

As Table 5 shows, the results of the dynamic loading tests on sleeper centres did not differ significantly from those of the static loading tests on the centres presented in Table 4.

3.5 Measured strains

Concrete strains were measured in each loading test. The results of strain measurements are, however, fully comparable only for the sleepers that had no cracks before loading. Cracks that formed in the sleepers or pre-existed in them were not necessarily in the measurement area.

The compression caused by pretensioning in the centres of B97 and BP99 sleepers is about 200 $\mu\text{m}/\text{m}$ and about 140 $\mu\text{m}/\text{m}$ at the rail due to the larger cross-sectional area.

In static loading tests on the B97 rail seat sections, strains were about 350-400 $\mu\text{m}/\text{m}$ at the loading level that produced the first crack. The corresponding strains on the BP99 sleepers were about 420-470 $\mu\text{m}/\text{m}$. Strains measured in the dynamic tests were of the same magnitude as those measured in the static loading tests.

Thus, the strain after reduced precompression is $\varepsilon_c = 0.0002$ or greater. In the case of concrete with a cube compressive strength $f_{c,\text{cube}} = 60$ MPa has a modulus of elasticity $E_{\text{cm}} = 37,000$ MPa [7], a strain of 0.0002 corresponds to tensile stress $\sigma_{\text{ct}} = E_{\text{cm}} \cdot \varepsilon_c = 7.4$ MPa, applying elastic tensile behaviour. According to Eurocode EN 1992-1-1 [7], the average tensile strength is $f_{\text{ctm}} = 4.1$ MPa. The flexural tensile strength of a structure that is 220 mm high is $1.38 \cdot f_{\text{ctm}} = 5.7$ MPa [7], which corresponds to strain increment $\varepsilon = 0.00015$ for elastic behaviour. Consequently, the sleepers could withstand greater tensile stresses than those calculated using the average concrete strengths of the Eurocode.

In loading tests on sleeper centres, strains corresponding to the formation of the first crack were about 420-500 $\mu\text{m}/\text{m}$ in the case of the B97 sleepers and about 480-580 $\mu\text{m}/\text{m}$ in the case of the BP99 sleeper. The strains measured for the B63, B75, and BV75 sleepers varied from 350-500 $\mu\text{m}/\text{m}$ at the formation of the first crack. The measured strains are slightly larger than those measured in rail seat section loading tests. This can be explained by the higher compression of concrete in the centre of the sleepers due to pretensioning.

3.6 Measured sleeper deflections

Deflections measured under static loading of the sleeper centres at the points shown in Figure 6 are presented in Figure 11.

Independent of sleeper type, deflections increased relatively evenly until the loading level of 50-60 kN. When the level exceeded 60 kN, deflections of the B63 and B75 sleepers increased above those of the others. The cross-sections of the used sleepers were smaller than those of the new ones as documented in Figures 1 and 2.

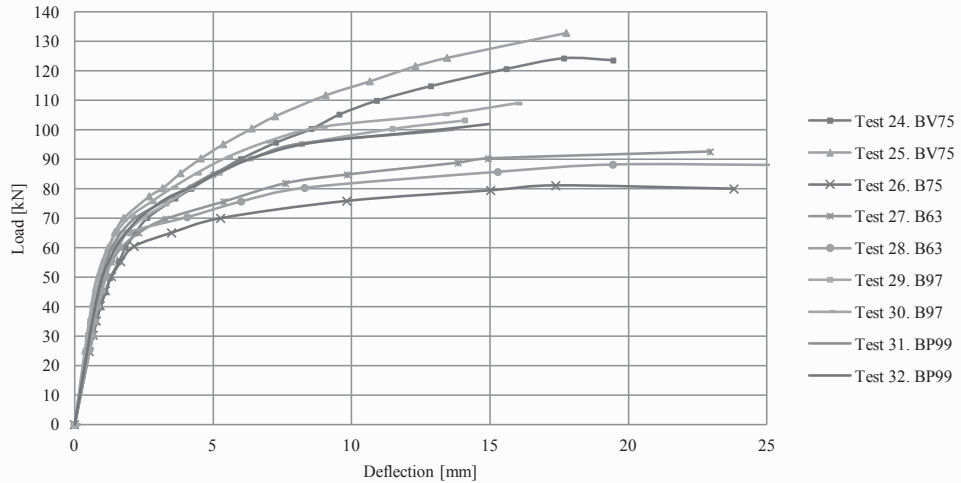


Figure 11 – Deflections measured in static loading tests on sleeper centres for B75, B63, B97, BP99, and two BV75 sleepers [6].

In the dynamic loading tests on rail seat sections, measured deflections increased very slowly until about 1 mm. Thereafter, they increased very fast, being 3-6 mm before failure, depending on the sleeper type. At the formation of the first crack, the measured deflections of the sleepers were only about 0.15-0.2 mm.

4. STRUCTURAL CALCULATIONS

Cross-section characteristics (e.g. moment of inertia I and section modulus W) were calculated first for all sleeper types at the rail seat section and sleeper centre to estimate the limit state of crack formation. The pre-stress and its location were taken into account, as well as the flexural tensile strength of the concrete. The compression strength of the concrete was estimated to be $f_{c,cube} = 60$ MPa. Accordingly, the flexural tensile strength was about 5.2 MPa. Values of tensile stress exceeding this value of strength would be expected to result in cracking.

Bending moment capacity was calculated by substituting breaking strength for tensile strength in the case of the outermost strands farthest from the compression side, while yield strength was substituted for tensile strength in the case of the strands closest to the compression side. The results are presented in Table 6.

Table 6 – Calculated bending moment capacities of tested sleepers.

Bending moment		BP99	B97	B63	B75	BV75
Rail seat section, positive						
M_{Rk} first crack	kNm	23.3	23.9	15.6	16.7	21.4
M_{Rk} failure	kNm	44.9	45.7	29.7	31.6	40.1
Sleeper centre, negative						
M_{Rk} first crack	kNm	15.2	14.6	12.4	12.4	13.1
M_{Rk} failure	kNm	33.7	32.8	26.4	26.4	29.3

The calculations performed to determine the load level associated with formation of the first crack in the rail seat section corresponded quite closely to the loading test results given in Table 2. On the other hand, the failure moments provided by the tests were typically much higher than the calculated failure moments, especially for the rail seat sections. The reasons for this are not clear. The strengths of the concrete and steel (tendons) were perhaps higher than reported by the manufacturers. For a short span, 0.6 m, the difference between loading capacity based on a strut-and-tie model and the bending model is about +5%.

The calculated moments corresponding to sleeper centre cracks were lower than the moments from the loading tests documented in Table 4. The average difference was 32% for sleeper type BV75, 24% for sleeper type B63, and 23% for the new sleepers. Calculated failure moments were also lower than the moments from the loading tests. The average difference was as high as 61% for sleeper type BV75, 32% for sleeper type B63, and 20% for the new sleepers. As the new sleepers were evaluated by calculating bending using the formula $M = FL/4 = 0,37m \cdot F$, the results for the new sleepers based on the tests and on the calculations were quite close. This could be done because it was obvious that the steel plate above the sleepers divided the loading force into two across a distance of about 120 mm, as illustrated in Figure 10.

5. CONCLUSIONS

Loading tests revealed a crack on the underside of every used sleeper at the rail seat. The lengths of the pre-existing cracks were in the range 30-100 mm, but the cracks were almost fully closed and thus extremely difficult to notice before loading. Based on the results of the loading tests, it can be estimated that occasional cracks are largely insignificant when a sleeper is subjected to static loading. No abnormal signs of corrosion were observed in any prestressed reinforcement in the vicinity of the cracks.

In rail seat section loading tests, sleepers B97 and BP99 met the criteria of standard EN 13230-2 well, and sleepers BV75 very well considering their age. Sleepers B63 and B75 fared clearly worse in the loading tests than the other sleeper types, but, based on visual inspection, their load bearing capacity was at least satisfactory considering their condition.

The results of dynamic loading tests on rail seat sections were lower than those of static tests. Results of dynamic loading tests on sleeper centres did not differ significantly from those of static loading tests on the centres.

Several used sleepers had cracks in the middle of the top side. As in the case of static loading tests on rail seat sections, the cracks were almost completely closed and thus difficult to notice. However, as loading progressed, the cracks opened up and continued to propagate. Nonetheless, on the basis of the results of the loading tests, it can be assumed that occasional cracks do not affect the strength properties of a sleeper much under static loading.

Deflections measured during tests on sleeper centres indicate that a deflection of about 1 mm is enough to produce a crack in the middle of a new sleeper.

Based on the tests on sleeper centres, the loading capacity of sleeper BV75 was at least as good as the capacities of sleepers B97 and BP99, which are presently being procured for the Finnish rail network. Sleepers B63 and B75 also passed the loading tests on sleeper centres surprisingly well considering their observed condition.

Considering that the loading force on the sleeper was equally divided in two over a 120 mm distance, the calculated limit state of crack formation corresponded quite closely to the observed bending behaviour. Assuming the same also applies to new sleepers, the calculated ultimate bending moment was close to the ultimate bending moments of the loading tests. The used sleepers were much more resistant to loading than predicted by calculations.

REFERENCES

1. Kerokoski O. Determination of longitudinal and transverse railway track resistance. JRC2010. Proceedings of the 2010 Joint Rail Conference. April 27-29, 2010, Urbana, Illinois, USA. Department of Civil Engineering, Tampere University of Technology, Finland. 9 pages. 2010.
2. Nurmikolu A., Kerokoski O., Rantala T. & Viitala T. Cyclic loading tests of concrete sleepers with varying ballast condition. JRC2010. Proceedings of the 2010 Joint Rail Conference. April 27-29, 2010, Urbana, Illinois, USA. Department of Civil Engineering, Tampere University of Technology, Finland. 9 pages. 2010.
3. Thun H. Assessment of fatigue resistance and strength in existing concrete structure. Luleå University of Technology. Department of Civil and Environmental Engineering. Division of Structural Engineering. ISBN: 978-91-85685-03-5. Sweden. 2006.
4. Gustavson R. Structural behaviour of concrete railway sleepers, Doctoral Dissertation, Chalmers Concrete Structures, Gothenburg. Chalmers University of Technology, Sweden. 2002.
5. EN 13230 Railway applications. Track. Concrete sleepers and bearers. Parts 1 & 2. European committee for standardization. 2009.
6. Rantala, T. Betoniratapölkyn vaurioitumismekanismit (Damage mechanisms of a concrete sleeper). Master of Science Thesis. Tampere University of Technology. 2011.
7. EN 1992-1-1 Eurocode 2: Design of concrete structures. Part 1-1: General rules and rules for buildings. 2004.

The Development of Microstructure of Portland Cement Mortars – From the Fresh to the Hardened State



Knut O. Kjellsen
Ph.D., Chief Engineer, Adjunct Professor
Norcem AS, N-3991 Brevik, Norway
Department of Structural Engineering, Norwegian University of
Science and Technology, N-7491 Trondheim, Norway,
e-mail: knut.kjellsen@norcem.no



Sidney Diamond
Ph.D., Professor Emeritus,
School of Civil Engineering, Purdue University,
550 Stadium Mall Drive, West Lafayette, IN 47907-1284,
United States

ABSTRACT

SEM-BSE examination of freshly-mixed, early age and late age Portland cement mortar specimens are reported. Freshly mixed mortars reveal complex features that appear to influence subsequent development of the hardened state microstructure. The larger cement grains were found to be distributed in-homogeneously within the paste of the freshly-mixed mortars, ‘pockets’ of paste being either relatively densely packed with large cement grains, or largely bereft of such grains. These ‘pockets’ gave rise to either ‘densely packed patches’ or ‘porous patches’ in the hardened mortars. Local indications of ITZ were occasionally observed in our visual examination. The microstructure of freshly-mixed mortar also contains layers of entirely water-filled space a few micrometers thick in the paste immediately adjacent to many sand grain surfaces. After a few hours, sparse deposits of calcium hydroxide, and later C-S-H and presumably other reaction products, may form in these spaces.

Keywords: Portland cement, fresh mortar, hardened mortar, microstructure, SEM

1. INTRODUCTION

Freshly mixed concrete is a suspension containing mixing water and solid particles of various composition, shape and size. The solid material consists of the micrometer-sized cement grains, the larger filler and sand particles, and the coarse aggregate particles which may be up to about 20 mm in diameter. Thus the particle size ranges over about four orders of magnitude. The particle shape, surface texture and mineralogy can vary widely. The particle suspension is mixed, more or less effectively, transported, placed in formwork and compacted. Once the reactive cement particles come in contact with the mixing water they

start to undergo partial dissolution. The mixing water rapidly becomes saturated with various ions from the dissolving cement phases, and reaction products (hydrates) precipitate out of the mixing water, and tend to fill up the space that were originally filled with water. This is a continuous process that starts immediately after water and cement is brought in contact and continues for days and even months.

From the description above one can easily perceive that concrete is a truly complicated material, both from the perspective of the large variability of the incorporated materials, the influence of the processing (mixing, placing, compaction), to the hydration processes. The question addressed in this paper is whether, for such a complicated and inhomogeneous material, there are some characteristic or recognizable patterns in how the various solid particles (in particular the cement grains) distribute themselves throughout the freshly mixed, placed and compacted suspension. And if there is, how will that influence the structure and properties of the hardened concrete. Previous research indicate that cement particles distribute themselves around and in between the larger aggregate particles in patterns that can be recognized in various concretes, for example in patterns like 'ITZ' (interfacial transition zones) and 'patchy structures'. This paper deals with these questions, and aims to provide a summary of the work that the present authors have done jointly in recent years.

2. EXPERIMENTAL

2.1 Materials, mixing, and curing

Mortars were mixed according to the European Standard EN 196-1 (Methods of Testing Cement. Part 1: Determination of Strength). The mixes were prepared at w:c ratios of 0.25 and 0.40, as well at the 0.50 w:c ratio specified in the Standard. In these mortar mixes the paste volume was kept constant at 42%, thus giving a constant sand volume of 58%. One bag (1350 g) of the siliceous reference CEN sand (cf. EN 196-1) was used for each mix batch. The cement used was a Swedish low-alkali sulfate-resistant cement (equivalent to ASTM Type V). The cement analysis gave the following percentages by weight: 22.3% SiO₂, 3.3% Al₂O₃, 4.6% Fe₂O₃, 64.3% CaO, 0.85% MgO, 0.56% K₂O, 0.17% Na₂O, 2.3% SO₃, and 0.71% ignition loss. The compositional data indicate that the cement was of low alkali content and contained almost no C₃A, the calculated Bogue composition being 57% C₃S, 21% C₂S, 0.8% C₃A, and 14% C₄AF. The Blaine specific surface area and density were 309 m²/kg and 3220 kg/m³, respectively.

In order to obtain workable mortars at the two lower water:cement ratios it was necessary to incorporate a superplasticizer. A modest dose of sulfonated naphthalene superplasticizer (Mighty 150) was employed with the w:c 0.40 ratio mix, and a heavy dose was needed for the w:c 0.25 mix. Batch compositions for all three mortar mixes are given in Table 1.

Table 1 - Composition of the mortars, grams per batch

w:c-ratio	0.25	0.40	0.50
Cement	650	515	450
Sand	1350	1350	1350
Water*	163	205	225
Superplasticizer	22.8	3	-

**total water, including water in plasticizer*

Mixing was carried out according to the EN 196-1, and involved the final mixing for 1 min. However, a second, more extensively mixed w:c 0.40 mortar batch was also prepared. The duration of the final mix sequence for this batch was 2 min instead of the 1 min specified in the standard method.

For each mortar a small sample was obtained for fast freezing immediately after mixing. The remainder of the batch was placed in a mould and conditioned as prescribed by the specified Standard Method. Curing took place at 100% RH and 20°C. Early age mortar samples were taken and specimens were prepared for SEM examination at 6 and 12 hours of hydration, and mature samples prepared after 28 days.

2.2 Specimen Preparation and SEM examination procedures

Specimens were freeze-dried immediately after mixing, and also after 6 hours, 12 hours, and 28 days. In each case, small (ca 0.25 g) portions of mortar were sampled from the mix and quenched in liquid nitrogen. The frozen samples were then subjected to low-pressure, low-temperature sublimation (at pressures between ca 10^{-4} and 10^{-2} mbars) over a period of three days. The degree of removal of water during this extended sublimation was checked against oven drying, and water removal was found to be complete. According to the ice - water vapor phase boundary in the water phase diagram, the pressures applied correspond to maintaining temperatures between ca -90°C and ca -60°C during the sublimations. Such temperatures would restrict (but probably not completely prevent) the Ostwald growth of some of the ice nuclei that were probably produced during the freezing step.

Specimen preparation, especially of the freshly-mixed mortars, is obviously a critical step in these investigations. On one hand, in fast freezing, the smaller the specimen the faster the freezing occurs, and the less the likelihood developing detectable ice formation artefacts. On the other hand, specimens of appreciable size are needed to obtain a representative volume of mortar for examination in different areas. The sample size selected, approximately 0.25 g, was a reasonable compromise. To check for possible effects of such ice crystal growth, additional samples of the w:c 0.40 mixes were dried (at 6 hours and beyond) using conventional drying at 60°C. The comparison did not reveal different microstructural features between the freeze-dried and oven-dried specimens [1].

The sublimed specimens, particularly of the freshly-mixed mortars, were exceedingly fragile and extremely careful handling was required to successfully impregnate and polish them for SEM examination. The specimens were vacuum impregnated with Epo-Tec 301 epoxy resin. The polishing procedures used are as described elsewhere [2]. Parallel observations in backscattered and secondary electron modes indicated that the as-prepared specimens were flat and fully impregnated.

The specimens were carbon coated and examined in the backscatter electron mode in a Hitachi model S-4300 Field-Emission SEM, with the accelerating voltage kept at 10 keV throughout. A number of areas of each specimen were examined to be certain that the images presented are representative of the specimens.

3. RESULTS AND DISCUSSION

3.1 Patchy microstructure and ITZ

Figure 1 shows a representative overview of the 0.50 w:c mortar hydrated for 6 hours. The siliceous sand particles are seen as the grains of a uniform darker gray appearance, whereas the bright smaller areas represent cement grains. The dark intermediate phase in between represents primarily water-filled pore space, some of which possibly contain some reaction products. There is little visual evidence of cement hydration at six hours, and the mortars were soft and weak, indicating that only some small degree of setting was attained. As only a very small fraction of the cement has hydrated, the image resembles quite well the spatial distribution of cement grains within the freshly-mixed mortar. The inhomogeneous spatial distribution of cement grains within the paste portion of the mortar is apparent. Closely-spaced aggregations of large cement grains are seen in the outlined area to the left. In contrast, the outlined area to the right contains only one cement grain of comparable size. The local w:c-ratio is obviously very different in the two outlined areas. Image analysis indicated a local w:c-ratio of about 0.35 in the outlined area to the left and about 1.5 in the outlined area to the right.

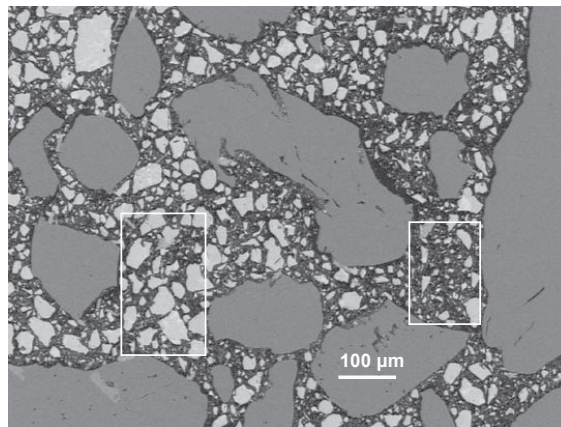


Figure 1 - Low magnification image of 6 hour old w:c 0.50 mortar.

The local variations in content of larger cement grains and w:c in the fresh and hardly hydrated mortar leads to corresponding variations in the hardened mortar. This local variation in w:c-ratio leads to a ‘patchy’ microstructure in the mature state. Figure 2, which shows the 0.50 w:c mortar hydrated for 28 days, illustrates this effect. A porous paste area with almost no residual cement grains are seen to the left just above the large multi-hued sand grain at the bottom of the image, while a dense paste area populated with large residual cement grains and containing little pore space is found to the right.

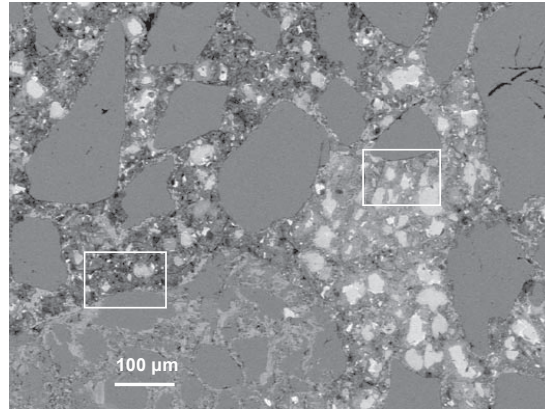


Figure 2 - Low-magnification view of w:c 0.50 mortar hydrated for 28 days

A detailed image of the porous patch outlined in Figure 2 is captured in Figure 3. The high porosity is evident. A number of hollow-shell pores (Hadley grains) are seen in the porous patch, some are indicated by an arrow. A predominance of hollow-shell pores in porous patches was noted by Diamond and Landis [3], and is consistent with the measurement of higher hollow-shell porosity at higher w:c ratios [4]. The dense patch in Figure 2 is reproduced at high magnification in Figure 4. The porosity is obviously much lower than in the porous patch, in fact only very few pores are seen. Also a number of relatively large residual cement grains are observed, corresponding to the closely-spaced assemblages of large cement grains in the fresh mortar (cf. Figure 1).

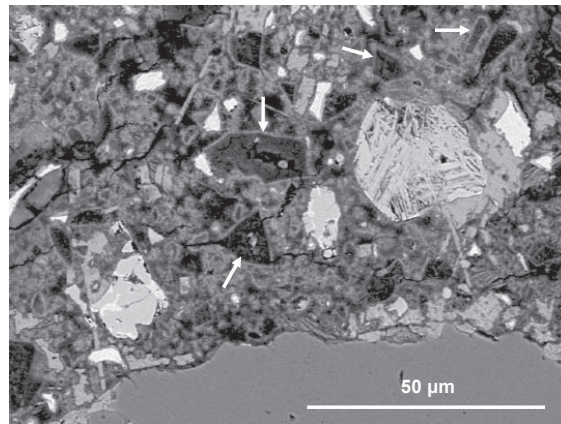


Figure 3 - High-magnification image of the porous area outlined in Figure 2.

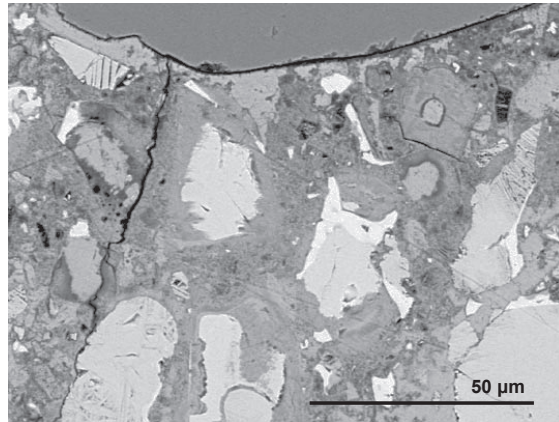


Figure 4 - High-magnification image of the dense area outlined in Figure 2.

The presence of dense and porous patches in the mature mortar was also observed in the 0.40 w:c mortars. On the other hand, in the mature 0.25 w:c mortars essentially the entire paste appeared dense, and a patchy microstructure was not clearly indicated by the visual examination.

It has been shown in a number of studies [e.g. 3, 5, 6] that both laboratory- and field mixed concrete or mortars may exhibit dense areas or patches of hardened cement paste which are sharply delineated from adjacent, highly porous areas. The reason for the existence of this patchy microstructure is not entirely clear, but it is a direct result of a variable spatial distribution of cement particles of the freshly mixed concrete or mortar. This is likely caused by insufficient dispersion of flocculated cement grains, or perhaps some other inability of mixing to disperse variably sized particles homogeneously. However, both addition of superplasticizer and extended periods of mixing have failed to eliminate this distinctive microstructure [5].

The geometry of the patchy microstructure appears to be different from that of the commonly accepted ITZ structure. Although the latter type of spatial structure also resembles an association between porous and denser paste areas, the ITZ concept predicts that the porous area will be in contact with the aggregate interface, and that there will be a gradual increase in density and presence of large cement grains with distance from the interface. The origin of the ITZ is commonly attributed to a so-called ‘wall effect’. A large aggregate particle placed at random in a cement paste (i.e. an assembly of cement grains) would ‘cut through’ previously existing cement grains. As this is impossible, in mixing the random packing is disrupted and it is anticipated that this disruption statistically gives rise to a zone of higher porosity and smaller grains in the zone closest to the aggregate [e.g. 7]. Scrivener et al. [7] found that at 1 day the deficiency in residual anhydrous grains, in particular larger grains, was only significant in a region of about 15 micrometers adjacent to the aggregate surface. In the mature state the deficiency in residual un-hydrated cement cores was apparent over a zone of about 40 micrometers, because the smaller anhydrous grains located closer to the aggregate surfaces will have reacted.

We can perceive that overlapping ITZ's from adjacent aggregate particles could be misinterpreted as porous patches. However, ITZ and patchy structures are indeed different spatial particle arrangements arriving from different mechanisms. Porous patches can exist up to several hundred micrometers within the 'bulk' paste, and may be in contact with only a small portion of the surface of a given aggregate particle. Indeed, some porous patches are seen (in two dimensions) to have no contact at all with aggregates, but are entirely or partly surrounded by and in close contact with dense patches, illustrated in [6].

According to our experience ITZ structures are not as easily visually observed as patchy microstructures, and can often probably only be discerned by statistical techniques such as image analysis and microanalysis [e.g. 8, 9]. Figure 5 reveals an image of the 0.25 w:c mortar hydrated for 6 hours. The outlined area to the left clearly reveals indication of a local ITZ structure, with a near interface zone largely bereft of larger cement grains and with the larger cement grains further away from the paste aggregate interface; indeed, there appears to be a certain gradient with respect to the sizes of cement grains. On the other hand, in the outlined area in the central part of Figure 5 it is observed that large cement grains are densely packed close to the aggregate surfaces, with no or very few small cement grains between them. A little further to the right a paste area is practically without cement grains, even in this w:c 0.25 mortar. We think Figure 5 and the other figures illustrate the large complexity and heterogeneity inherent in mortar and concrete microstructures. The spatial particle arrangement and the structure in concrete and mortar is very complex, and appears to comprise 'ITZ' structures, 'patchy' structures, and other structures as well – as will be discussed next.

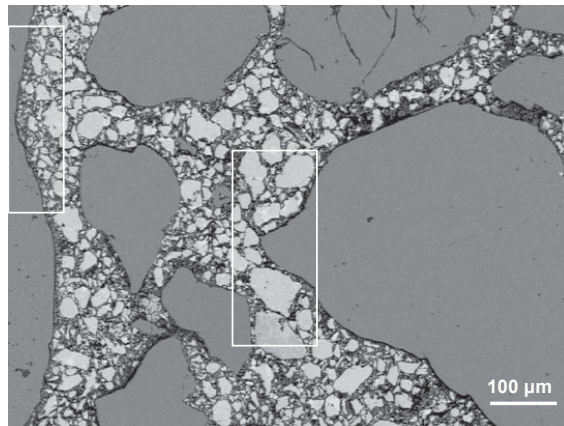


Figure 5 - Low magnification image of 6 hour old w:c 0.25 mortar.

3.2 Apparently water filled-layers adjacent to sand grains

In the SEM examination of the freshly-mixed and early age mortar specimens it is observed that some of the areas adjacent to the sand grain surfaces are filled with epoxy, and are seen to be locally free of cement grains or hydration products. An example can be observed in Figure 6 showing a field of the 0.50 w:c mortar fast frozen immediately after mixing. Such layers which are water filled in the fresh state are a few micrometers wide. Similar well defined

water-filled layers adjacent to many sand grains were found in all fresh mortar specimens and also in all of the early age specimens, both oven-dried and freeze-dried. It was seen that the outline of the black (water filled) layer follows the local convolutions of the sand grain surfaces with considerable fidelity.

After a few hours sparse deposits of calcium hydroxide (CH) are formed within these water-filled layers, as observed in Figure 7, which provides a detailed view of the w:c 0.40 mortar fast-frozen after 6 hours hydration.

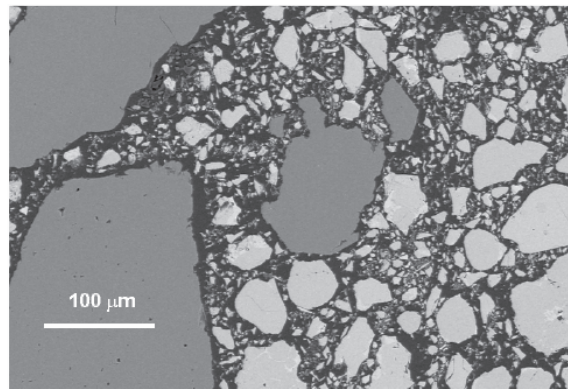


Figure 6 - Image of the w:c 0.50 mortar fast frozen immediately after mixing

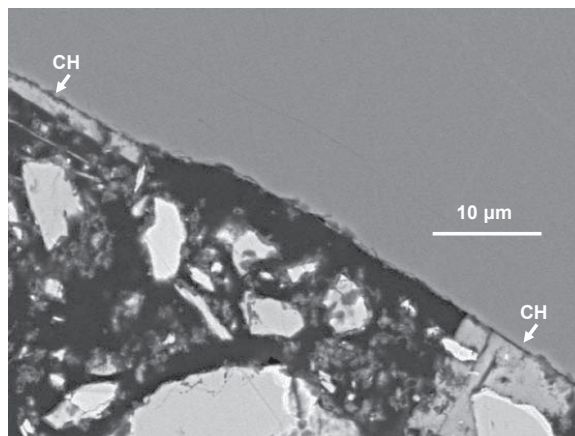


Figure 7 - High-magnification image of the w:c 0.40 mortar fast-frozen after 6 hours hydration.

Later on, C-S-H may fill in, but the layers persist as recognizable features for at least 12 hours. It appears to us that the existence of such deposits of hydrates provides an objective proof that the layers represent zones that were filled with water in the original mortars, and were not induced by either method of specimen preparation.

These water-filled layers in the fresh mortar appear to be associated with the common occurrence in hardened concretes of oriented layers of calcium hydroxide of roughly the same thickness along aggregate surfaces; Figure 1 in Kjellsen et al. [9] can be taken as an example. Possible explanations are the previously discussed ‘wall effect’, ‘bleeding’ or ‘syneresis’. We call attention to Diamond and Kjellsen [10] for a more in depth discussion.

3. CONCLUSIONS

The highly heterogeneous nature of concrete microstructure is sometimes appreciated by researchers, but probably not to the extent it should. Real concrete microstructures appear to be much more complicated than predicted by the simple concept of ‘ITZ’ structures.

The conventional notion of a nearly uniform gradient of cement grain packing extending outwards from all aggregate surfaces, so as to produce a corresponding nearly uniform gradient of porosity (i.e. a conventional ‘interfacial transition zone’), is far from what is typically observed. Rather, there seems to be a very variable packing of cement grains near sand grains in different areas, which results in corresponding variable near-interface microstructure in the hardened state. Conventional uniform gradients of cement grain packing (i.e. ITZ) are visually observed occasionally, but in other fields, large cement grains are densely packed close to the sand grains. In some fields, particularly in congested areas, practically no cement grains exist at all. Also, water filled layers a few micrometers wide are found around parts of many sand grains in freshly mixed mortars. These water-filled layers in the fresh mortar appear to be the sites of the subsequent development of oriented layers of calcium hydroxide of roughly the same thickness along portions of the aggregate surfaces in hardened concretes.

REFERENCES

1. Kjellsen, K. O. and Diamond, S., “Investigations into the Microstructure of Fresh Portland Cement Mortar,” Proceedings, 12th International Congress on the Chemistry of Cement, Montreal, 2007, paper TI-04.2
2. Kjellsen, K. O., Monsøy, A., Isachsen, K. and Detwiler, R. J., “Preparation of Flat-Polished Specimens for SEM-Backscattered Electron Imaging and X-ray Microanalysis – Importance of Epoxy Impregnation,” *Cement and Concrete Research*, Vol. 33, 2003, pp. 611-616.
3. Diamond, S. and Landis, E., “Microstructural Features of a Mortar as Seen by Computed Microtomography,” *Materials and Structures*, Vol. 40, 2007, pp. 989-993.
4. Kjellsen, K. O., Lagerblad, B. and Jennings, H. M., “Hollow-shell Formation – an Important Mode in the Hydration of Portland Cement,” *Journal of Materials Science*, Vol. 32, 1997. pp. 2921-2927.
5. Diamond, S. “The Patch Microstructure in Concrete: The Effect of Superplasticizer,” *Cement and Concrete Research*, Vol. 36, 2006, pp. 776-779.
6. Diamond, S. and Thaulow, N., “The Patch Microstructure in Concrete: Evidence that it Exists and is not a Backscatter SEM Artifact”, *Cement and Concrete Research*, Vol. 28, 2006, pp. 606-612.

7. Scrivener, K., Crumbie, A. K. and Laugesen, P., "The Interfacial Transition Zone (ITZ) Between Cement Paste and Aggregate in Concrete," *Interface Science*, Vol. 12, 2004, pp. 411-421.
8. Scrivener, K.L, Crumbie, A.K., and Pratt, P.L., "A Study of the Interfacial Region Between Cement Paste and Aggregate in Concrete," *Materials Research Symposium Proceedings*, Materials Research Society, Pittsburgh, 1988, Vol. 114, pp. 87-88.
9. Kjellsen, K.O., Wallevik, O.H., and Fjallberg, L., "Microstructure and Microchemistry of the Paste-Aggregate Interfacial Transition Zone of High Performance Concrete," *Advances in Cement Research*, Vol. 10, 1998, pp. 33-40.
10. Diamond, S. and Kjellsen, K. O., "Scanning Electron Microscopic Investigations of Fresh Mortars: Well-defined Water-filled Layers Adjacent to Sand Grains," *Cement and Concrete Research*, Vol. 38, 2008, pp. 530-537.

Model for Concrete Strength Development Including Strength Reduction at Elevated Temperatures



Peter Fjellström
M.Sc., Ph.D. Student
Luleå University of Technology
Dept. of Structural Engineering
SE - 97187 Luleå
peter.fjellstrom@ltu.se



Dr. Jan-Erik Jonasson
Professor
Luleå University of Technology
Dept. of Structural Engineering
SE – 97187 Luleå
jan-erik.jonasson@ltu.se



Dr. Mats Emborg
Head of R&D, Betongindustri AB
Professor, Head of Department
Luleå University of Technology
Dept. of Structural Engineering
SE – 97187 Luleå
mats.emborg@ltu.se



Dr. Hans Hedlund
Adj. Professor
Skanska Sverige AB
Technology
Bridge and Civil Engineering
SE – 405 18 Göteborg
hans.hedlund@skanska.se

ABSTRACT

When casting concrete structures, one of the most important properties is the concrete strength development. The need of actions on site is different at various stages of hardening, from the fresh concrete to the hardened concrete. The paper defines a model analysing maturity and associated strength growth within three important time periods. The model can be applied separately within each of these periods depending on test data available.

It is shown in the paper that the temperature plays an important role on the strength development of concrete structures. The hydration rate increases with increased temperatures, which can be described by maturity functions. If the concrete temperature remains high, strength reduction at later ages usually occurs compared to hardening at lower temperature, which may be denoted strength reduction at elevated temperatures or cross over effects. Both these phenomena have been implemented in the model for strength growth presented in the paper. The functionality of the model is demonstrated by evaluation of laboratory tests for five concrete mixes and

two types of cement.

Key words: Concrete hardening, Maturity function, Strength development, Construction stages, Strength reduction, Cross over effects.

1. INTRODUCTION

The range of commercial cements in Sweden has been relatively small. For each type of cement the variation in properties is very small, both in time and between cement plants. One consequence is that the so called tendency strength curves from the cement producers in practice are considered as “true” strength development. Therefore, strength controls on construction sites in Sweden are very rare.

The present situation will probably change with respect to the general demands of lowering the environmental impact of concretes. There is reason to believe that cements with lowered CO₂ loading will show larger variation both in cement properties and concrete compositions, as new non-reactive fillers as well as different kinds of SCMs (supplementary cementitious materials) will be introduced to lower the environmental impact. Besides, since Sweden entered the European Union about 10 years ago, the import of cement has increased gradually, and today the import of cement is about 18%. Thus, there will probably be an increased need to test and evaluate new compositions in the future. Resulting parameters can be applied both in the planning stage of a concrete casting as well as in the follow up procedure at construction site.

In order to model strength development, it is common to describe the strength growth at a reference concrete temperature together with the maturity function for the concrete in question.

There are two situations where it is important to estimate concrete strength development

- 1) Pre-calculations of temperature and strength development prior the casting of concrete.
- 2) Follow-up an in situ casting to translate measured concrete temperatures to estimated strength development.

For both situations the maturity function and strength development have to be known. In addition, to be able to calculate the concrete temperature, the first situation needs information concerning heat of hydration.

Application in situation 1) means pre-calculation of temperature and strength development in any specific point in a construction. This is essential during the planning stage to analyse choice of materials and measures to be able to fulfil demands concerning strength. Such analyses may comprise variation of concrete mix, casting sequence, framework stripping, insulation, cooling, heating etc.

Another application of situation 1) is when something unexpected has happened, where calculation with known boundary conditions may be a helpful tool to analyse consequences on site.

In situation 2) above, the temperature inside the concrete construction has to be measured. The application means estimation of strength based on known strength development and maturity function for the concrete in use.

The paper presented deals with a model for strength development based on laboratory tests at variable curing temperature for five concrete mixes and two types of cement.

2. AIMS AND PURPOSES

The aims and purposes in this paper are

- To define and motivate time periods concerning strength growth in concrete with respect to rational information on site affecting production behaviour.
- To analyse and develop a model for strength development in concrete including early age behaviour as well as strength reduction at elevated curing temperatures.

3. A BRIEF HISTORY OF THE MATURITY CONCEPT

It has been generally known since long that the temperature and moisture state in concrete plays an important role for the hardening process, and therefore also for the strength growth. A rational way to take into account variable temperature effects on strength growth is presented by diagrams for practical use in [1], although no models were established. During the planning stage of the Hoover dam [2] a more complex role of temperature on concrete hardening was observed. Higher strength growth at higher temperatures was confirmed at early ages, but for long-term strength a strength reduction at higher temperatures was seen in some of the tests. The latter phenomenon is today known as a cross over effect.

The temperature is fairly easy to measure and calculate, while moisture is hard to measure and calculate. A consequence is that the application for use in practice prefers to use only temperature as base for strength prediction. The first model analysing the single influence of the concrete temperature was presented in [3]. The author used a basic age index, defined as the cumulative area below the temperature-time curve down to a datum temperature as the fundamental parameter related to the strength growth. This opened a door for an inviting way of taking temperature and time into consideration analysing strength development at variable temperature. Tests on strength rate using steam curing [4] showed that initially steam cured cement paste showed accelerated strength growth for early ages, but also a drop in 28 day strength compared with air cured specimens. These observations confirmed the findings in [2]. In [5] it was stated that for early age concrete a datum temperature of -10°C worked sufficiently enough for curing at normal temperature variations, and this was established as the well-known Nurse-Saul maturity function formulated by

$$M = \sum_0^t (T - T_0) \cdot \Delta t \quad (1)$$

where M = maturity at time t ; T = concrete temperature; T_0 = datum temperature; t = time after mixing.

The Nurse-Saul maturity function was quickly adopted in the Scandinavian countries as a technique to estimate the concrete maturity and associated strength when casting in cold climate conditions [6, 7, 8, 9]. With $T_0 = -10^\circ\text{C}$ Eq. 1 in Sweden became known as the TT factor method (TT = temperature-time), and it has alternatively been expressed as Eq. 2 which opens the possibility to describe the equivalent time of maturity, see Eq. 3. The author in [6] confirmed that the use of $T_0 = -10^\circ\text{C}$ was satisfactory analysing several test series from the literature as well as on own tests. About the same datum temperature ($-11,7^\circ\text{C}$) was presented in [10].

$$\beta_T = \frac{T - T_0}{T_{ref} - T_0} \quad (2)$$

$$t_e = \int_0^t \beta_T \cdot dt \quad (3)$$

where β_T = temperature dependent rate factor, usually denoted maturity function;
 T_{ref} = reference concrete temperature; t_e = equivalent time of maturity.

In [5] it was shown that a strength reduction occurred if the steam curing temperature of 95°C was reached before seven hours after casting, i.e. the rate of hardening at very early ages seems to play an important role for the final strength. The findings in [11] were of importance for concrete casting in cold climate conditions, where the test results for curing temperatures about 6°C showed a compressive strength as high as or higher for equivalent age larger than 7 days compared with curing at room temperature. Shortly thereafter [12] cross over effects for curing temperatures between -4°C to 49°C were demonstrated, which again verifies the findings in [2], [5] and [11]. So, the twofold effects of the curing temperature on strength: that higher curing temperatures accelerate the hardening at early ages but might result in lower final strength, has been known at least since the 1950s. In [12] and [13] possible causes of the cross over effects are discussed, and the structure of the hydration products is assumed to be dependent on the curing temperature. This might explain the low final strength at high curing temperatures, and vice versa for low curing temperatures.

The importance of using the maturity concept at cold weather concreting was pinpointed by two collapses of concrete structure in U.S. with fatal consequences in the 1970s. These disasters started a number of investigations [14, 15], which resulted in the first versions of the standard ASTM C1074, and the current version is given in [16].

Until the mid 1970s the maturity function has been formulated empirically, but in the Scandinavian countries [17, 18] the temperature dependency was shown to work with respect to the chemically defined activation energy formulated by

$$\beta_T = \exp \left[\frac{E}{R} \cdot \left(\frac{1}{293} - \frac{1}{T + 273} \right) \right] \quad (4)$$

where E [J/mole] = apparent activation energy; R [J/mole K] = general gas constant = 8,314J/mole K; T [°C] = concrete temperature.

Unfortunately, the activation energy, E , was not always constant, which means that the so called Arrhenius equation is not used in a theoretically strict way. Nevertheless, the formulation according to Arrhenius equation is inviting, as the activation energy has a theoretical meaning in thermal activation of chemical reactions. An empirical expression for the apparent activation energy was introduced in [19] expressed as

$$\theta = \frac{E}{R} = \theta_{ref} \cdot \left(\frac{30}{T+10} \right)^{\kappa_3} \quad (5)$$

where θ [K]= “activation temperature”; θ_{ref} [K] and κ_3 [-] are empirically constants useable in most practical situations.

With the help of mercury intrusion and backscattered electron image analysis it was shown in [20] that the porosity increased with increased curing temperature at the same degree of hydration. It was also found in [21] that low curing temperatures gave a uniform distribution of hydration products, and elevated temperatures resulted in a coarser pore structure. Additionally, tests on one mortar mix showed that the maturity concept directly could be applied up to about 50% degree of hydration [22]. Above 50% degree of hydration, the tests indicate that the apparent activation energy also changes with the degree of hydration. This latter finding means that the hydration rate is decreased at higher degree of hydration, which might be designated a hydration retarding effect due to densification of the hydration products.

The “first model generation” completing the maturity concept with the cross over effect was established by separate adjustments of the strength growth by functions only dependent on the temperature without taking the retarding effect into account [23-27]. Later models [28-37] have used different techniques adding the retarding effect, either by adjusting the apparent activation energy by time or introducing separate retarding functions decreasing by time.

Another effect that retards the rate of hydration is drying, both external drying to the environment and self-desiccation at sealed conditions. The moisture effect is well known from laboratory tests [38] and observed in field tests [39], and this is taken care of by rules concerning moisture hardening in standards and specifications all over the world. Considering the drying effect separately is too difficult for most applications in practice, as the moisture state in a structure is rather complex to measure or calculate. The combined effect on hydration of temperature, moisture and retarding due to densification is possible to take into account for special applications, where the moisture plays a significant role, see for instance [40-41]. The maturity models only based on temperature might theoretically be denoted “temperature maturity models”, but this refined notation is usually not considered.

It is interesting to conclude that the maturity concept also is applicable for the stiffening during the time between initial and final set, see [42-44]. This means that a comprehensive maturity model also should include this very early stage of concrete hardening.

Most results from the literature concerning maturity and evaluation of apparent activation energy is shown for separate concrete mixes, but some attempts are presented where the

activation energy is estimated based on information concerning chemical and physical properties of the binder [45-46].

The maturity concept, as a method to follow up the strength growth in concrete structures, has been used for up to 50 years in several countries. When the concrete maturity properties are well known, the general conclusion is that the maturity concept is a good quality control tool for assessments of in-situ strength in concrete structures during hardening [47-48]. One consequence is that field cubes in Sweden have been replaced by temperature measurements on site since the beginning of the 1990s. In contrast to this, some countries in Europe still use field cubes and compression tests when estimating strength on site, probably due to “traditional” use of existing local standards and since long established practical procedures.

4. MODEL FOR STRENGTH DEVELOPMENT

4.1 Choice of time periods

It is important that different time periods are defined with respect to the behaviour on site, and that the periods can be defined from properties of concrete. Starting from casting, three periods connected to the treatment of concrete are here defined as

- I. Fresh concrete period
- II. Surface finishing period
- III. Hardening period

These three time periods are in line with what is used in [42, 43, 44], see Figure 1. Some preliminary tests have shown that the influence of the temperature might be different within these time periods, and the modelling presented below is structured to take this into account.

Here the first period is denoted “fresh” concrete as the contractor is able to place and vibrate the concrete without damaging the structure of the cement paste.

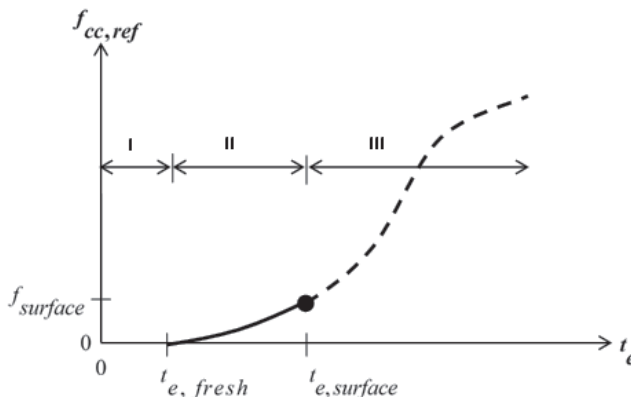


Figure 1 – Reference strength ($f_{cc,ref}$) as a function of equivalent time (t_e). Note that t_e may be calculated differently within each period, see further Eqs. 9, 11 and 14.

The second period in Figure 1 may approximately be regarded as the time between initial and final setting, which in practice means that the contractor is able to process the surface finishing within this period. The limits for the surface finishing period are usually defined by penetration resistance in cement paste [44] or mortar. Here, concrete strength is used to describe the surface finishing period by

$$f_{fresh} = 0 \text{MPa} \quad (6)$$

$$f_{surface} = 0,5 \text{MPa} \quad (7)$$

where $f_{fresh} = 0 \text{MPa}$ from casting to the equivalent time at the end of the fresh concrete period, $t_{e,fresh}$, when the concrete mix no longer is workable; $f_{surface}$ = the strength value when the surface no longer can be processed, which occurs at the equivalent time, $t_{e,surface}$, at the end of the surface finishing period. The notation strength is here used for compression tests performed on 100mm or 150mm cubes.

4.2 Strength development during the fresh concrete period

The parameter $t_{e,fresh}$ may be taken as the time when the concrete surface is walkable with a permanent imprint of about 5–10mm [49]. The strength growth and the equivalent time during the fresh concrete period are described by

$$I : f_{cc,ref} = 0 \quad \text{for} \quad 0 \leq t \leq t_l \quad (8)$$

and

$$I : t_e = \beta_{\Delta} \cdot \int_0^t \beta_T \cdot dt + \Delta t_{e0} \quad \text{for} \quad 0 \leq t \leq t_l \quad (9)$$

where $f_{cc,ref} [\text{MPa}]$ = strength growth at reference conditions as a function of equivalent time, $t_e [\text{h}]$; $t [\text{h}]$ is real time; $t_l [\text{h}]$ is the time when $t_e = t_{e,fresh}$ using Eq. 9 with $\theta_{ref} = \theta_{ref,l}$ and $\kappa_3 = \kappa_{3,l}$ for calculation of β_T , see Eqs. 4-5; and $\beta_{\Delta} = \beta_{\Delta,l}$. The parameters $t_{e,fresh} [\text{h}]$, $\theta_{ref,l} [\text{K}]$, $\kappa_{3,l} [-]$, $\beta_{\Delta,l} [-]$ and $\Delta t_{e0} [\text{h}]$ are evaluated from fitting of test data.

4.3 Strength development during the surface finishing period

The strength $f_{surface}$ is here proposed to be 0,5MPa. In practice it has been shown that the actual surface finishing normally can be performed between the strength of about 0,1MPa to 0,4MPa [50] which is within the limits defined by Eqs. 6 and 7. Exact limits for different kinds of surface finishing treatments must be tested separately for each mix. The strength growth and the equivalent time during the surface finishing period are described by

$$II : f_{cc,ref} = f_{surface} \cdot \left(\frac{t_e - t_{e,fresh}}{t_{e,surface} - t_{e,fresh}} \right)^{n_{surface}} \quad \text{for} \quad t_I < t \leq t_{II} \quad (10)$$

with

$$II : t_e = t_{e,fresh} + \beta_{\Delta} \cdot \int_{t_I}^t \beta_T \cdot dt \quad \text{for} \quad t_I < t \leq t_{II} \quad (11)$$

where $f_{cc,ref}$ [MPa] = strength growth at reference conditions as a function of equivalent time, t_e [h]; t_{II} [h] is the time when $t_e = t_{e,surface}$ using Eq. 11 with $\theta_{ref} = \theta_{ref,II}$ and $\kappa_3 = \kappa_{3,II}$ for calculation of β_T , see Eqs. 4-5; and $\beta_{\Delta} = \beta_{\Delta,II}$. The parameters $n_{surface}$ [-], $t_{e,surface}$ [h], $\theta_{ref,II}$ [K], $\kappa_{3,II}$ [-] and $\beta_{\Delta,II}$ [-] are evaluated from fitting of test data.

4.4 Tendency curve during the concrete hardening period

The strength growth according to Eurocode 2 [51] is expressed by

$$f_{cc,ref} = f_{cc,28d} \cdot \exp \left\{ s \left[1 - \left(\frac{672}{t} \right)^{1/2} \right] \right\} \quad (12)$$

Where $f_{cc,28d}$ [MPa] = 28 days compressive strength for reference conditions; s [-] is a coefficient which depends on the type of cement; and t [h] is the time for mean temperature of 20°C and moist curing.

From the basic formulation in Eq. 12, the strength growth during the hardening period (III) is here modified as

$$III : f_{cc,ref} = f_{cc,28d} \cdot \exp \left\{ s \left[1 - \left(\frac{672 - t^*}{t_e - t^*} \right)^{n_{cc,28d}} \right] \right\} \quad \text{for} \quad t > t_{II} \quad (13)$$

with

$$III : t_e = t_{e,surface} + \beta_{\Delta} \cdot \int_{t_{II}}^t \beta_T \cdot dt \quad \text{for} \quad t > t_{II} \quad (14)$$

where $f_{cc,ref}$ [MPa] = strength growth at reference conditions as a function of equivalent time, t_e [h]; t_{II} [h] is the time when $t_e = t_{e,surface}$, see Eq. 11. Application of Eq. 13 means that Eq. 14 shall be used with $\theta_{ref} = \theta_{ref,III}$ and $\kappa_3 = \kappa_{3,III}$ for calculation of β_T , see Eqs. 4-5, and $\beta_{\Delta} = \beta_{\Delta,III}$. The parameters $f_{cc,28d}$ [MPa], s [-], $n_{cc,28d}$ [-], $\theta_{ref,III}$ [K], $\kappa_{3,III}$ [-] and $\beta_{\Delta,III}$ [-] are evaluated from fitting of test data. t^* [h] is introduced to fit the data point $(t_{e,surface}, f_{surface})$, which means

that the end point of time period II has to be the same as the start point of time period III, see Figure 1. The numerical value of t^* has no physical meaning and is calculated by

$$\begin{aligned}
 &\text{let} && f_{\text{surface}} = f_{cc,ref} \left(t_{e,surface} \right) \\
 &\text{calculate using Eq.13} && \delta_c = \left(1 - \ln \frac{f_{\text{surface}}}{f_{cc,28d}} \cdot \frac{1}{s} \right)^{1/n_{cc,28d}} \quad (15) \\
 &\text{and finally} && t^* = \frac{672 - \delta_c \cdot t_{e,surface}}{1 - \delta_c}
 \end{aligned}$$

When evaluating a specific recipe for the first time the parameters $\beta_{\Delta,j} [-]$ $\{j=I, II, III\}$ are usually set = 1, and parameter Δt_{e0} is usually set = 0. Then, if only the type of admixture is changed, it might be possible only to introduce $\beta_{\Delta,j} \neq 1$ and/or $\Delta t_{e0} \neq 0$ as additional parameters to existing model data for a basic recipe.

4.5 Strength reduction

The typical behaviour when cross over effects occur is shown in Figure 2. The notation cross over originates from plotting linear strength as a function of real time, see left part of Figure 2. When time is transformed to equivalent time it is possible to use the term strength reduction for temperatures above a chosen reference temperature, here 20°C, see right part of Figure 2. The strength for temperatures below reference temperature also shows a cross over effect (or strength gain), but this part is here ignored and might be regarded as an extra margin.

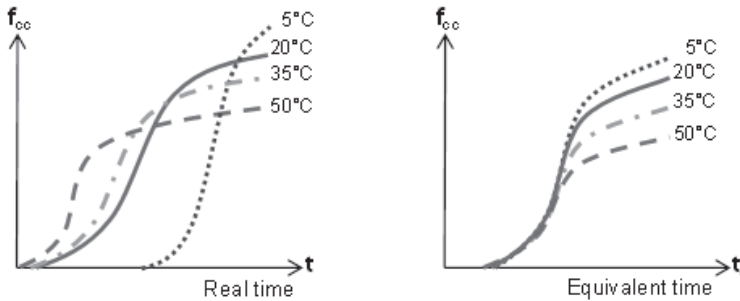


Figure 2 – Typically strength results for specimens cured between 5°C and 50°C, at left plotted in real time and to the right in equivalent time.

The strength reduction due to elevated hardening temperatures is only calculated for the hardening period (III) by

$$f_{cc} = f_{cc,ref} - \gamma_{drop} \cdot \Delta_{drop,28d}^{\max} \cdot f_{cc,28d} \quad \text{for} \quad t > t_{II} \quad (16)$$

where $\Delta_{drop,28d}^{\max} [-]$ = maximum strength reduction at $t_e = 672\text{h}$; $\gamma_{drop} \{0,1\}$ is the factor taking into account the temperature effect on strength reduction.

The technique to describe the reduction in strength according to Eq. 16 is here characterized by the following observations

- 1) The drop in strength starts at some minimum temperature, reflected by γ_{Temp} (Eq. 20).
- 2) Elevated temperatures influence the strength drop after a certain time, reflected by γ_{time} (Eq. 21).
- 3) The retarding effect at later ages [22] is here modelled by the “relative” rate of reaction ($d\alpha^* / dt_e$, see Eqs. 22 and 23).

These three phenomena can be described by the following material related empirical model

$$\gamma_{drop} = \frac{\delta_{drop}}{\delta_{ref}} \quad (17)$$

with

$$\delta_{drop} = \int_0^{t_e} \gamma_{Temp} \cdot \gamma_{time} \cdot \frac{d\alpha^*}{dt_e} \quad (18)$$

and

$$\delta_{ref} = \int_0^{672h} \gamma_{time} \cdot \frac{d\alpha^*}{dt_e} \cdot dt_e \quad (19)$$

The functions reflecting temperature and time effects, γ_{Temp} and γ_{time} , see Eqs. 20 and 21, are chosen to be exponential formulas, which are inviting to use within a certain range as they are within the interval $\{0,1\}$. This gives a robust type of modelling, and they can easily be extended to a broader range, if such test data are added afterwards.

$$\gamma_{Temp} = \exp\left(-\left[\frac{T}{Temp_D}\right]^{-\kappa_{Temp}}\right) \quad (20)$$

$$\gamma_{Time} = \exp\left(-\left[\frac{t_e}{time_D}\right]^{-\kappa_{time}}\right) \quad (21)$$

Where $Temp_D$ [°C]; $time_D$ [h]; κ_{Temp} [-] and κ_{time} [-] together with $\Delta_{drop,28d}^{\max}$ are evaluated by fitting against test data where strength reduction has occurred.

The hydration rate is described in Eq. 22 from [52]. The derivative with respect to the temperature equivalent maturity age is presented in Eq. 23.

$$\alpha^* = \exp\left(-\left[\ln\left(1 + \frac{t_e}{t_1}\right)\right]^{-\kappa_1}\right) \quad (22)$$

$$\frac{d\alpha^*}{dt_e} = \frac{\alpha^*}{t_1 + t_e} \cdot \kappa_1 \cdot \left[\ln\left(1 + \frac{t_e}{t_1}\right)\right]^{-(\kappa_1 + 1)} \quad (23)$$

where α^* [-] is the “relative” degree of hydration; t_1 [h] and κ_1 [-] are parameters decided from calorimetric tests. The notation relative means that $\alpha^* = 1$ reflects the ultimate heat of hydration (corresponding to ultimate degree of reaction) in relation to the individual final value for a tested concrete.

The use of Eqs. 22 and 23 is based on the existence of test data from calorimetric measurements, which at Luleå University of Technology is a standard behaviour testing early age concrete. Eq. 23 starts and stops at $d\alpha^*/dt_e = 0$. Somewhere in between, it has a maximum value mainly depending on the type of cement and the w/c ratio. Hereby, the rate of hydration depending on cement composition and w/c ratio is taken into account in a material related way.

5. TEST RESULTS AND EVALUATION ACCORDING TO PROPOSED MODEL

5.1 Test setup

Strength developments on 100mm cubes cured in water baths of different temperature levels, 20°C, 35°C and 50°C respectively, have been performed [52]. All cubes for each recipe originate from one physical mix to avoid variations due to differences in mix conditions [53]. The concrete temperatures are registered and the individual temperature-time behaviour is considered in the evaluation. The main test and evaluation methodology is given in [53]. The cements used are Anlåggningscement (AnlC) and Byggcement (ByggC), and the cement compositions are presented in Table 1. Totally five concrete recipes have been tested, see main constituents in Table 2.

Table 1 – Oxides, clinker minerals and specific surface of tested cements. ByggC is of type CEM III/A-LL 42,5 R containing about 13% LL, and AnlC is of type CEM I 42,5 N MH/SR/LA (CEMENTA AB).

Cement	Oxides [%]					Clinker minerals [%]				Specific surface [m ² /kg]
	CaO	SiO ₂	Al ₂ O ₃	Fe ₂ O ₃	SO ₃	C ₃ S	C ₂ S	C ₃ A	C ₄ AF	
ByggC	61,4	18,7	3,9	2,8	3,5	54,1	8,9	5,1	7,8	460
AnlC	64,1	22,4	3,7	4,5	2,4	48,0	28,0	2,1	13,8	316

Table 2 – Main constituents of tested concretes.

Recipe	Cement	Cement content [kg/m ³]	w/c
1	ByggC	285	0,70
2	ByggC	360	0,55
3	ByggC	470	0,38
4	AnlC	340	0,55
5	AnlC	455	0,38

5.2 Evaluation procedure

The evaluation procedure for the model outlined here is aimed to be performed in three steps, one separate evaluation for each time period (I, II and III) in Figure 1. A possible “complete sequence of evaluation” behaviour is presented below.

If tests have been performed concerning time period I the evaluation can be done as follows

- Ia) For an individual, basic recipe $\theta_{ref,I}$ and $\kappa_{3,I}$, see Eq. 5, and $t_{e,fresh}$, see the denotation list in connection to Eq. 9, are determined for $\Delta t_{e0} = 0$ and $\beta_{\Delta,I} = 1$.
- Ib) When a basic evaluation exists, a possibility is to use $\Delta t_{e0} \neq 0$ and $\beta_{\Delta,I} \neq 1$, when effects from other types of admixtures are analysed.

If tests have been performed in time period II the evaluation can be done as follows

- IIa) For an individual, basic recipe $\theta_{ref,II}$ and $\kappa_{3,II}$, and $t_{e,surface}$, see the denotation list in connection to Eq. 11, are determined for $\beta_{\Delta,II} = 1$.
- IIb) When a basic evaluation exists, a possibility is to use $\beta_{\Delta,II} \neq 1$, when effects from other types of admixtures are analysed.

If tests have been performed in time period III the evaluation can be done as follows

- IIIa) For an individual, basic recipe $\theta_{ref,III}$, $\kappa_{3,III}$, s , $n_{cc,28d}$ and $f_{cc,28d}$, are determined for $\beta_{\Delta,III} = 1$, see Eqs. 13-14. The parameter t^* in Eq. 13 has no physical meaning and is not an independent fitting parameter. t^* is calculated separately according to Eq. 15.
- IIIb) When a basic evaluation exists, a possibility is to use $\beta_{\Delta,III} \neq 1$, when effects from other types of admixtures are analysed.

A complete evaluation sequence is only possible when test data exist within all three time periods. Many other alternatives are possible in practice.

Here, only test data exist within the hardening period (III), and the consequence is that the strength development can only be estimated with high credibility within time period III. The parameters for time periods I and II are here chosen as follows

$$\theta_{ref,I} = \theta_{ref,II} = \theta_{ref,III} = \theta_{ref} \quad \text{and} \quad \kappa_{3,I} = \kappa_{3,II} = \kappa_{3,III} = \kappa_3 \quad (24)$$

The meaning of Eq. 24 is that the maturity function has only two fitting parameters (θ_{ref} , κ_3) formally valid for all time periods.

Besides, here the evaluations are regarded as individual basic recipes, which is described by

$$\Delta t_{e0} = 0 \quad \text{and} \quad \beta_{\Delta,I} = \beta_{\Delta,II} = \beta_{\Delta,III} = \beta_{\Delta} = 1 \quad (25)$$

The meaning of Eq. 25 is that the parameters Δt_{e0} and $\beta_{\Delta,j}$ are excluded from the evaluation sequence.

The remaining parameters for time periods I and II are here set to reasonable “theoretical” values chosen to be the same for all recipes by

$$t_{e,fresh} = 3\text{h}, \quad t_{e,surface} = 5\text{h} \quad \text{and} \quad n_{surface} = 3 \quad (26)$$

The parameters in Eq. 26 are probably functions of the water-cement ratio (w/c), but such test data are not available for the concretes analysed here.

The remaining parameters for the strength reference curve for each recipe ($f_{cc,28d}$, s and $n_{cc,28d}$), and the corresponding maturity functions (θ_{ref} , κ_3) have to be determined by fitting procedure by regression analysis using the so called least square method. With this procedure it was recognized that $n_{cc,28d} \approx 0,5$, $\theta_{ref} \approx 2750\text{K}$ and $\kappa_3 \approx 0$ for all analysed recipes. Therefore, these three parameters were fixed to these values, see Table 3. So, the remaining fitting parameters for each recipe analysed here are $f_{cc,28d}$ and s , respectively. The final resulting parameters are shown in Table 3 and the corresponding reference curves are presented in Figure 3 and Figure 4 as the plotted curves denoted f_cc_ref.

In Figure 3 the blue squares, the green triangles and the red rotated squares are test results at the temperature levels shown in the legend. The larger green square is the evaluated 28 days strength, $f_{cc,28d}$ in Eq. 13, and the larger red square represents the maximum possible strength reduction for evaluated temperatures, $\Delta_{drop,28d}^{\max}$ in Eq. 16. The continuous line marked f_cc_ref in Figure 3 means the reference curve at $T \equiv 20^\circ\text{C}$, see Eq. 13, and the three lines marked T20 C, T35 C and T50 C are calculated strength developments based on measured temperatures for each temperature level.

As can be seen in Figures 3 and 4 the different temperature levels are measured up to equivalent age of about 200h. The reason is that the primarily interest is to create information to predict or estimate strength growth at variable temperature the first days after casting. Hereby, decisions can be taken on site with respect to time and need of measures for frost protection, time of post tensioning and time of form striking. In addition, we are always measuring and evaluating the 28-day-strength (28d = 672h), which is a “key” parameter in concrete design.

Basically, the same notations are used in Figure 4 as in Figure 3, but, without strength reductions.

So far the reference curve is evaluated, and the cross over effect or strength reduction is ignored. It is obvious in our test series that concretes with ByggC show strength reduction, but cement AnIC does not show any significant strength drop. Earlier tests on strength growth at Luleå University of Technology have also shown strength reduction using ByggC [54] but not when

using AnlC [55]. AnlC is a moderate heat cement, formally an OPC with reduced production of hydration heat. AnlC is aimed for use in civil engineering structures and ByggC is aimed for more general castings. Civil engineering structures means structures exposed to severe environmental conditions, for example bridges, tunnels, harbours, water towers etc. In Sweden the production of AnlC is about 16% of the total cement production.

Table 3 – Model parameters received for maturity function and reference strength by using regression analysis with Eqs. 4 - 6.

w/c	Recipe	$f_{cc,28d}$ [MPa]	S [-]	$n_{cc,28d}$ [-]	$t_{e,fresh}$ [h]	$t_{e,surface}$ [h]	$f_{surface}$ [MPa]	$n_{surface}$ [-]	θ_{ref} [K]	κ_3 [-]	Δt_{e0} [h]	β_{Δ} [-]
0,70	1	33,2	0,190	0,5	3	5	0,5	3	2750	0	0	1
0,55	2	49,6	0,163	0,5	3	5	0,5	3	2750	0	0	1
0,38	3	79,9	0,122	0,5	3	5	0,5	3	2750	0	0	1
0,55	4	49,4	0,350	0,5	3	5	0,5	3	2750	0	0	1
0,38	5	83,8	0,237	0,5	3	5	0,5	3	2750	0	0	1

5.3 Strength reduction

The modelling of strength reduction is described in Eqs. 16 – 23. Fitting using the least square method resulted in individual parameters for recipe 1 – 3, see Table 4. According to the test results in Figure 4 the use of cement type AnlC did not seem to show any significant strength reduction, which in Table 4 is shown by $\Delta_{drop,28d}^{\max} = 0$.

Table 4 – Model parameters for strength reduction and relative degree of hydration.

Recipe	Strength reduction					Degree of hydration	
	$\Delta_{drop,28d}^{\max}$ [-]	$Temp_D$ [°C]	κ_{Temp} [-]	$time_D$ [h]	κ_{time} [-]	t_1 [h]	κ_1 [-]
1	0,41	39	7	25	2,00	8,57	1,31
2	0,45	38	5	35	1,75	6,52	2,18
3	0,48	36	3	40	1,50	5,19	3,25
4	0	-	-	-	-	7,56	1,80
5	0	-	-	-	-	19,0	0,62

The strength reduction functions, γ_{Temp} and γ_{time} (Eqs. 20 and 21), for the concretes using ByggC are dependent on the w/c ratio. Also the value of $\Delta_{drop,28d}^{\max}$ is higher for lower w/c ratios, see Table 4. The observed dependency of the w/c ratio indicates that these functions reflect differences in the pore structure in the paste matrix.

From Figure 5 it is seen that the relative rate of hydration is strongly dependent on the w/c ratio for concretes using ByggC, which probably contributes to the higher strength reduction for lower w/c ratios, see Figure 3. Figure 5 also shows that the relative rate of hydration using AnlC is dependent on the w/c ratio, but the values are lower than using ByggC. No significant strength reduction was observed using AnlC in the tests, see Figure 4, which probably is a consequence of both cement composition and a lower value of specific surface, see Table 1. Although, in Figure 4, there is a tendency that the lower w/c ratio (0,38) indicates a strength reduction from about 100h equivalent time. But, with no information at later ages, strength reduction for AnlC is not regarded here. To clarify this, further tests are needed.

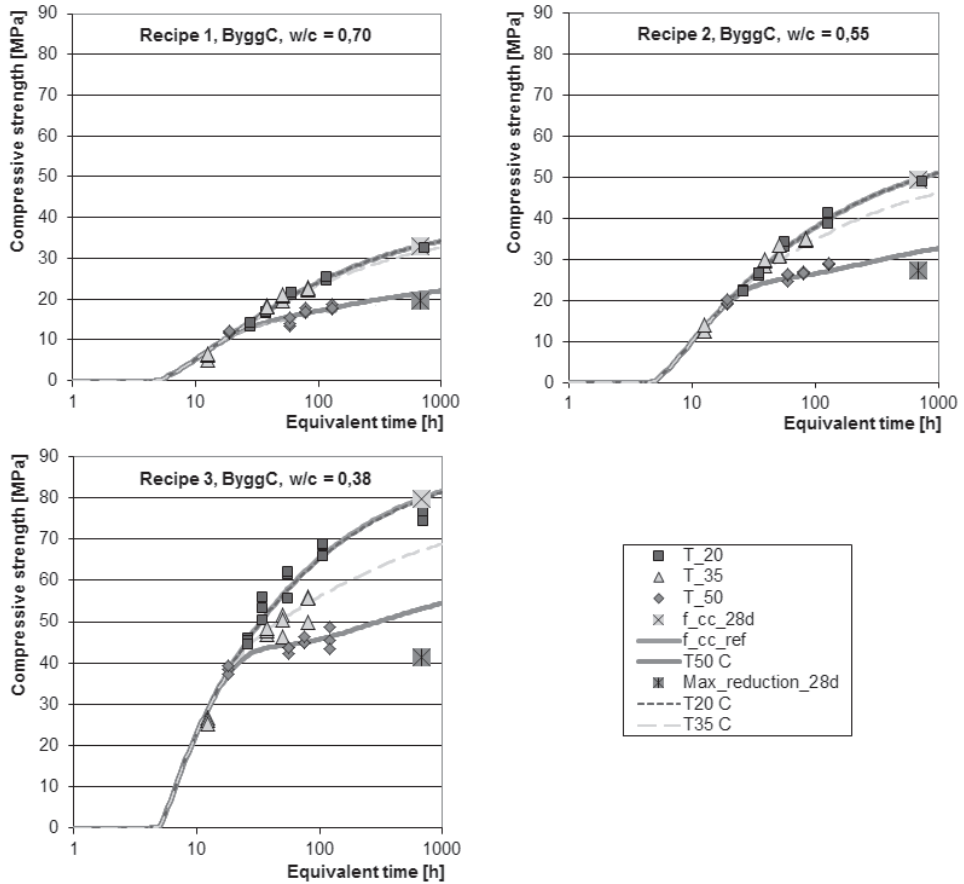


Figure 3 – Reference and strength reduction curves for all ByggC recipes.

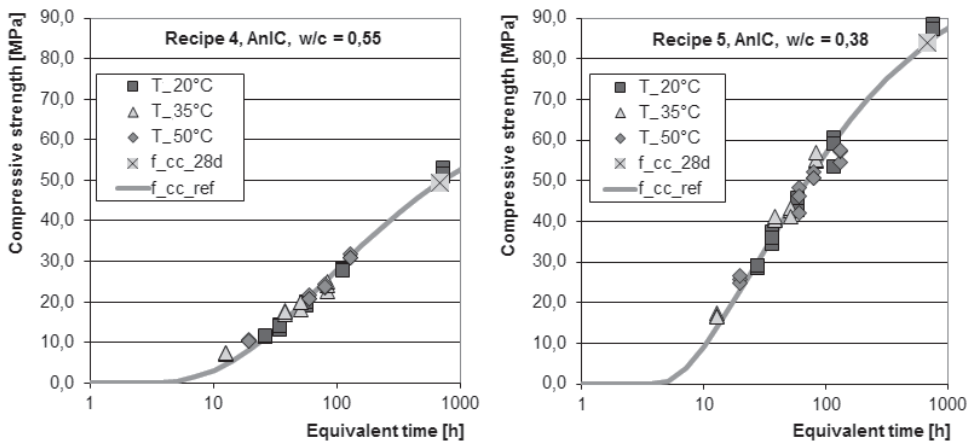


Figure 4 – Reference strength curves for recipe 4 – 5, AnlC.

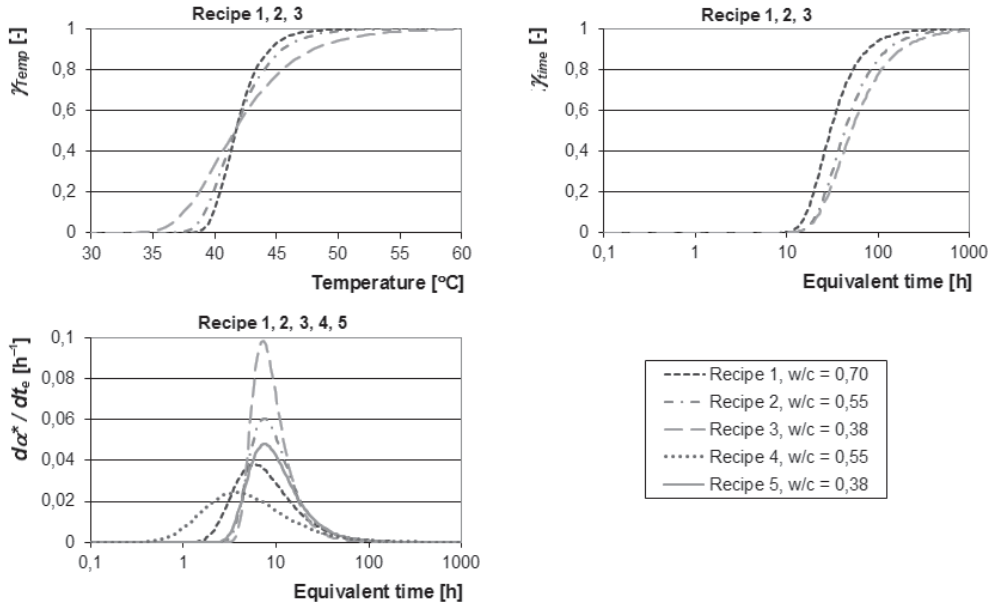


Figure 5 – Functions used in modelling strength reduction for analysed concretes, recipe 1 – 5. Numerical values for use of Eqs. 20, 21 and 23 are given in Table 4.

6. SUMMARY AND CONCLUSIONS

- The defined time periods for different models of strength growth are strongly adapted to the contractors behaviour on site, denoted I) Fresh concrete period, II) Surface finishing period and III) Hardening period. By introduction of individual strength growth and maturity functions within each time period, tests and modelling may be treated separately within the periods. This opens a possibility to study and analyse the period that is of most interest for a specific application. In the most comprehensive modelling all three periods may be combined to a complete sequence. In the paper it is shown that if tests results only are available during the time period III, high credibility can be achieved with reasonable assumptions also within time periods I and II. In summary, the presented model with three time periods is shown to be very flexible with respect to available test data.
- The strength development is modelled separately within time period II and III. Within time period III the model is based on an established formula in Eurocode 2, and modifications are introduced with respect to continuation in strength at the end of time period II. This modification is straight forward and simple to apply for the strength at reference conditions, which here means curing at 20°C. For curing at elevated temperatures, a robust model has been developed taking into account effects of time, temperature and rate of reaction. These three areas are modelled separately which seems to be appropriate with respect to observed strength developments. In the paper the model has been applied successfully for five concrete mixes. The tests were performed with two types of cements, of which one showed strength reduction.

ACKNOWLEDGEMENTS

The authors of the paper acknowledge The Swedish Research Council Formas, Cementa AB and Betongindustri AB. The laboratory tests have been performed in cooperation with personnel from Complab at Luleå University of Technology, which is hereby acknowledged.

REFERENCES

1. McDaniel, A.B., "Influence of Temperature on the Strength of Concrete," Bulletin No. 81, University of Illinois, Engineering Experiment Station, July 1915. pp. 24.
2. Davis, R.E., Carlson, R.W., Troxell, G.E., and Kelly, J.W., "Cement Investigations for the Hoover Dam," Journal of the American Concrete Institute - Proceedings at the 29th annual Convention, Chicago, February 21-23 1933, pp. 413-431.
3. McIntosh, J.D., "Electrical Curing of Concrete," *Magazine of Concrete Research*, Vol. 1, No. 1, January 1949, pp. 21-28.
4. Nurse, R.W., "Steam Curing of Concrete," *Magazine of Concrete Research*, Vol. 1, No 2. June 1949, pp 79-88.
5. Saul A.G.A., "Principals Underlying the Steam Curing of Concrete at Atmospheric Pressure," *Magazine of Concrete Research*," Vol. 2, No. 6, March 1951, pp. 127-140.
6. Bergström, S.G., "Curing Temperature, Age and Strength of Concrete," *Magazine of concrete research*, Vol. 5, No 14, December 1953, pp. 61-66.
7. Rastrup, E., "Heat of Hydration in Concrete," *Magazine of Concrete Research*, Vol. 6, No. 17, September 1954, pp 79-92.
8. Nykänen, A., "Hardening of Concrete at Different Temperatures, Especially Below the Freezing Point," Proceedings, RILEM Symposium on Winter Concreting – Theory and practice, Session BII, Danish Institute for Building Research, Copenhagen, Denmark, 1956.
9. Jonasson, J-E., "Early Strength Growth in Concrete - Preliminary Test Results Concerning Hardening at Elevated Temperatures," Proceedings, 3rd International RILEM Symposium on Winter Concreteing, Espoo, Finland, 1985, pp. 249-254.
10. Plowman, J. M., 1956, "Maturity and the Strength of Concrete," *Magazine of Concrete Research*, Vol. 8, No. 22, March 1956, pp. 13-22
11. McIntosh, J. D., 1956, "The Effects of Low-temperature Curing on the Compressive Strength of Concrete," Proceedings, RILEM Symposium on Winter Concreting – Theory and practice, Session BII, Danish Institute for Building Research, Copenhagen, Denmark, 1956.
12. Klieger, P., "Effects of Mixing and Curing Temperature on Concrete Strength," *Journal of the American Concrete Institute* Vol. 54, No. 12, June 1958, pp. 1063-1081.
13. Verbeck, G. J., and Helmuth, R.H., 1968, "Structure and Physical Properties of Cement Paste," Proceedings, 5th International Symposium on the Chemistry of Cement, Part III, Tokyo, Japan, 1968, 1-32.
14. Leyendecker, E.V., and Fattal, S.G. "Investigation of the Skyline Plaza Collapse in Fairfax County, Virginia," Center for Building Technology, Institute for Applied Technology, National Bureau of Standards, Washington D.C. 20234, 1977, pp. 90.
15. Lew, H.S., Fattal, S.G., Shaver, J.R., Reinhold, T.A., and Hunt, B.J. "Investigation of Construction Failure of Reinforced Concrete Cooling Tower at Willow Island, West Virginia," Center for Building Technology, National Engineering Laboratory, National Bureau of Standards, Washington, D.C. 20234, 1977, pp. 195.

16. ASTM Standard C1074 – 11, “Standard Practice for Estimating Concrete Strength by the Maturity Method,” ASTM International, West Conshohocken, PA, 2011. www.astm.org.
17. Freiesleben Hansen, P., and Pedersen, E.J., “Maturity Computer for Controlled Curing and Hardening of Concrete,” *Nordisk Betong*, Vol. 1, No. 19, 1977, pp. 21-25.
18. Byfors, J., “Plain Concrete at Early Ages,” Swedish Cement and Concrete Research Institute, Report Fo/Research 3:80, Stockholm 1980, 345 pp.
19. Jonasson, J-E., “Slipform Construction – Calculations for Assessing Protection Against Early Freezing,” Swedish Cement and Concrete Research Institute, Report Fo/Research 84:4, Stockholm 1984, 70 pp.
20. Kjellsen, K.O., Detwiler, R.J., and Gjrv, O.E., “Pore Structure of Plain Cement Pastes Hydrated at Different Temperatures,” *Cement and Concrete Research*, Vol. 20, No. 6, November 1990, pp. 927-933.
21. Kjellsen, K.O., Detwiler, R.J., and Gjrv, O.E., “Development of Microstructures in Plain Cement Pastes Hydrated at Different Temperatures,” *Cement and Concrete Research*, Vol. 21, No. 1, January 1991, pp. 179-189.
22. Kjellsen, K.O., and Detwiler, R. J., “Reaction-Kinetics of Portland-Cement Mortars Hydrated at Different Temperatures,” *Cement and Concrete Research* Vol. 22, No. 1, January 1992, pp. 112-120.
23. Emborg, M., “Thermal Stresses in Concrete Structures at Early Ages,” Doctoral thesis 1989:73D, Luleå University of Technology, Luleå 1989.
24. Tank, R.C., and Carino, N.J., “Rate Constant Functions for Strength Development of Concrete,” *ACI Materials Journal*, Vol. 88, No. 1, January 1991, pp. 74-83.
25. Jonasson, J-E., “Modelling of Temperature, Moisture and Stresses in Young Concrete,” Doctoral thesis 1994:153D, Luleå University of Technology, Luleå 1994.
26. Carino, N.J., and Lew, H.S., "The Maturity Method: From Theory to Application." Proceedings, ASCE Conference on Structure Congress & Exposition, Washington, D.C, 2001.
27. Brooks, A.G., Schindler, A.K., and Barnes, R.W., “Maturity Method Evaluated for Various Cementitious Materials,” *Journal of Materials in Civil Engineering*, Vol. 19, No. 12, December 2007, pp. 1017-1025.
28. Chengju, G., “Maturity of Concrete – Method for Predicting Early-Stage Strength,” *ACI Materials Journal*, Vol. 86, No. 4, July 1989, pp. 341-353.
29. Kjellsen, K.O., and Detwiler, R.J., “Later-Age Strength Prediction by a Modified Maturity Model,” *ACI Materials Journal*, Vol. 90, No. 3, May 1993, pp. 220-227.
30. Chanvillard, G., D'Aloia, L., “Strength Estimation at Early Ages: Modification of the Method of Equivalent Age,” *ACI Materials Journal*, Vol. 94, No. 6, November 1997, pp. 520-530.
31. Kim, J.K., Han, S.H., and Lee K.M., “Estimation of Compressive Strength by a New Apparent Activation Energy Function,” *Cement and Concrete Research*, Vol. 31, No. 2, February 2001, pp. 217-225.
32. Pane, I., and Hansen, W., “Concrete Hydration and Mechanical Properties Under Nonisothermal Conditions,” *ACI Materials Journal*, Vol. 99, No. 6, November 2002, pp. 534-542.
33. Kim, J.K., Han, S.H., and Song, Y.C., “Effect of Temperature and Aging on the Mechanical Properties of Concrete - Part I. Experimental Results,” *Cement and Concrete Research*, Vol. 32, No. 7, July 2002, pp. 1087-1094.
34. Kim, J.K., Han, S. H., Park, S.K., “Effect of Temperature and Aging on the Mechanical Properties of Concrete - Part II. Prediction Model,” *Cement and Concrete Research*, Vol. 32, No. 7, July 2002, pp. 1095-1100.

35. Yi, S.T., Moon, Y.H., and Kim, J.K., "Long-Term Strength Prediction of Concrete with Curing Temperature," *Cement and Concrete Research*, Vol. 35, No. 10, October 2005, pp. 1961-1969.
36. Kim, T., and Rens, K.L., "Concrete Maturity Method Using Variable Temperature Curing for Normal and High-Strength Concrete I: Experimental Study," *Journal of Materials in Civil Engineering*, Vol. 20, No. 12, December 2008, pp. 727-734.
37. Kim, T., and Rens, K.L., "Concrete Maturity Method Using Variable Temperature Curing for Normal-Strength Concrete Mixes. II: Theoretical Study," *Journal of Materials in Civil Engineering*, Vol. 20, No. 12, December 2008, pp. 735-741.
38. Powers, T.C., "A Discussion of Cement Hydration in Relation to the Curing of Concrete," Research Laboratories of the Portland Cement Association, Bulletin 25, Chicago, 1948, pp. 178-188.
39. Radlinski, M., Olek, J., and Nantung, T., "Influence of Curing Conditions on Strength Development and Strength Predictive Capability of Maturity Method," Laboratory and Field-Made Ternary Concretes. Transportation Research Record, Vol. 2080, Transportation Research Board of the National Academies, Washington D.C., 2008, pp. 49-58.
40. Norling Mjörnell, K., "Moisture Conditions in High Performance Concrete: Mathematical Modeling and Measurements," Doctoral thesis, Chalmers University of Technology, Gothenburg 1997.
41. Jonasson, J-E., Mjörnell, K. and Carlsson, C.A., "Modeling of Simultaneous Temperature and Moisture transportation in modern concrete," Proceedings, International RILEM Symposium on Concrete Modeling - ConMod '08, Delft, Netherlands, 2008, pp. 665-672.
42. Pinto, R.C.A., and Hover, K.C., "Application of Maturity Approach to Setting Times," *ACI Materials Journal*, Vol. 96, No. 6, November 1999, pp. 686-691.
43. Schindler, A.K., "Prediction of Concrete Setting," Proceedings, International RILEM Symposium on Advances in Concrete through Science and Engineering, Evanston, Illinois, March 2004.
44. Garcia, A., Castro-Fresno, D., and Polanco, J.A., "Maturity Approach Applied to Concrete by means of Vicat Tests," *ACI Materials Journal*, Vol. 105, No. 5, September 2008, pp. 445-450.
45. Schindler, A.K., "Effect of Temperature on Hydration of Cementitious Materials," *ACI Materials Journal*, Vol. 101, No. 1, January 2004, pp. 72-81.
46. Riding, K.A., Poole, J.L., Folliard, K.J., Juenger, M.C.G., and Schindler, A.K., "New Model for Estimating Apparent Activation Energy of Cementitious Systems," *ACI Materials Journal*, Vol. 108, No. 5, September 2011, pp. 550-560.
47. Myers, J.J., "The Use of the Maturity Method as a Quality Control Tool for High-Performance Concrete Bridge Decks," Proceedings, PCI/FHWA/FIB International Symposium on High Performance Concrete, L.S. Johal, Ed., Precast/Prestressed Institute, Chicago, 2000, pp. 316-330.
48. Bagheri-Zadeh, S.H., Kim, H., Hounsell, S., Wood, C.R., Soleymani, H., and King, M., "Field Study of Concrete Maturity Methodology in Cold Weather," *Journal of Construction Engineering and Management-ASCE*, Vol. 133, No. 11, November 2007, pp. 827-835.
49. Concrete Handbook, "Workmanship: Design and Construction," Svensk Byggtjänst and Cementa AB, 2nd Ed, 1992, pp. 837. (In Swedish).
50. Petersson, Ö., and Johansson, A., "Controlling Trowelling Hardness," Technical Report, Cement and Concrete institute, 1991, pp. 76. (In Swedish).
51. EN 1992-1-1:2004, "Eurocode 2: Design of Concrete Structures – Part 1-1:General Rules and Rules for Buildings," Brussels, Belgium 2004

52. Jonasson, J-E., and Fjellström, P., "Measurements and Modeling of Strength and Heat Development in Concrete with Swedish Cements," Technical report, Luleå University of Technology, Luleå 2011, pp. 30. (in Swedish).
53. Ekerfors, K., "Maturity Development in Young Concrete, Temperature Sensitivity, Strength and Heat Development," *Licentiate Thesis 1995:34*, Luleå University of Technology, Luleå 1995. (in Swedish).
54. Hedlund, H., and Jonasson, J-E., "Heat and Maturity Development for Portland-Lime Cement," Technical report 1999:13, Luleå University of Technology, Luleå 1999, pp. 34. (in Swedish).
55. Hedlund, H., "Hardening Concrete - Measurements and Evaluation of Non-elastic Deformation and Associated Restraint Stresses," *Doctoral Thesis 2000:25*, Luleå University of Technology, Luleå 2000.

The influence of temperature on water absorption in concrete during freezing



Tomas Sandström
M. Sc., Lic.tech
WSP Group
Skeppargatan 11
SE-803 20 Gävle, Sweden
E-mail: tomas.sandstrom@wspgroup.se



Katja Fridh
Ph.D, Assistant Professor
Division of Building Materials, Lund University
Box 118, SE-221 00 Lund, Sweden
E-mail: katja.fridh@byggttek.lth.se



Mats Emborg
Professor
Division of Structural and Construction Engineering
Luleå University of Technology, SE971 87 Luleå, Sweden
Head R&D
Betongindustri AB, SE-100 74 Stockholm, Sweden
E-mail: mats.emborg@ltu.se
mats.emborg@Betongindustri.se



Manouchehr Hassanzadeh
Ph. D., Professor Vattenfall Research and Development AB
BU Engineering/BD Asset Development , SE-162 87 Stockholm,
E-mail: manouchehr.hassanzadeh@vattenfall.com

ABSTRACT

A large part of the Nordic hydropower concrete structures are in direct contact with water and are therefore subjected to several transport mechanisms. External water can be transported into a porous material in three ways; by diffusion, capillary suction or by externally applied hydraulic pressure and all three mechanisms are active in a hydraulic structure. The presence of moisture is important in most destructive processes affecting the durability of porous construction materials. The combination of water uptake and harsh climate in which most of the structures of the hydropower industry are situated, explain why damage due to freezing is common. Principally, the environment is a prerequisite for internal freezing to occur but also surface scaling has been found on these structures. Since there presently do not exist any analytical models that can describe the moisture transport for these specific situations of a hydraulic structure, a new test set up has been developed. The

purpose is to study the possible effect of ambient temperature on water absorption properties of concrete. Thus, a test apparatus was constructed where bottom of concrete cylinder specimens of concrete could be placed in direct contact with water and the top was facing the ambient air with varying temperature. The results show that cycling the air temperature from +20 °C to -20 °C increases the water uptake compared to constant room temperature (+18 °C). With a constant temperature gradient (+2°C to -17°C) was the absorption found to be less, but since a large part of the specimens were frozen during a large part of the test, the absorption still was remarkable. Different parts of hydraulic structures are exposed to both of the climate conditions tested and an enhanced risk of frost damage exists.

Key words: Absorption, Temperature, Freeze/thaw, Durability, Hydropower concrete structures.

1. INTRODUCTION

1.1 General

The concrete structures of the Nordic hydropower industry are old; the mean age of the concrete dams in Sweden is approximately 70 years /1/ and /2/. This means that some of the structures are close to reach their designed service life and many have already exceeded it. Thus, the need is increased for maintenance and repair of the old and often worn concrete structures. To be able to do that in a durable manner it is of great importance to understand the active destruction mechanisms. One of the key factors in many destruction mechanisms is the moisture state of the structure. External water can be transported in to a porous material in three ways; by diffusion, capillary suction or by externally applied hydraulic pressure. A large part of the hydropower concrete structures are in direct contact with water and therefore are subjected to all these transport mechanisms. The combination of water uptake and the harsh climate, in which most of the infrastructures of the hydropower industry are situated, explain why it is believed that a common destruction mechanism is freeze action. Principally, this environment is a prerequisite for damage due to internal freezing to occur, since the material has endless amounts of water available during its entire lifetime and long periods of low temperature.

The expression “*freeze action*” is intentionally used here as it is often used when describing the inflicted damage caused by the expansion of the absorbed capillary water in concrete materials as it transforms from liquid to solid state. The commonly used expression “*freeze/thaw action*” implies that concrete is damaged due to some sort of fatigue load, which probably is not the case for structures subjected to long freezing periods. It is shown in experiments on moisture sealed specimens that it is in fact the phase change that damages the material during freezing and not the different thermal expansion coefficients of ice and concrete /3/. However, the freeze/thaw cycling does *indirectly* affect the materials resistance to damage caused by internal freezing, because it increases water uptake, which will be shown here.

According to /4/, damage of any concrete specimen due to freezing is in most cases a consequence of very few freeze cycles. In /5/ it is concluded that solely one freezing will damage the material, presuming that the volume of freezable pore water is large enough at the given temperature. The underlying mechanism causing damage due to freezing has been dealt in several research reports, see e.g. /6/ - /12/. The prerequisite for damage to occur due to freezing

is that the critical degree of saturation (S_{CR}) is transgressed simultaneously with sub-zero temperatures. The amount of freezable water is dependent on the freezing temperature. Hence, the lower the freezing temperature, larger volume of absorbed water will be able to freeze. Thus, the lower the temperature is the higher the risk is to transgress the S_{CR} .

Since the concrete structures constituting the waterways are in direct contact with water, and in most cases have been so for a very long time, it is inevitable that S_{CR} of certain areas within the concrete structures will, at some point in time, be reached. As hydraulic structures also are submitted to sub-zero temperatures the risk of frost damage is high.

Unfortunately it is impossible to predict the moisture state in hydropower structures such as dams and other type of structures as there are many different factors, both material and climatic ones, which influence the water uptake. At most hydropower sites annual temperature variations are large. Long periods of really low temperatures (-20°C) are followed by long periods of moderate temperatures ($+15^{\circ}\text{C}$). It is difficult to predict how the wetting and drying of different parts of the structure varies over time. In concrete there is a hysteresis of freezing and thawing which to some extent can be explained by bottle-neck shaped pores in the material and this may also influence the water absorption as well as cycling temperature creating alternating freezing and thawing, see e.g. /13/ and /14/. How much the temperature cycling affects the rate of absorption and what is the driving mechanism it is not entirely known, even though different theories exist that perhaps might explain this phenomenon, /15/ and /16/. In view of the fact that no analytical models exist that can describe this specific situation, an attempt has been made in this research to study the possible effect of the surrounding air temperature on the water absorption properties of concrete.

2. METHOD AND MATERIALS

2.1 Method

The test set up was designed to create a situation where one side of concrete specimens was subjected to air (with temperature, T_a), while the other side of the specimens was in direct contact with water of temperature T_w , see Figure 1 /10/. The purpose of this approach was to simulate existing situation for hydropower concrete structures. Three temperature cases were studied:

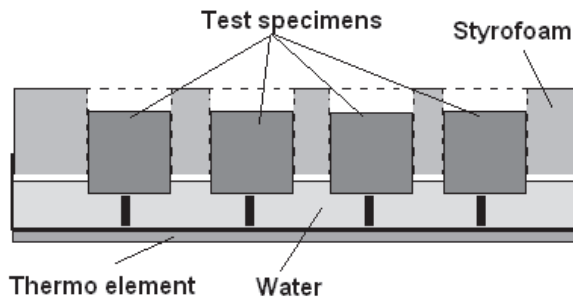
- A) Specimens subjected to one-sided capillary suction at 18°C . $T_w = T_a = 18^{\circ}\text{C}$ (reference, also denoted “room temperature” in Figure 3).
- B) Specimens subjected to one-sided capillary suction in a freezer with cyclic air temperature variation (160 cycles) and almost constant temperature of water. $T_w = 0$ to 1°C ; $T_a = -20$ to $+20^{\circ}\text{C}$, see Figure 2.
- C) Specimens subjected to one-sided capillary suction in a freezer with almost constant air temperature and almost constant temperature of water. $T_w = 1$ to 2°C , $T_a = -17$ to -20°C (temperature variations due to improper temperature control in freezer).

A steel container 490x540x80 mm, was fitted into the available space in a freezer. Twelve steel pins were welded perpendicular to the bottom surface of the container to support concrete cylinders, see Figure 1. The container was partially filled with water and the top of the container was covered with a 100 mm thick insulation block of Styrofoam. Twelve holes corresponding to the diameter of the test specimens were drilled through the block of Styrofoam see Figure 1. A thermo element was placed in the bottom of the container controlling the water temperature.

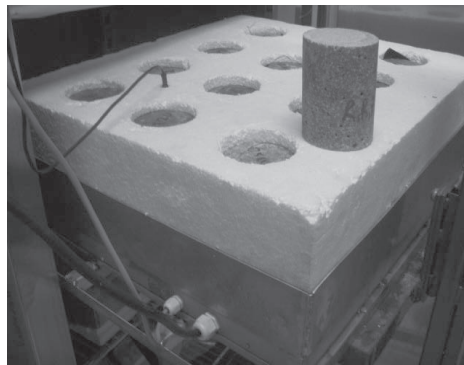
The change in saturation of the concrete during the test was documented as follows;

1. The weight of each core specimen was measured throughout the test.
2. At the end of the test the pore volume of the core specimens was calculated after vacuum saturation and drying at 105 °C.

To verify that no damage had occurred in the specimen during the test, the results from the measurement of the pore volumes was compared with the pore volumes for reference core specimens, stored in the same climate room but not used in the test. Alternatively, ultrasonic pulse velocity measurements could have been used detecting possible damage.



a)



b)

Figure 1 – Test Setup a) sketch b) photo /10/.

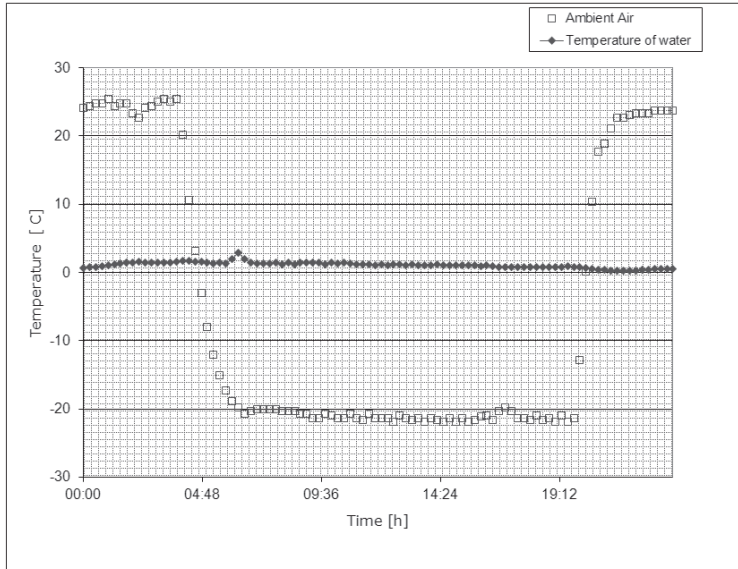


Figure 2 – Temperature cycle in set up B /10/.

To describe the amount of absorbed water by the specimens the degree of saturation, S , was used. The amount of absorbed water at an actual moment in time S_{act} can thus be defined as the degree of saturation of the material, Fagerlund /5/:

$$S_{act} = V_w / V_p \quad (1)$$

The volume of absorbed water (V_w) is the total amount of absorbed water, which will dry out at 105 °C. The open porosity (V_p) includes all type of pores and cavities in the specimen that are accessible to water. As a material continues to absorb water, S_{act} will increase. Experimentally S_{act} can then be determined as follows:

$$S_{act} = \frac{m_{act.} - m_{105}}{m_{sat.} - m_{105}} \quad (2)$$

Where,

S_{act} = actual degree of saturation [-]

$m_{act.}$ = mass of the specimen at a given time [kg]

$m_{sat.}$ = mass of the specimen after vacuum saturation [kg]

m_{105} = mass of the specimen after drying at 105 °C until constant mass is obtained [kg]

2.2 Materials

In the experiment four concrete types were used, see Table 1. Two recipes had a w/c ratio of 0.50, one with and one without air entraining agent (AEA). The other two recipes had w/c ratios

of 0.60 and 0.70, both without AEA. The cement type was a CEM I SR LA and the aggregate was mostly granite.

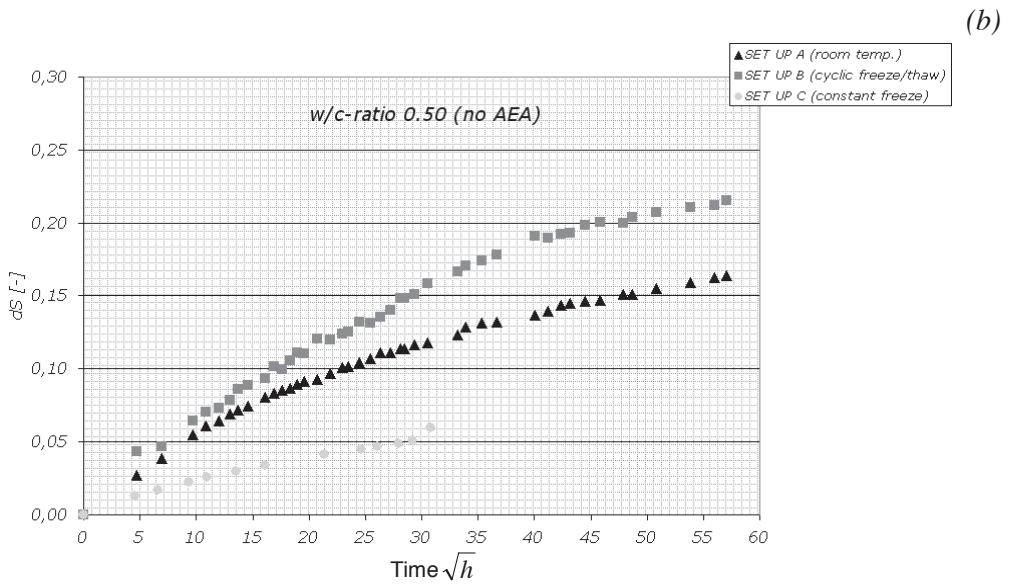
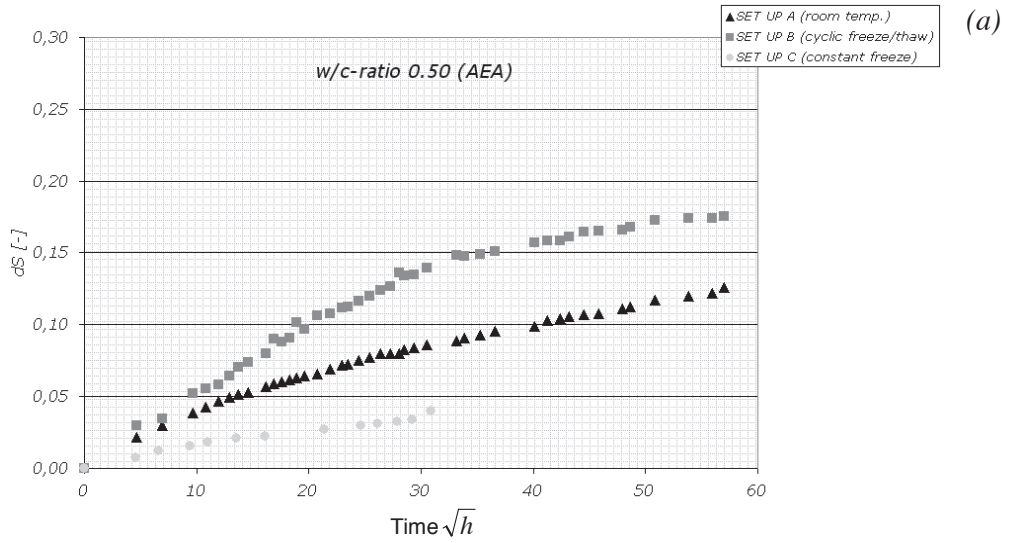
One slab of each recipe was manufactured. The slabs had the approximate dimensions of 600x400x120 mm and they were moisture sealed for one week. After this week cores (diameter 75 mm, length 120 mm) were drilled out of the slabs. The cores were placed in a water tank for a month and thereafter the specimens were placed in a climate chamber (20 °C, RH 80 %) for at another 2 months prior to the start of the experiment.

Table 1 - Mix compositions and test data of concretes studied in the experiment /10/

	Concrete 1	Concrete 2	Concrete 3	Concrete 4
w/c ratio	0.50	0.50	0.60	0.70
AEA	Yes	No	No	No
Cement	340 kg/m ³	340 kg/m ³	340 kg/m ³	340 kg/m ³
Water	170 kg/m ³	170 kg/m ³	204 kg/m ³	238 kg/m ³
Aggregates 8-16	550 kg/m ³	550 kg/m ³	520 kg/m ³	495 kg/m ³
Aggregates 0-8	1230 kg/m ³	1230 kg/m ³	1170 kg/m ³	1105 kg/m ³
Aggregates 2-5	80 kg/m ³	80 kg/m ³	70 kg/m ³	66 kg/m ³
Porosity, V _p	18 ± 0.1 %	14 ± 0.1 %	17 ± 0.1 %	19 ± 0.1 %
Sact at the start	49 ± 4 %	71 ± 3 %	70 ± 4 %	68 ± 1 %

3. RESULTS

The results from the measurements of the change in degrees of saturation (dSact), for the four mixtures are presented in Figures 3a-d. The change is normalised with the degree of saturation at the start of the experiment according to Table 1 and is described as units of Sact, according to Eq (1) and (2). The duration of the experiment (x-axis) is presented as the square-root of the time. It can be noted that Sact at the start was lower for the specimens used in set up C as this test was conducted after A and B i.e. the specimens were stored for a longer time in the climate chamber, subjected to enhance drying.



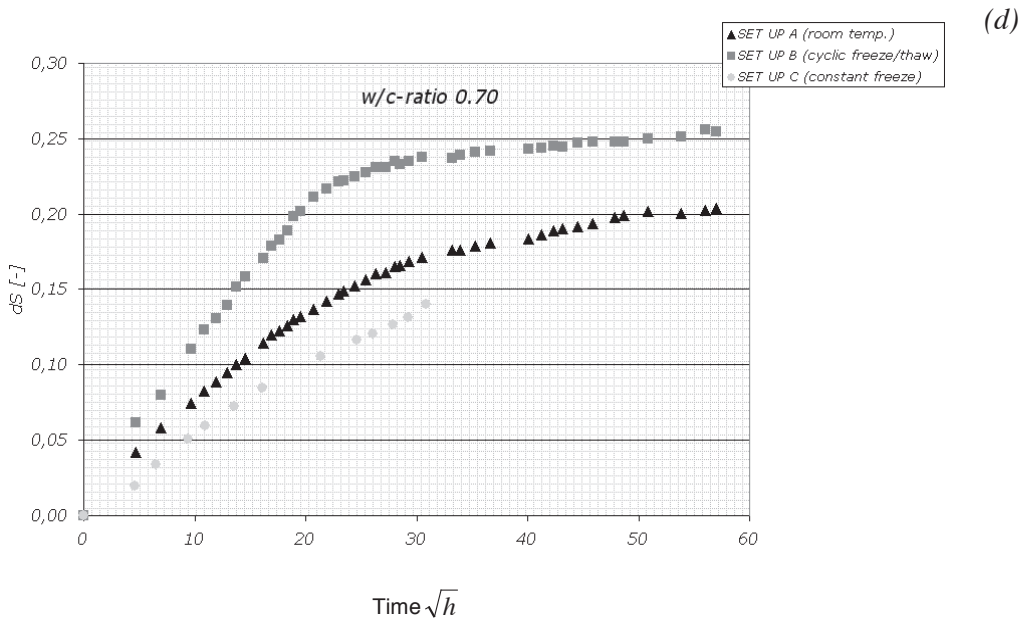
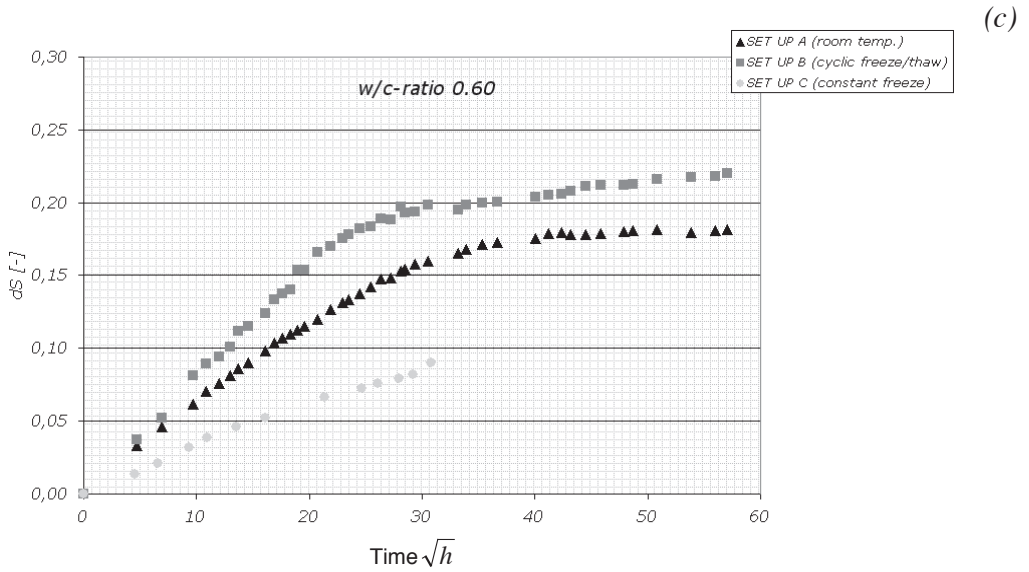


Figure 3 Change in degrees of saturation, dS_{act} from its value at start of test, S_{act} (see Table 1) due to capillary suction as a function of the square root of time: Mix design see Table 1,

4. DISCUSSION AND CONCLUSIONS

4.1 Remarks and discussion

As can be observed in Figures 3a-d the temperature conditions of the ambient air affects the absorption noticeably. Cyclic temperature variations increase the absorption significantly. On the other hand, a constant temperature gradient, as in set up C, results in less absorption than for set up A and B.

The first part of a capillary suction curve represents the filling of the well-connected capillary pores. This is a somewhat rapid process which can be seen in the rather steep slopes in the Figures 3a-d. When the well-connected pores are filled, the filling of the not so well connected capillary pores and air voids starts. The mechanism of filling these pores is more of a diffusion process which is a much slower process and the slope of the curve decreases. Therefore, there is a knick point in the curves when the dominating mechanism is changed as also is mentioned in /17/. It is obvious that, changing the temperatures during capillary suction, creating freezing and thawing in the pores (as documented in /15/ and /16/) which has a lower free energy than the water which creates a driving force towards the ice which results in a larger absorption. If the specimens were damaged during freezing this would also have led to an increased water uptake. However, no change in porosity was observed and probably no internal damage occurred. Nevertheless, this is emphasized in previous studies on completely submerged specimens where no difference was observed of the absorption at constant temperature (+20 °C) or during daily cycling the temperature (from +20 °C to +5 °C) /18/. This is despite the fact that during parts of the cycle, sections of the specimen is frozen and not active in the water uptake. Structures subjected to this kind of environment are thus more likely to be affected by frost damage due to higher moisture levels.

The degree of saturation in relation to time of absorption for specimens with w/c ratios 0.60 and 0.70 is presented in Figure 4. Trend lines, which help to visualize the difference in absorption properties of the materials, are added. It is seen that the rate of absorption is higher for specimens subjected to freeze/thaw cycling (set up B) than for set up A (reference). By comparing line 1 for both the cases it is clear that the slope is much steeper for set up B, proposing an increased rate of capillary suction. The knick point, separating line 1 from line 2 appears to be reached earlier for specimens subjected to freeze/thaw cycling, and at a higher degree of saturation.

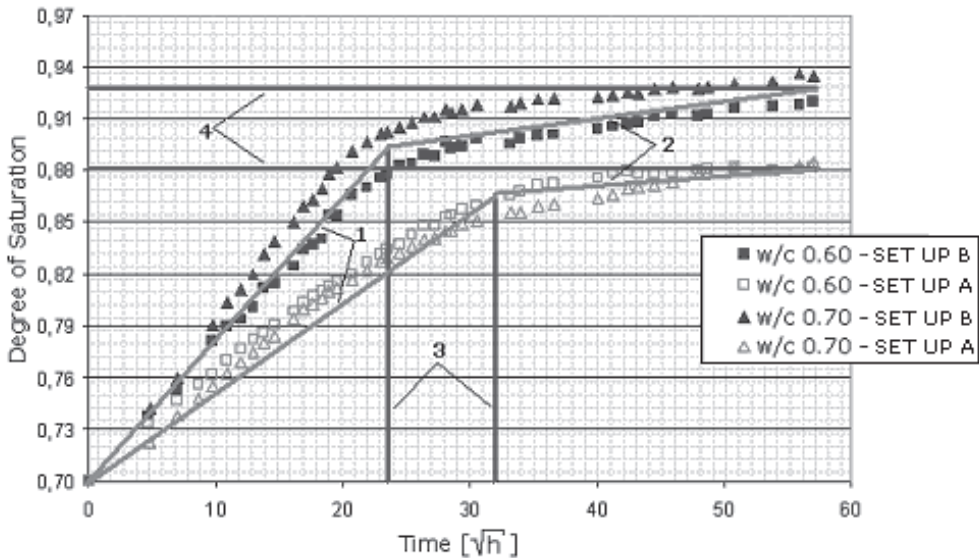


Figure 4 – Comparison of the absorption properties (here as degree of saturation, S_{act}) of specimens with w/c-ratios 0.60 and 0.70 in set up A and B [10].

Comparing lines 2 in the figure, the slope of the line appears to be somewhat steeper for the specimens subjected to freeze/thaw cycling (set up B). This indicates that the freezing and thawing of the specimen increases the rate of filling the more isolated capillary pores and the air voids. This increases the chance of the concrete being damaged by frost, when the air which is supposed to work as a space where the ice can expand tensionless disappears.

The over capillary range also appears to be reached much earlier in the specimens exposed to freeze/thaw cycling (set up B) than for the specimens not subjected to freeze/thaw action (set up A). The nick point (line 3) appears approximately 500 hours earlier for specimens exposed to freeze/thaw cycling, compared to the specimens which air temperature was constant at +20°C.

At the end of the experiment, after about 3500 hours (or about 145 cycles of freezing and thawing), the degrees of saturation measured in the two set ups show a significant and critical difference in the uptake of water. Hence, line 4 shows that specimens subjected to freeze/thaw cycling almost reach a degree of saturation of 0.94, while specimens not exposed to freeze/thaw cycling “only” reach about 0.88.

The influence of w/c-ratio was found to be as expected, see Figure 5. The higher the w/c-ratio, the higher degree of saturation after the same time of absorption. The slope of the first part of the curves (referred to as line 1 in Figure 4) represents the large, connected capillary pores and the higher the w/c-ratio is, the larger is the amount of these types of pores. Comparing concrete for the w/c-ratio 0.50 with and without AEA interesting observations can be made regarding difference in water uptake where the difference in recorded dS_{act} is due to different amount of air voids in the two materials.

During long periods of time the hydro power concrete structures are exposed to water absorption when it is simultaneously subjected to a temperature gradient. Although this is a well-known fact experiments of water absorption during a temperature gradient are rare. The influence of w/c-ratio on absorption in these temperature conditions was the same as for the two other set ups. Absorption was higher the higher w/c-ratio, see Figure 6. But it seems as if the differences in absorbed amount between the w/c-ratios are larger. This is most likely due to ice lenses forming in the capillary pores which are enhancing the absorption. Since the measuring time was relatively short, it is most likely so that the less accessible pores are not activated yet. Even though the rate is only half of the rate during freezing and thawing, it should be remembered that a large part of the specimen is frozen during a large part of the experiment and do not participate in the water uptake. That considered, is the water uptake remarkable and structures subjected to these climate conditions at risk for frost damage.

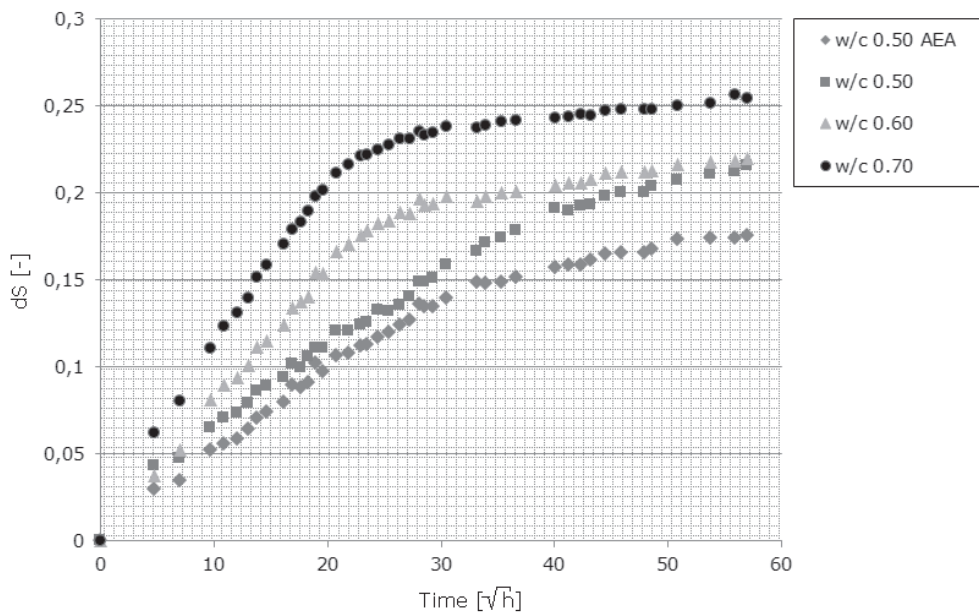


Figure 5 – Change in degree of saturation of the specimens in set up B.

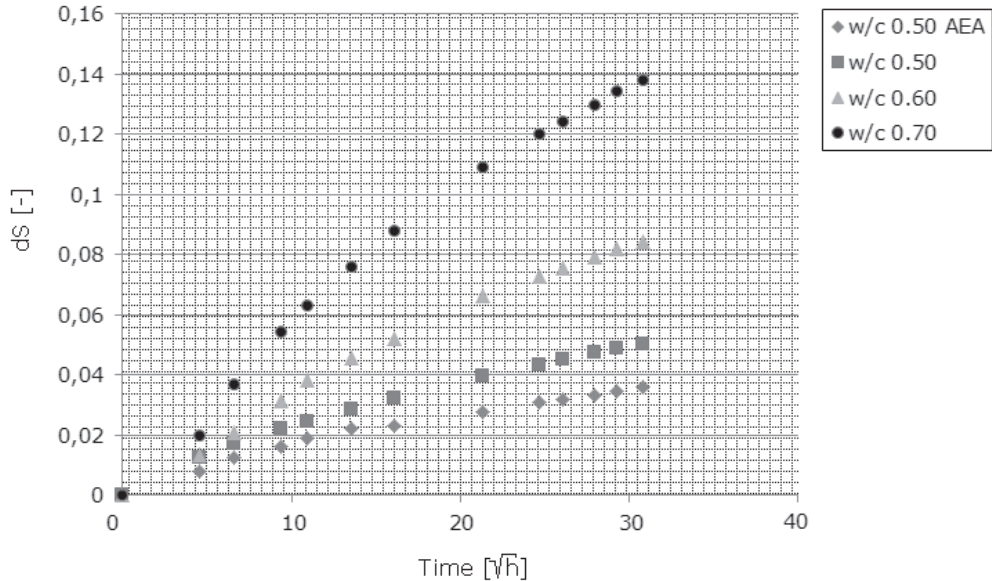


Figure 6 – Change in degree of saturation of the specimens in set up C.

4.2 Conclusions

There is a rather strong resemblance between the set ups of the experiment and the situation for a hydraulic structure. The observation made for set up B applies for the water line of hydraulic structures and forces us to wonder what the physical performance of our oldest dam structures is. It is therefore of great interest to translate these laboratory results to the conditions present in reality, although indeed it is a difficult task, and it is clear that further investigation both in laboratory and in full scale is needed. However, taking these results into account as indications it seems likely that there are reasons to be concerned regarding the conditions of the concrete structures subjected to freezing and thawing cycling at the same time as they are in direct contact with (unfrozen) water.

The following conclusions were drawn from the observations made in the tests presented in this paper:

- The temperature of the ambient surroundings significantly affects the absorption properties of concrete.
 - Water absorption increases with time at constant temperature.
 - Freeze/thaw cycling noticeably increases the rate of absorption due to microscopic ice lens formation. The temperature cycling itself does not increase the rate.
 - The absorption during a constant temperature gradient is slow but still significant since a large part of the specimens were frozen during the test.
- Water-uptake at constant temperature gradient seems to affect concrete with high w/c-ratio much more than concrete with lower w/c-ratio. The reasons for this need further investigation.

- Since different parts of hydraulic structures are exposed to water absorption in all this climatic conditions tested in the study, thorough investigations are needed on the state of our oldest concrete dams with respect to possible damages due to internal freezing.

The results of this study created many new questions and led to several new studies /18/ and /19/ and a PhD project concerning both frost damage mechanisms and its influence during selecting refitting methods.

ACKNOWLEDGEMENT

The Swedish Hydro Power Industry (SVC) and the Swedish Research Council (Vetenskapsrådet) financed the work in collaboration with the Technical University of Luleå, Lund University of Technology and Vattenfall Research and Development which is gratefully acknowledged

REFERENCES

1. Rosenqvist M, Persson M, Hassanzadeh M, Fridh K ” Frost Damage in Concrete in the Waterline of Porsj Hydro Power Plant”, International Symposium on Modern Technologies and Long-term Behavior of Dams, Zhengzhou, ISBN 978-7-5084-9018-2, 2011.
2. Bernstone C. ”Automated performance monitoring of concrete dams”, Doctoral thesis, Lund Institute of Technology, Engineering Geology, Faculty of Engineering, Report TVGV-1020, Lund 2006
3. Fridh K., “Internal Frost Damage in Concrete”, Doctoral Thesis, Lund Institute of Technology, TVBM-1023, Lund 2005
4. Svensk Byggtjänst, “Betonghandbok – Material”, Utgåva 2, Avsnitt 21.5, Stockholm, 1994
5. Fagerlund G. ”The critical degree of saturation method of assessing the freeze/thaw resistance of concrete”, CBI Reports 6:77, Volume 10N-58, Stockholm 1977
6. Powers T. C. Helmuth R. A. “Theory of Volume Changes in Hardened Portland-Cement Paste During Freezing”, Highway Research Board 32, 1953
7. Powers T.C. Brownyard, T. L., “Studies of the physical properties of hardened cement paste. Part 8: the freezing of water in hardened cement paste”, Bulletin 22, The Research Laboratory of the Portland Cement Association, 1948
8. Fagerlund G “A service life model for internal frost damage in concrete”, TVBM-3119, Lund Institute of Technology, Div. Building Materials, Lund, 2004
9. Lindmark S., ”Mechanisms of Salt Frost Scaling of Portland Cement-bound Materials: Studies and Hypothesis”, Doctoral Thesis, Lund Institute of Technology, Report TVBM-1017, Lund 1998
10. Sandström T. “Durability of Concrete Hydropower Structures When Repaired with Concrete Overlays”. Technical Licentiate Thesis. Luleå University of Technology, 2009, ISBN 978-91-7439-074-2, 179 pp
11. Setzer et al. “Frost resistance of concrete”, Proceedings, RILEM Publications S.A.R.L, Canchan, 2002.
12. Bager D.H and Sellevold E.J. “Ice formation in Hardened Cement Paste Part I – Room Temperature Cured Pastes with Variable Moisture Contents, Cement and Concrete Research, vol 16, pp. 835-844, 1986.

13. Statens Vattenfallsverk ”Vattenfalls Betonghandbok – Anvisningar för utförande och kontroll av betongarbeten”, ISBN-91-7186-003-7, Stockholm 1972
14. Neville A. M., “Properties of Concrete”, Fourth and final edition, Reprinted 2008, Edinburgh Gate, 2008
15. Jacobsen S, “Scaling and cracking in unsealed freeze/thaw testing of Portland cement and silica fume concrete”, Doctoral thesis, Division of Structural Engineering, Concrete section, The Norwegian Institute of Technology, 1995.
16. Setzer M.J, “Development of the micro-ice-lens model”, Frost resistance of concrete, Proceedings, Editors, Setzer, Auberg, Keck, Rilem Publications S.A.R.L, Canchan, 2002.
17. Fagerlund G. “Moisture design with regard to durability”, TVBM-3130, Lund Institute of Technology, Div. Building Materials, Lund, 2006
18. Wikström T. “Concrete’s water absorption capacity under different temperature conditions”, (In Swedish) TVBM-5084, Lund Institute of Technology, Div. Building Materials, Lund, 2012.
19. Persson, M., Rosenqvist, M., “Frost damage in concrete dams”, TVBM-5074, Division of Building Materials, Faculty of Engineering, Lund University, Lund, 2009. (In Swedish)

Finite element simulation of shotcrete exposed to underground explosions



Lamis Ahmed
Ph.D. student
KTH Royal Institute of Technology
Division of Concrete Structures
SE-100 44 Stockholm, Sweden
E-mail: lamis.ahmed@byv.kth.se



Richard Malm
Ph.D., Researcher
KTH Royal Institute of Technology
Division of Concrete Structures
SE-100 44 Stockholm, Sweden
E-mail: richard.malm@byv.kth.se



Anders Ansell
Ph.D., Associate Professor
KTH Royal Institute of Technology
Division of Concrete Structures
SE-100 44 Stockholm, Sweden
E-mail: anders.ansell@byv.kth.se

ABSTRACT

An elastic finite element model is used to simulate the induced stress waves from blasting, propagating in rock towards shotcrete on a tunnel wall. Due to the inhomogeneous nature of the rock, the stress waves attenuate on its way from the point of explosion towards the shotcrete on the rock surface. Material damping for the rock-mass is estimated from in-situ measurements. The vibration resistance of the shotcrete-rock support system depends on the material properties of the shotcrete. Age-dependent material properties are varied to investigate the behaviour of young shotcrete subjected to blast loading. Finally, finite element analysis results are presented and verified through comparison with other numerical models, measurements and observations.

Keywords: Shotcrete, rock, vibration, blasting, finite element analysis.

1. INTRODUCTION

The use of shotcrete as a support element became common in the 1960s [1] and at the same time the first calculation methods based on the mode of action of shotcrete in hard rock were developed. In these methods, the aim is to make the rock carry its inherent loads, and thereby assuming that the main design principle for the support system is to provide rock confinement immediately after excavation, giving the rock support to stabilize itself around the opening. The performance of shotcrete interacting with rock is influenced by a number of parameters. The

most fundamental parameter is the ability to adhere to a surface, forming a bond that depends on the bond strength between shotcrete and rock. In general, the rock support is designed for static loading conditions. However, in many cases the openings are also subjected to dynamic loads, e.g. a local rock burst or a detonation of explosives during excavation of tunnels and underground spaces. The detonation gives rise to an impulse that propagates as a stress wave through the surrounding rock. As the wave moves radially outwards, the stress level decreases but may still cause severe damage to permanent installations and support systems within the rock, such as shotcrete. Most construction work in underground rock involves the use of explosives for excavation. The search for a more time-efficient construction process therefore naturally puts focus on the possibilities of reducing the time of waiting between stages of construction. This means that supporting systems in one tunnel are likely to be affected by vibrations from a neighbouring tunnel under construction.

The first step towards reliable guidelines for how close, in time and distance, to young and hardening shotcrete blasting can be performed was taken through a series of tests conducted in the underground mine at Kiirunavaara, Sweden [2]. Sections of plain, un-reinforced shotcrete were projected on tunnel walls and exposed to vibrations from explosive charges detonated inside the rock. The response of the rock was measured with accelerometers mounted on the rock surface and inside the rock. It was concluded that sections with sudden loss of bond at the shotcrete-rock interface appeared for vibration velocities within 0.5–1.0 m/s, while ejected rock was found for vibration velocities higher than 1 m/s. The results also agreed with tests performed on fully hardened reinforced shotcrete in Canada [3]. These tests have been evaluated using numerical modelling, with a one-dimensional elastic stress wave model and two structural dynamic models with vibrating masses and beams connected through elastic springs [4–6], in the following referred to as the mass-spring and the beam-spring models. The advantage of these simplified models is the efficient analytical procedure that, with relatively small computational effort, makes it possible to compare a large number of calculations with various combinations of input data and the straightforward interpretation of the results. The numerical results have been verified through comparisons with observations and measurements from in-situ testing [4] and from full scale mining operations [5]. The beam-spring model has also been used for studying the vibration resistance for young and hardening shotcrete [6]. The three numerical models have been compared and it was shown that the models give comparable results [7], although the definition of the dynamic loads is slightly different. For the stress wave model the dynamic load is defined as a time dependent velocity while a time dependent acceleration is used for the other two models. All of these models are based on linear elastic material theory and thus not able to describe partially damaged structures, e.g. partial debonding of shotcrete. The models can, however, be used to identify the limit for damage through series of calculations with increasing load level until either the tensile strength or the bond strength is exceeded. The effect of impact loading and wave propagation was also studied using non-destructive laboratory experiments [8]. Finite element modelling was used to verify the test results, which showed that the laboratory model with an impacting hammer could produce the same type of stress waves that is the result from blasting in good quality rock. In this paper, two-dimensional (plane strain) dynamic finite element models of shotcrete and rock subjected to stress waves have been developed and refined through comparisons with results from the previous studies. The goal is to suggest a type of finite element models, load formulations and boundary conditions that leads to realistic results, also for more complex geometries and shotcrete material properties than tested before.

2. MATERIAL PROPERTIES

The purpose of the investigation in this paper is to study the effect of stress waves in shotcrete on rock. No rock bolts or mesh reinforcements are included as supporting elements and the material properties for shotcrete and rock are chosen as typical representative average values to exclude the effect of extreme material strengths, etc. To facilitate comparisons the same material properties as used in the previous numerical models [7] were chosen.

2.1 Shotcrete

This study assumes un-reinforced shotcrete, without fibre content and with a standard composition containing water glass as accelerator. The material properties chosen for the examples resembled that of the shotcrete used in the Kiirunavaara tests [2] resulting in a density (ρ_{shot}) of 2100 kg/m³ and a modulus of elasticity ($E_{28\text{d}}$) of 27 GPa after 28 days. The development of the E_{shot} for hardening shotcrete is herein assumed to follow an average curve, derived from a large number of tests [9]. The relation between E_{shot} and the age of shotcrete t_s (in days) is

$$E_{\text{shot}} = 1.062 E_{28\text{d}} e^{-0.446 t_s^{-0.8}} \quad (1)$$

Alternatives to this relation are presented and commented in [6].

The bond strength between fully hardened shotcrete and rock is usually determined through pull-out tests in the direction perpendicular to the rock wall. These in-situ tests usually give results between 0 and 2 MPa but at conditions normal for tunnelling, values higher than 0.5 MPa are realistic. In the following, bond strength (f_{cb}) of 1.0 MPa is assumed, which correspond is to shotcrete on a sufficiently cleaned surface of hard granite [4]. There are almost no reliable test results published on the development of f_{cb} for hardening shotcrete on rock. However, for the studied case preliminary laboratory results [8] from tests with mortar on concrete will provide a good approximation. The tests, based on a newly developed method [10], indicated a relatively rapid development of the bond strength which reached 1 MPa after 24 hours. This is in good correspondence to the range of 0.6–1.1 MPa that has been reported from other investigations on 1–2 days old shotcrete and mortar, [10]. The development of the bond strength thus follows

$$\frac{f_{\text{cb}}}{f_{\text{cb},24\text{h}}} = 2.345 e^{-0.858 t_s^{-0.97}} \quad (2)$$

where the average strength at 24 hours is $f_{\text{cb},24\text{h}} = 1.0$ MPa.

2.2 Rock

The rock properties are here chosen to represent hard granite type Scandinavian bedrock which typically has a density (ρ_{rock}) of 2500 kg/m³ and a Poisson's ratio ν that is 0.15 [7]. It is difficult to define material properties for a large rock mass since its behaviour is site-specific with geological discontinuities and fractures that affect the characteristics of propagating stress waves. The modulus of elasticity (E_{rock}) for intact granite is in the range 40–80 GPa [5], but due to the heterogeneous nature of the rock a lower average value is often assigned to a larger rock

mass. For this study the modulus was set to be within 16–40 GPa. The higher limit thus corresponds to high quality intact rock while the lower corresponds to a slightly fractured rock mass [11].

2.3 Vibration resistance

Shotcrete sprayed on rock exposed to blasting will thus be affected by incoming stress waves that reflect at the interface between shotcrete and rock. When exposed to incoming stress waves, the inertia forces caused by the accelerations acting on the shotcrete give rise to stresses at the shotcrete-rock interface which may cause bond failure. The shotcrete-rock load carrying system fails if either the bond or the rock material fails. It is difficult to define a reliable damage criterion for rock but various suggestions are available. One of the common criterions is the damage criterion. Table 1 show an example of damage criterion for Swedish hard rock [12], where it should be noted that the threshold damage (incipient damage) occurs at a peak particle velocity (PPV) of 1.0 m/s. These values should be compared to the observed damage limits for shotcrete on rock, here compiled in Table 2. It should be noted that the highest limits are between those for incipient damage and fragmentation in rock, as given in Table 1.

Table 1 – Vibration velocities PPV at damage for hard Scandinavian bedrock [12].

PPV at damage	Effect
0.70 m/s	Incipient swelling
1.00 m/s	Incipient damage
2.50 m/s	Fragmentation
5.00 m/s	Good fragmentation
15.0 m/s	Crushing

Table 2 – Vibration velocities PPV when shotcrete damage occurs based on in-situ measurements. Compilation from [5].

	PPV at damage	Comments:
Kiirunavaara tests [2]	0.50–1.00 m/s	Young shotcrete
Japanese tunnelling [13]	0.70–1.45 m/s	
Mining, full scale [14]	app. 1.00–1.80 m/s	
Canadian tests [3]	1.50–2.00 m/s	Steel fibre reinforced

3. STRESS WAVES IN ROCK

A rock burst or an explosive detonation within the rock mass gives rise to stress waves that propagate towards possible free rock surfaces. The wave motion in homogenous un-fractured rock can be compared to that of an elastic medium and described as movement of energy through the material, by particles translating and returning to equilibrium after the wave has passed [15]. The propagation velocity is governed by the type of rock and the wave motion can be divided into three main wave types; compression waves (P-waves), shear waves (S-waves) and surface waves. The P-wave propagates faster than other waves and is therefore the first to reach an observation point when different types of waves have been generated simultaneously.

3.1 Wave propagation

As each wave passes, the motion of the particles in the rock can be described in three dimensions, either as displacements, velocities or accelerations. When a wave-front reflects at a free surface, for instance a tunnel, the particle velocities are doubled and the stresses are zero over the surface. This means that a compressive wave reflects backwards as a tensile wave, etc. The propagation velocity c of P-waves in an elastic material is given by its stiffness and the density ρ of the material [15], following

$$c = \sqrt{\frac{E}{\rho}} \quad (3)$$

where E is the elastic modulus. In the following it is assumed that the stress wave and thereby the PPV has a cosine shaped time history that would correspond to a sinusoidal shaped particle acceleration and displacement. The particle velocity of the propagating stress is here

$$v(t) = 0.5v_{\max} \cos(2\pi f t) - 0.5v_{\max} \quad (4)$$

where f is frequency of the incoming stress and, v_{\max} the maximum PPV. This shape of velocity wave have previously [7] been tested and evaluated for use in numerical calculations. In rock, layers and cracks have a filtering effect on propagating vibration waves. Certain frequencies within a spectrum of a wave will be amplified while others will be damped out, depending on the characteristics of the medium, which can be rock with minor cracks. Therefore, a frequency spectrum of a measured acceleration signal only contains a limited number of peaks, i.e. the characteristic frequencies. For modelling purposes, this can be used to forecast accelerations from known explosive charges. An amplified frequency f depends [15] on the layer thickness H and wave propagation velocity c as

$$f = \frac{c}{4H} \quad (5)$$

For rock containing more than one characteristic distance between imperfections, H should be varied to calculate multiple characteristic frequencies.

3.2 Attenuation of rock vibration with distance

Particle velocities that can be measured remote from a vibration source in rock will show a decrease in magnitude with increasing distance. This attenuation is caused by geometrical spreading and damping in the rock [15]. For waves generated by explosives this is governed by equations on the form

$$v_{\max} = v_0 \left(\frac{R}{\sqrt{Q}} \right)^{-\beta} \quad (6)$$

where v_0 and β are constants and v_{\max} is the PPV at a distance R from an explosive charge with the weight Q . The equation is valid only for situations where R is large compared to the length of the explosive charge, thus assuming a concentration of the explosives. The examples in this paper have been performed for hard quality granite for which Eq. (6) can be used with $v_0 = 700$ mm/s and $\beta = 1.5$, as in [2], giving

$$v_{\max} = 700 \left(\frac{R}{\sqrt{Q}} \right)^{-1.5} \quad (\text{mm/s}) \quad (7)$$

where R in meters and Q in kg.

The damage depth in rock at different amount of explosives can be calculated using empirical formulas similar to Eq. (6). In the following examples a damage limit at 0.9 m/s for granite is assumed, which is on the safe side with respect to incipient damage according to Table 1. From Eq. (7), the depth of the damage zone R_{ppv} , where the particles velocity reaches the threshold PPV, will thus be

$$R_{\text{ppv}} = 0.846 \sqrt{Q} \quad (\text{m}) \quad (8)$$

In the present study, waves with high frequency content are used and therefore the contribution of material damping has a great effect on the results. The shorter the wavelength, the higher is the influence from material damping on the attenuation [15]. There are many methods for estimating damping but one of the practical methods is to calculate the damping ratio from the acceleration representation in the frequency domain using the so-called half-power bandwidth method, see [16]. This method applied to the relatively limited data from the measurements in Kiirunavaara [2] resulted in a damping ratio (ζ) close to 8 %, which is in good correspondence with other observations in-situ, e.g. [17] where up to 10% damping has been reported. For shotcrete a material damping ratio of 2.5 % was used, in accordance with the previously presented modelling examples, [6] and [7].

4. FINITE ELEMENT MODEL

In this study, dynamic finite element models of rock and shotcrete subjected to stress waves have been developed using the ABAQUS/Explicit finite element program [18]. The simulations were performed using two-dimensional (2D) plane strain elements. The models describe two cases with respect to the geometry of the tunnel and position of the detonation point. The fundamentals of the models are shown in Figure 1. The first case is shown in Figure 1(a), where the wave propagates through the rock from the detonation point at the centre of the charge towards the tunnel side. The second case is used for studying the effects of stress wave

propagation along the tunnel sides, as shown in Figure 1(b). The detonation is introduced in the model from a circular area within the rock where an impulsive particle velocity is applied. An incident PPV wave caused by an explosion is applied as a boundary condition at the perimeter of the circular area, with the radius R_{PPV} calculated according to Eq. (8). This distance thus corresponds to the limit for rock damage and therefore can elastic properties be assigned to the rock outside this area. In the real case, the rock area immediately around the hole containing the explosives will be severely cracked. However, there is no need to include this effect in the present model since the load here is applied at a long enough distance from this point.

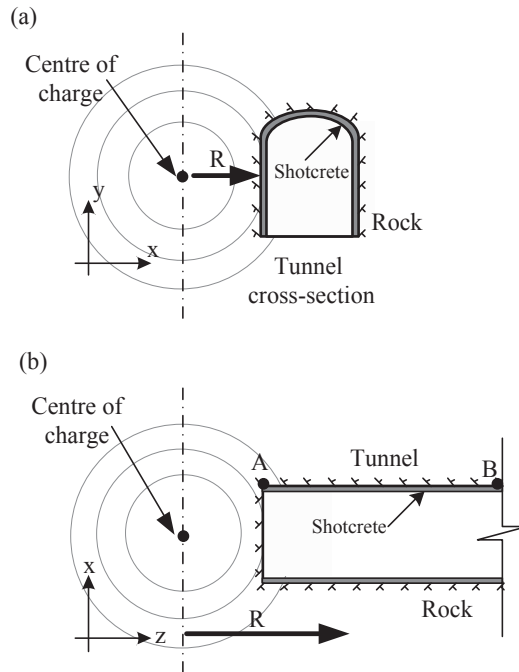


Figure 1– Two cases of detonation close to a tunnel in rock; (a) orthogonal to a tunnel wall (profile), and (b) ahead of tunnel face (horizontal plane). A and B are reference points.

An example of meshing and use of finite elements is shown in Figure 2, describing a model of case (a) in Figure 1. A fine mesh was used around the loading area and tunnel opening with coarser mesh used further away from the tunnel opening. Infinite elements were utilized to represent the non-reflecting boundaries and prevent the wave reflections. The rock and the shotcrete behave in a strictly elastic manner and possible failure thus occurs when the stresses at the shotcrete-rock interface exceeds the bond strength. That is, no plastic deformations or permanent failure, for example, crushing or cracking, were considered within the models and a linear elastic relationship between stress and strain was assumed. The horseshoe shaped tunnel for case (a) (see Figure 2a) has a height of 6 m and width of 5 m. The tunnel is assumed to be situated 11.5 m below the ground surface. The material surrounding the excavation is discretized with first-order 4-node plane strain elements of type (CPE4R), which is recommended for simulations of impact and blast loading using ABAQUS/Explicit [18]. The infinite extent of the rock is represented by a 20 m wide mesh that extends from the surface to a depth of 45 m below the surface. Far-field conditions on the bottom and right-hand side boundaries are modelled

using infinite elements of type (CINPE4). The interaction between rock and shotcrete was modelled using tie constraints, i.e. no relative displacement between the materials was assumed. The element size of the shotcrete part is $0.01 \times 0.1 \text{ m}^2$ for all models, with different element sizes used for the rock part. Depending on the accuracy and details of the solution, some regions of the rock would be discretized with a refined mesh. More refinement adjacent to the tunnel opening and loading area was done, due to the significant deformations expected at these regions. The model consists of about 28000 nodes and 2500 elements.

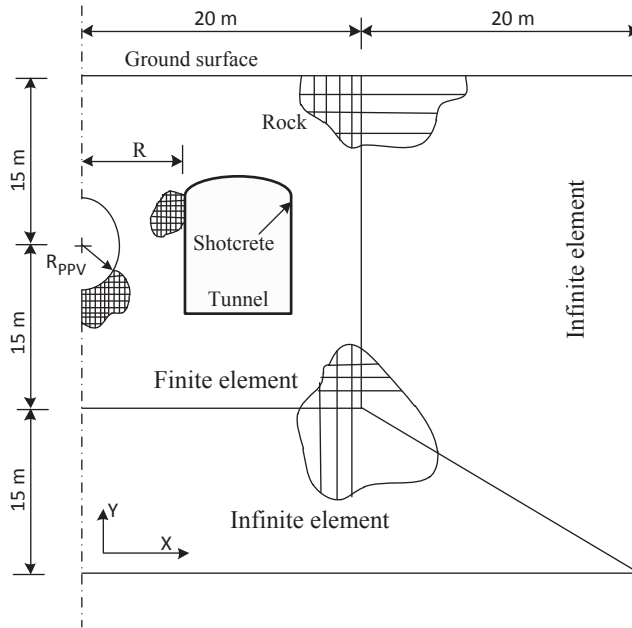


Figure 2 – Configuration of a finite element model for case (a).

5. EXAMPLES

The four examples given in the following sections are based on the material properties given in sections 2.1–3 and are valid for cases where 100 mm shotcrete is sprayed on rock subjected to stress waves from detonation of $Q = 2 \text{ kg}$ of explosives, corresponding to ANFO (ammonium nitrate and fuel oil). The radius of the loading area is $R_{ppv} = 1.2 \text{ m}$, given by Eq. (8). The density of the shotcrete ρ_{shot} is 2100 kg/m^3 and the rock ρ_{rock} is 2500 kg/m^3 . The bond strength between fully hardened shotcrete and rock is set to 1.0 MPa. The E_{shot} for the hardened shotcrete is 27 GPa while both E_{rock} equal to 16 GPa and 40 GPa are investigated for the rock. The damping within the rock material is set to 8 % and 2.5 % for the shotcrete. The rock mass is assumed to contain cracks and imperfections spaced $H = 0.5 \text{ m}$. This affects the principal frequency of the applied load, formulated as in Eqs. (4) and (7), depending on the propagation velocity c in the rock, according to Eqs. (3) and (5). The maximum value $E_{\text{rock}} = 40 \text{ GPa}$ will thus give $c = 4000 \text{ m/s}$ and $f = 2000 \text{ Hz}$ while the corresponding values for $E_{\text{rock}} = 16 \text{ GPa}$ are $c = 2530 \text{ m/s}$ and $f = 1265 \text{ Hz}$, respectively. It should be noted that both these frequencies correspond to a wavelength of 2 m and that the longest distance between nodes (element length) used for the

fine mesh of rock in the model that is 0.133 m. Thus, there are 15 first-order elements per wavelength and this number of node intervals is more than the 10 intervals that are recommended [18] for an accurate analysis. Therefore, no systematic mesh convergence studies were conducted.

5.1 Homogeneous rock

First, the propagation of the waves in rock without tunnel openings was investigated with the purpose to demonstrate the effect of material damping and the choice of elastic modulus. The finite element model here consists of rock and infinite boundary conditions without the tunnel opening. In this model, the rock mass is assumed to be either intact or fractured with E_{rock} equal to 40 or 16 GPa, respectively. Figure 3 shows the attenuation results for various particle velocity loads, measured along a horizontal line from the centre of the charge through the rock. Results obtained without damping and with the damping ratio of 8 % are compared with results from the empirical formula from Eq. (7). As seen, the results obtained with damping included are much closer to the empirical values than the un-damped cases. Also note that the curves representing the two different E_{rock} values almost coincide.

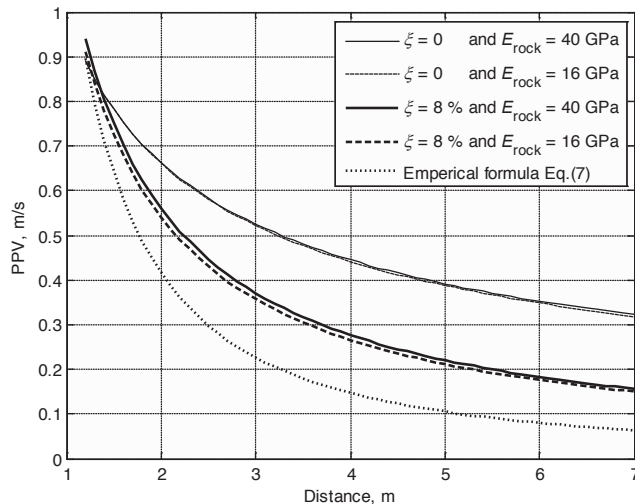


Figure 3 – Maximum PPV in the rock vs. horizontal distance from the centre of the explosive charge ($Q=2\text{kg}$).

5.2 Tunnel profile, case (a)

The results from six models of case (a), as shown in Figure 2, with distances R of 2.2, 3.0, 4.0, 5.0, 6.0 and 7.0 m from the centre of the charge are presented in Figure 4. The calculations were carried out with a damping ratio of 8 % and E_{rock} equal to 16 and 40 GPa. The results are plotted as two curves for the maximum bond stresses at the shotcrete-rock interface vs. distance. These results are compared with the results from the previously presented numerical models [7]. The curves are compiled by the maximum values from curves as those shown in Figure 5, i.e. time

histories of stresses at the shotcrete element closest to the rock surface, for the curves shown calculated for R equal to 3, 5 and 7 m. A load with $v_{\max} = 0.9$ m/s, as given by Eq. (7) for $R = R_{ppv} = 1.2$ m, was applied at the edge of the loading area.

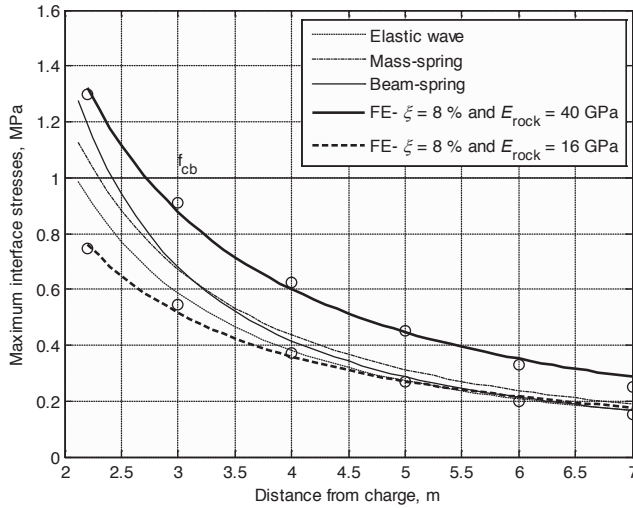


Figure 4 – Maximum bond stresses in the interface between shotcrete and rock versus distance from the centre of the explosives ($Q=2\text{kg}$), compared to previously presented results [7].

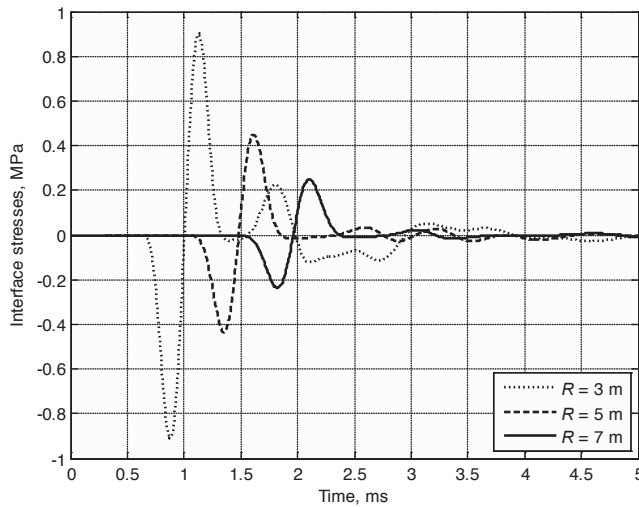


Figure 5 – Stress in the interface between the shotcrete and the rock for various distances from the centre of the explosives ($Q=2\text{kg}$). Calculated for $E_{\text{rock}} = 40$ GPa ($f = 2000$ Hz).

5.3 Tunnel plane, case (b)

This example investigates the maximum tensile stresses that occur at the interface between shotcrete and rock along the length of the tunnel when the explosion occurs in front of the tunnel face, as shown in Figure 1(b). In this modelling approach, appropriate simulation of infinite boundary conditions must be considered, here applied around the finite element of the rock, representing a horizontal section of the ground. Figure 6 shows the response of the shotcrete element closest to the rock surface and its variation along the wall of the tunnel from point A to point B (see Figure 1(b)), perpendicular and parallel to the wall surface of the tunnel.

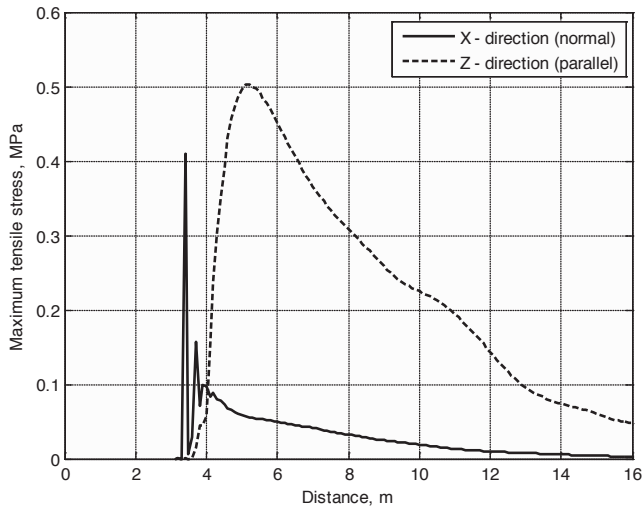


Figure 6 – Maximum tensile stresses in the shotcrete element closest to the rock along the wall of the tunnel; perpendicular to the wall of the tunnel (z -direction) and parallel to the wall of the tunnel (x -direction), for the distance $R = 3$ m, for $E_{rock} = 40$ GPa ($f = 2000$ Hz).

5.4 Young shotcrete

This last example demonstrates how the development of the shotcrete modulus of elasticity affects the stresses at the shotcrete-rock interface, i.e. the bond stress. The model used is case (a), as in the second example, but here E_{shot} is assumed to be a variable according to Eq. (7). Multiple calculations have been performed for a shotcrete age between 1 and 24 hours, for R equal to 2.2, 3.0 and 5.0 m, respectively. The results are presented in Figure 7 and compared to the bond strength curve according to Eq. (8).

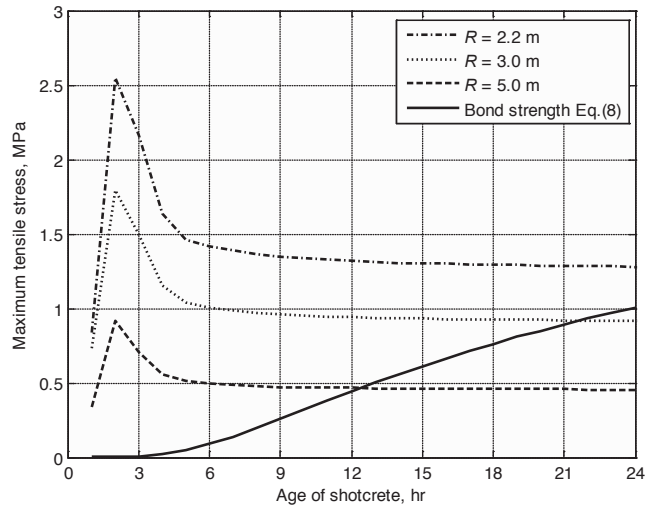


Figure 7 – Tensile stress in hardening shotcrete, at the shotcrete-rock interface. Calculated for $E_{rock} = 40 \text{ GPa}$ ($f = 2000 \text{ Hz}$).

6. DISCUSSION

The calculated results were in good agreement with observations and measurements in-situ and with the previous numerical modelling results [7]. Compared to the previous models, using a sophisticated finite element program, such as ABAQUS/Explicit, will facilitate modelling of more complex geometries and also provide more detailed results. The models must, however, also include the rock mass to provide an accurate description of the attenuation of the propagating stress waves, due to geometric spreading and material damping. For the rock mass representative average values for the modulus of elasticity must be used, accounting for the occurrence of cracks and imperfections, also in combination with a certain amount of damping that should be based on measurements in-situ. This is necessary so the attenuation of the PPV with increasing distance follows the empirical relations that often exist as a result from numerous in-situ measurements. The application of the dynamic load, i.e. the stress wave, must be done in a correct manner. The presented examples demonstrate the method here used, with a circular front of PPV applied along the perimeter of a circular area surrounding the centre of the explosives. Empirical relations are used to give the correct level of PPV. The results from the suggested type of models contain much more detailed information than the three previously used numerical models [7]. The displacement field is two dimensional and therefore the effect from both P and S-waves originating from the same event can be studied. This is highly important for cases where shear stresses will be dominant.

6.1 Examples and previous results

The effect of introducing damping was investigated in the first example. From the results in Figure 3 it is clear that the introduction of damping gives results closer to the empirical curve from Eq. (7). The latter is based on in-situ measurements and therefore includes most factors that influence the attenuation of vibration velocity with distance. In the presented examples a damping ratio of 8 % is used, based on in-situ measurements. From Figure 3, it can be seen that this level of damping does not give a perfect fit to the empirical formula and that the choice of E_{rock} has a marginal effect on the PPV levels. Parametric studies showed that a very close fit to Eq. (7) is achieved for a relatively high damping ratio of 20 %, but it is here preferred to base the damping on in-situ results. The effect of using different values of E_{rock} for the rock is demonstrated in the second example and shown in Figure 4. It can be seen that FE model with $E_{\text{rock}} = 40$ GPa gives higher stresses compared to the previous results [7] in which the dynamic load was applied directly at the interface between the rock and shotcrete. In the finite element model the stress waves propagate from the edge of the loading area, making it difficult to calculate reliable results for very short distances R . The lower value of the elastic modulus, $E_{\text{rock}} = 16$ GPa, gives a good fit to the previous results for higher values of R . Thus, when calculating stresses it is important to use a representative modulus of elasticity since this governs the relation between displacement and stresses in the material. The assumption of a good quality rock mass with a high E_{rock} will always give over-estimated, safe distances. Lower, more realistic values for E_{rock} can be used if the rock quality is well defined, allowing blasting closer to the shotcrete. It can also be seen that when compared to the bond strength f_{cb} of 1.0 MPa, the limiting safe distance is about 1.8–2.8 m, depending on E_{rock} . This can be compared to 3.2 m as given in [4] where the results are based on a higher frequency, $f = 2500$ Hz. The variation of stresses with time at the shotcrete-rock interface is shown in Figure 5. It is clearly demonstrated that the peak stress occur later for longer distances while the stress levels decrease. The effect of damping can also be seen. The wave arrives at the points of observation as a compressive stress (negative sign) directly followed by the tensile maximum, which is critical with respect to bond failure at the interface.

The third example shows a case with detonation ahead of a tunnel front and the stresses that occur along the tunnel walls, a geometry not previously studied. The centre of the explosive charge was here located 3 m from the front. This is, when compared to the results in Figure 4, a safe distance with respect to damage at the front where the vibration velocity is $v_{\text{max}} = 0.47$ m/s, as given by Eq. (7), i.e. just below the damage limit of 0.5 m/s previously defined [2]. Accordingly, no damaging stress levels will appear in this example, as can be seen in Figure 6 where the stresses parallel with the tunnel wall (z -direction) and normal to the walls (x -direction) are shown. The results show dominance by stresses in the z -direction, i.e. shear stresses. Of the three previously used numerical models [7], shear stresses could only be described by the beam-spring model. In the study of large scale blasting during mining operations [5], where stress waves reached the shotcrete in an oblique angle, a domination of shear stresses was also observed. It can be seen that the only high normal stresses (x -direction) appear locally just behind the tunnel face while the maximum shear stresses (z -direction) are situated 2 m into the tunnel. Also note that the shear stresses are present more than 10 m into the tunnel.

The last example demonstrates the variation of maximum stress at the shotcrete-rock interface as the shotcrete hardens. The results are in agreement with previously published results [6] which show that 100 mm shotcrete will never survive waves from $Q = 2$ kg explosives at 2 m distance and 4 m can be seen as the limit, which is verified here. The stress peaks that occur within 1–5

hours of age are characteristic and this phenomenon has also been observed for cast concrete. Previous investigations [19] show that hardening, cast concrete goes through a phase during a period of 3–11 hours after casting where it has a low resistance to vibrations. Here, it should be noted that the stress levels are dependent on the thickness of the shotcrete layer, where lower stress peaks are obtained for thinner layers [6].

6.2 Conclusions

It was demonstrated that wave propagation through rock towards shotcrete can be modelled using two dimensional elastic finite elements in a dynamic analysis. The models must include the properties of the rock and the accuracy of the material parameters used will greatly affect the results. However, this also means that it will be possible to describe the propagation of the waves through the rock mass, from the centre of the explosion to the reflection at the shotcrete-rock interface, also after this has occurred. Using a sophisticated finite element program with elastic models in dynamic analyses gives a relatively efficient and fast analysis process. It is acceptable to use elastic material formulations until the material strengths are exceeded, i.e. until the strains are outside the elastic range which thus indicates a material failure. It is in this case of little interest to continue the analysis for a partially damaged supporting structure. The higher complexity of this type of model, compared to the previous numerical models used [7], will make it more demanding to validate the results since the relation between input-output is more complex. The advantage is that more sophisticated geometries can be modelled. There is no immediate need to extend the modelling concept to three dimensions, as long as the area of observation is a horizontal or vertical plane.

For the future research, this type of finite element models will be used to study more realistic cases, with respect to varying shotcrete material properties and complex geometry. Cases that need focus are construction of multiple tunnels, parallel tunnels, crossing tunnels and stress waves with oblique impacts. Cases with multiple explosive charges will also be studied, aiming at finding the least damaging sequence of detonation using different delay times. The effect of additional reinforcing elements, such as rock bolts, cables and wire mesh, can also be included. Of special interest is the study of how vulnerable young and hardening shotcrete is when exposed to impacting vibrations. The goal is here to find limits for safe blasting, with respect to both shotcrete age and distance to the vibration source.

REFERENCES

- [1] Holmgren, B.J., ‘Shotcrete Research and Practice in Sweden – Development over 35 Years’, Proceedings of the third international conference on engineering developments in shotcrete, Queenstown, New Zealand, March 2010, pp. 135–141.
- [2] Ansell, A., ‘In-situ Testing of Young Shotcrete Subjected to Vibrations from Blasting’, Tunnelling and Underground Space Technology, Vol. 19, No. 6, June 2004, pp. 587–596.
- [3] Wood, D.F., Tannant, D.D., ‘Blast Damage to Steel Fibre Reinforced Shotcrete’, In: Banthia N, Mindess, S, editors. Fibre-reinforced Concrete – Modern Developments. Vancouver: University of British Columbia Press; 1994, pp. 241–250.
- [4] Ansell, A., ‘Recommendations for Shotcrete on Rock Subjected to Blasting Vibrations, Based on Finite Element Dynamic Analysis’, Magazine of Concrete Research, Vol. 57, No. 3, March 2005, pp. 123–133.
- [5] Ansell, A., ‘Shotcrete on Rock Exposed to Large-scale Blasting’, *Magazine of Concrete Research*, Vol. 59, No. 3, March 2007, pp. 663–671.
- [6] Ansell, A., ‘Dynamic Finite Element Analysis of Young Shotcrete in Rock Tunnels’, *ACI Structural Journal*, Vol. 104, No. 1, January 2007, pp. 84–92.
- [7] Ahmed, L. and Ansell, A., ‘Structural Dynamic and Stress Wave Models for the Analysis of Shotcrete on Rock Exposed to Blasting’, *Engineering Structures*, Vol. 35, February 2012, pp. 11–17.
- [8] Ahmed, L. and Ansell A., ‘Laboratory investigation of stress waves in young shotcrete on rock’, Accepted for publication in Magazine of Concrete Research, 2012.
- [9] Chang, Y., ‘Tunnel Support with Shotcrete in Weak Rock- a Rock Mechanics Study’, PhD thesis, Division of Soil and Rock Mechanics, Royal Institute of Technology (KTH), Stockholm, Sweden, 1994, 166 pp.
- [10] Bryne, L.E., Holmgren, J. & Ansell, A., ‘Experimental investigation of the bond strength between rock and hardening sprayed concrete’, Proceedings of the Sixth International Symposium on Sprayed Concrete, Norwegian Concrete Society, Tromsø, September 2011, pp. 77–88.
- [11] Bieniawski, Z., ‘Determining Rock Mass Deformability: Experience from Case Histories’, *International Journal of Rock Mechanics and Mining Sciences and Geomechanics abstracts*, Vol. 15, 1978, pp. 237–247.
- [12] Persson, P. A., ‘The Relationship between Strain Energy, Rock Damage, Fragmentation, and throw in Rock Blasting’, *Fragblast – International Journal of Blasting and Fragmentation*, Vol. 1, January 1997, pp. 99–110.
- [13] Nakano, N., Okada, S., Furukawa, K., Nakagawa, K., ‘Vibration and Cracking of Tunnel Lining Due to Adjacent Blasting’, Proceedings of the Japan Society of Civil Engineers, 1993, pp.53–62. (In Japanese, Abstract in English).

- [14] Kendorski, F.S., Jude, C.V., Duncan, WM., 'Effect of Blasting on Shotcrete Drift Linings', *Mining Engineering*, Vol. 25, No. 12, December 1973, pp. 38–41.
- [15] Dowding, C.H., 'Construction Vibrations', Upper Saddle River: Prentice-Hall, 1996, 610 pp.
- [16] Paz, M., 'Structural dynamics. Theory and computation', 3rd Ed., Van Nostrand Reinhold, New York, 199, 626 p.
- [17] Sun, X. and Sun, J., 'Research on the Damage Fracture of Rock Blasting Based on Velocity Response Spectrum', *Applied Mechanics and Materials*, Vol. 105-107, 2012, pp. 1521-1527.
- [18] ABAQUS User's Examples and Theory Manual, Version 6.10, Simulia, Providence, 2011.
- [19] Ansell, A., Silfwerbrand, J., 'The vibration resistance of young and early age concrete', *Structural Concrete*, Vol. 4, September 2003, pp. 125–134.

Lessons Learned – Swedish Design and Construction of Industrial Concrete Floors



Jerry Hedebratt
M.Sc., Licentiate of Technology
Tyréns
Peter Myndes Backe 16
SE-118 86 Stockholm
E-mail: Jerry.Hedebratt@tyrens.se



Johan Silfwerbrand
Professor, President
Swedish Cement and Concrete Research Institute (CBI) and KTH Royal
Institute of Technology
Drottning Kristinas Väg 26
SE-100 44 Stockholm
E-mail: Johan.Silfwerbrand@cbi.se

ABSTRACT

Long term studies on several industrial floor productions show where typical damages occur, highlighting common design and construction flaws. Development of the building process has brought new demands in the exaggerated hunt for low cost and profit; often the purpose of building floors is lost in the process. The main part of the pile supported slabs in this study was cast with reinforced steel fibre concrete. These floor slabs is investigated for damages. After a few years of usage a detailed study was made on floors that were completed the preceding 5 years before 2006. Now in 2012 a follow up-study is made. Possible ways of increasing the quality and the experience with new Swedish recommendations from 2008 are discussed.

Key words: Long term studies, design criteria, pile supported floors, steel fibre concrete, damages, integrated design and construction.

1 INTRODUCTION

1.1 General

Industrial floors are commonly constructed with concrete. Problems with cracking, curling and damaged joints are not only most difficult for the client to treat but are also difficult to repair with a durable result. The licentiate thesis of Hedebratt [1] deals with the development of an integrated method for design and construction of industrial floors. The thesis work and results are discussed. A wide range of industrial, commercial and house building projects where concrete floors have been constructed with steel fibre concrete or in a combination with steel or steel mesh only, have been designed by the first author. The floor design, construction and the resulting floor are discussed.

1.2 Aims and limitations of the article

The aim is to briefly present the authors' experiences of floor design and construction and to conclude lessons learned from the past years.

2 INTEGRATED DESIGN AND CONSTRUCTION OF INDUSTRIAL FLOORS

In the licentiate thesis [1] a proposal for integrated design and construction of industrial floors was developed. A design process that integrates the construction process of industrial floor must fulfil some basic demands:

- add cost and time efficiency
- be value adding
- minimize waste
- minimize occurring damages
- return improvements in future processes

The cost and time reduction should give advantages and revenue for each part in the value chain to get all actors interested to work in an integrated manner with the joint project. If the design and construction process integrates without adding value or even decreasing the value, the client gets *less bang for the bucks*, which is of no one's interest and least of all for the client. Therefore the process must be value adding, and also resulting in a distinguishing mark of the actors that – *less is more*. Using such a manner i.e., the Toyota method, states that all waste (material, time and time-laps etc.) in the project must be reduced. To improve the quality and be able to add value also the occurring damages must be minimised. And to further develop and build even better with less energy, time and environmental footprint spent on each new project, the integrated design and construction process must return improvements for future building processes.

2.1 Long term studies on real projects

Through studies on used demands on industrial floors and more or less frequently occurring damages, ideas have developed to perform further and more detailed studies. Parts of the pilot studies, which were preceded by three years of studies, are presented in a licentiate thesis [1].

Three industrial floors were instrumented (let's call them a, E and I); it was investigated where efforts in design and construction are most efficient for the quality of the floor. A first pilot study aimed to investigate the effects of floor shrinkage and shrinkage cracking that is a frequent problem in industrial concrete floors. The measuring of slab shrinkage would be a way to verify methodology improvements. A minor part of an industrial floor was studied constituting of a high racking storage on approximately 3 000 m² of the total of 21 500 m² slab on gravel. The floor was constructed for Company E which built and own the central distribution centre at Svista industrial estate in Eskilstuna, Sweden. The floor (a), is of type slab on grade with steel fibre concrete, (SFC), on a compacted layer of blast rock filling. Floor projects and companies are denoted as in table 1, provided they are of type slab on pile, with small letter they are of type slab on grade.

A second pilot study for the new wholesale trade, built and owned by (contractor E/ client E), in Tumba, Botkyrka municipality, Sweden, proceeded in the same way but this time the measuring

was made automatically for parts of the floor. A larger part of an industrial floor was studied. Slightly more than half of the floor consisted of pile supported floors and the remaining part of slab on ground, the total floor area was approximately 30 000 m². The floor is constructed of steel fibre concrete or a combination of steel fibre concrete and reinforcing bars.

An integrated method is based on co-operation between the participants in the building process, education, improvement of guidelines, control and measurement together with follow-ups. With a proposal for an integrated method a third pilot study started, where selected parts of the method were used in a sharp project, to improve partly in the design but mostly in the construction of a medical research centre for company H, Gärtuna in Södertälje, Sweden. The building area of approximately 7 000 m², equalling half of the building, constitutes of a slab on ground. A strip reinforced steel fibre concrete floor slab was constructed over the piled part. The integrated design and construction method was aimed to involve the floor production team in the design process together with meetings with the main contractor, the floor contractor and the owners' representative and consultants. A meeting was arranged where the two authors had a "crash course" in floor design and construction damages on floors. Also in the building process it was expressively marked that the production team should come up with ideas for change of solutions or construction during preparation of work and in the production. Some ideas won interests and become incorporated in the design, i.e.:

1. Design the floor with even thickness over most part of the floor instead of making haunches. This makes the reinforcement work and pouring of concrete easier.
2. Design the floor with even thickness over most part of the floor instead to make the installation of heavy equipment i.e. laboratory machines easier.
3. Cast the thick slab areas of concrete in layers that later are vibrated together.
4. Use bent bar stirrups, i.e., cat's-feet instead of reinforcement beams.
5. In the transmission between thinner slabs and thicker slabs the slab is designed with a thickness that is gradually increasing using a longer slope of the graded material instead of 45 degrees inclination to make a haunch.

Measurements of floor shrinkage and shrinkage of prismatic reference beams were performed from moment of pouring of concrete, during the curing and until 224 days of maturing. Also the humidity and temperature were logged.

The extent of the thesis [1] involved detailed studies on design and construction, dialog and meetings with the worker team, worker team leaders, project leaders and designers in industrial building projects together with literature studies for planning of experiments and analysis of results. For limitation the measuring studies were directed towards shrinkage, temperature in air and in the floor together with air humidity. The analysis of every pilot study includes assessments of results from measured data and diagrams and also a damage analysis and structural analysis.

Some concluding remarks show that:

- overwhelmingly shrinkage movements (after 224 days in level of the code values for final shrinkage) may occur in the floor and that
- the shrinkage of concrete varies considerably (200 to 1200 μ -strain)
- measurements prove that the concrete creep is large in early stages
- the quality of the industrial floor is largely dependent on the participant's competence

- co-operation in the construction process may lead to solutions that are more effective and less expensive in design, material selection and increased flexibility for the contractor and the client
- *The Integrated design and construction method* is a step in the right direction and works as intended.

Several proposals for future research turned-up during the time of the studies:

- long term effects for pile supported steel fibre concrete slabs.
- steel fibre concrete slabs or combined reinforced slabs, how are they working statically and dynamically and what is happening when severe cracking occurs?
- the load concept on floors – how is it perceived and how is it used?
- how is the quality in the building process of floors influenced by the human factor?
- further development of the integrated method for design and construction of industrial floors is needed.

The first three suggestions were later forming the base for continuing PhD studies and full scale tests of a pile supported floor [6, 7, 10, and 11].

2.2 Development of the construction process

Over the recent years concepts as *Lean Construction* have been developed for the building construction industry. The ideas have until today not been up for discussion in general floor construction. *Lean Construction* an origin from the Toyota Company's development of the car manufacturing process has now come to be of large interest in the Swedish construction industry. By using 3/4/5D models and Building Information Models (BIM) to plan, adjust and visualise the building and the construction process. Especially when constructing complex structures the buildings are constructed more efficiently with fewer damages and less waste. BIM therefore adds more value to the process. The insight of where structural problems (collisions) and where difficulties and bottlenecks in construction and planning occur is helpful for everyone wishing to perform better in one or another way.

The floor industry has anyway dealt with the production problems "as they occur". Needs of increasing the production speed has developed new techniques for spreading out concrete and to screed the surface. The slow and un-healthy heavy work with placement of reinforcement bars and meshes has brought wishes of ready mix reinforced concrete to the introduction of steel fibre concrete, (SFC) also referred to as steel fibre reinforced concrete (SFRC). The development has been fast and maybe not always so thoughtful. The designs open up for low cost construction techniques where the production cost is minimized and have often won over more serious and long lasting designs. In other words "*Quantity has often won over quality*" even with small differences in the total production costs. This was also the problem in early car production where the mass production techniques ruled.

If the acting companies constituting the value chain for floor construction co-operates with the ordinary construction process (one step above in the chain) and with help of the thoughts and almost religious believe in the *Lean Movement* probably 50 % cost savings could be the results for everyone and the double profit could be a fact [5]. A change agent in the floor business has been the technical platform that comes with the steel fibre concrete concept; another has been the use of laser levelling and laser screed equipment for compacting levelling and placing of floor concrete and screed. Now rather the companies have problems with management when the

concrete workers have less involvement in the total construction process of the floor and become more specialised. The mass production followed by a “leaner” building process of floors that before was the bottleneck has minimised each work team’s time spent on each square metre of floor. The faster production has also led to the fact that the management becomes rather overloaded and a bottle-neck in the construction process.

3. DESIGN FOR LOW COST

The actors in the construction process pay more and more attention for keeping the total building cost low, meaning fast and just-in-time production with low cost material. Buying the subcontractors and materials abroad is one solution, another is to redesign to match the construction methods and cheapen design and construction solutions.

3.1 Designing for increased productivity

Often less reinforcement is a great concern for the contractor wanting to increase the productivity. The reinforcement work is often heavy, slow and considered to be costly. On the other hand, reinforcement is not often placed in excess of the structural needs therefore the possibilities to decrease the amount of reinforcement is small. Furthermore, it is a fact that in common floor designs less reinforcement than the actual need is placed in corners, edges and at other critical positions of the concrete floor slab.

Typical methods to design quality floors with high productivity in the construction phase:

1. Adding steel fibres to the concrete.
2. Avoid haunches and other thickness deviations.
3. Use stiff and adjustable stop ends in dilatation joints with tight tolerances.
4. Install as few joints as the construction method allows for providing that the reinforcement ratio is sufficient.
5. Proportionate as workable concrete as possible, that will perform well in the spreading, screed and power floating moments (without getting to thick laitance layer, no segregation and short waiting time between the working phases).
6. Open space design allows for larger and therefore more efficient equipment and less disturbances.

Less traditional reinforcement may be considered by adding a moderate content of steel fibres for structural reinforcement and crack control. Of importance is that even when the fibre dosage is significant there is a need to strengthen parts of the slab with reinforcement mesh and bars that seldom could or should be avoided.

Steel fibre concrete is common in concrete floors. The floor slabs could be pile supported or placed on graded material. In the case of foundation on compacted graded material of good quality the need of reinforcement becomes less. For foundations with pile support the need of reinforcing the slab concrete is usually present at strained sections. The need for reinforcement is due to structural safety and strength of different sections. Primary the sheared sections around pile-head are to be controlled for punching and bending moments, also straight yield lines may become dimensioning. However, if the slab also cracks due to insufficient stress redistribution the possibility to have wild and wide cracks lead to other geometric boundary conditions with considerable more severe moments and shear actions for the floor slab to handle. The need of

crack control becomes obvious. A steel fibre only solution is interesting in many perspectives but lacks to prove the long term properties. If designing today with scientifically tested design methods, only elastic properties of fibre concrete could be used for serviceability limit state. The long-term performance of fibre concrete structural solutions are not yet determined; but could be evaluated with experimental methods [10, 11]. Even if advanced SFC design and construction techniques exist they may not covering all design criteria's that ought to be considered in some cases.

Combined reinforced floors have been common in Sweden since the beginning of 2000. Over 40 floor productions had 2006 successfully been constructed in both small and larger projects where the total area built is over 400 000 m². The fibre content has most often been 35 kg/ m³ of Dramix RC/65-60-BN. In one reported case the contribution to time saving was 50 days for a combined solution relative the traditional steel rebar solution that should take 75 days according to the best bid (DHL, Örebro, 2004) [6, 7]. In floors undertaking more severe conditions (impenetrability, free of cracks, large area pouring and severe restraints) up to 50 kg/m³ have been used. The requirements have led to residual strength factors between 60 % and 80 % and the pile distance has been 2 to 7 m where the average is 4.5 m [7].

3.2 Damages and discrepancies in various projects

Table 1 inscribes approximately 5 % of all pile supported floors designed and constructed in Sweden during the years 2001-2006 and that are designed at Tyréns by the first author. The 25 floors are mostly combined reinforced but substantial parts are also steel fibre concrete floors without conventional reinforcement of structural type slab-on-grade. The projects, cities, floor area, Client, consultants and contractors and year of building are given in the table. For consideration sake of the actors of other companies than Tyréns the names are un-identifiable.

1. The first floor at project A, Gothenburg (built 2001) initiated the combined reinforced floor system (Bekaert FOP) in Sweden. The floor was rather difficult to reinforce and had a triangular shape and steel columns penetrating the concrete surface without isolation joints. The cracks around the restraining columns were rather wide, also a narrow section had been broken and showed visible through cracks shortly after construction.

2. The English property developer B built a car manufacturing facility for a new car model in Trollhättan, Sweden (built 2001/2002). The work with placing concrete was troublesome for the floor contractor B because this was planned to start prior to New Year 2001 (at -5°C outside). A large tent placed over the nearly frozen ground could with help of fan heaters increase the ground and air temperature, see *Figure 1*. Only for one slab section the concrete reported to become frozen. At some gate framings the floor was not isolated for preserving free movements. The edge beams were only mechanically attached to the floor with thin steel wires allowing for elastically restraint possibility for shrinkage movement. No severe cracking or other damages were reported before 2006. In October 2009 the first author was contacted by a consultant engineer that made a Technical Due Diligence for the property owner. The consultant had noticed cracks in the floor also in unloaded free movement areas and wanted information about the load capacity and if the cracks were hazardous for the usage of the floor. We could conclude that the floor had reinforcement in strips and that the cracks had developed in yield lines as the design method suggests and that the load capacity remains as designed.



Figure 1 –Placing of concrete over the preinstalled reinforcement in strips was trough the tent roof. Here the last moments before power floating, placing of the hard concrete screed using a LASER ARM® laser screed machine and manually bull-floating the surface of screed (2).

3. At the project C, a Central Distribution Centre in Hallsberg (built 2002) the pile deviations were extreme with up to 1.5 m, partly because of large conduits disturbing the sub layers. A serious redesign of the floor, from real measured pile positions, added about one rebar with diameter 16 mm per 100 mm deviation. No severe cracking or other damages reported were reported before 2006.

4. At the project D, Jönköping (built 2001) the slab span over 6 m from pile to pile with pile depth up to 110 m. The flooring was relatively stiff marble clinker tiles. No cracking or other damages has been reported before 2006. At a meeting with a consultant engineer in October 2009 he reported that there was cracking in the visible concrete floor in the back storage but there was no signs of damages in the sales areas that has clinker tiles. The engineer had been consulted regarding actions for crack repair. The first author has verified the cracking in spring 2010 to be located to yield lines in mesh reinforced areas with slab thickness 250 mm, the mesh has bar diameter 8 mm, spaced 200 mm. The fibre concrete floor has all been covered with tiles in mortar.

5. The whole sale trade, project E (built 2002), was mainly cast during summer time. Parts of the slabs were instrumented in a pilot study that was running besides the consultant commission by the first author. The floor concrete shrinkage was measured and the overall performance of the slabs was studied. After 224 days the slab shrinkage was nearly 300μ –strain. The free shrinkage of concrete was about 600μ –strain. At many edges and corners the parts that are slab-on-grade have some large cracking exceeding 0.5 mm. The pile supported slab that is thicker has only a few cracks caused by divergent joint division (partly not rectangular).

6. From the project F, Örebro (built 2002) and 7. Project G, Malmö (built 2002) no damages are reported.

8. From project H, Nykvarn (built 2002) no damages are reported. The first author visited and inspected the floor in August 2003. The day joints had opened about 5 mm and there were no visible damages.

9. At the project V (built 2002) the half part of 8 000 m² consist of slab-on-grade and the rest of pile supported floor. Even though the pile supported slab in *Figures 2 and 3* was 400 mm thick some edge rising were measured. Two different types of damages could be found, cracking at the crossfall of the scuppers (a thickness reduction at the discharge wells with-out water trap) and restraining joints caused of erroneous assembling. In 2010 the managing design officer Kenneth Douhan, Tyréns, only had revived the owners' good feedbacks.



Figure 2 –The concrete is placed in layers due to its thickness 400 mm. It was windy inside due to uninstalled facade windows, but this fact did not seem to impair the quality in this case (9).



Figure 3 – Placing of the hard concrete screed using a LASER ARM laser screed machine in the narrow environment between precast concrete columns in this heavy building (9).

10. At project J, Haninge (built 2002), the pouring was outside at autumn; below freeze temperatures and snow was covering the slab just the day after casting. No severe cracking or damages are reported probably due to the fact that the flooring constructed at spring time consisted of clinker tiles in mortar.

11. Project K (built 2003), an shopping centre has floors and edge beams of SFC. No damages have been reported. The first author has several times visited the finished shopping centre during the years and may confirm this by the latest visit in August 2010. He has talked with the managing design officer from consultant company H, which only has heard good reports from the contractor.

12. The floors at project L (built 2003) in Gothenburg and also 13. project M (built 2003) in Gothenburg (Do-It-Yourself stores) have been up for discussions and damage investigations because of their individual damages. Initially the projects were meant to have the same flooring system and both of them situated on the Beach of Gotha River, having subsoil's consisting of deep clay.

The project L (12.) had problems even before start. The contractor would not allow the floor-layer to vibrate the concrete because this procedure was not usual in Germany, with their concretes. The reinforcement grid was turned 45 degrees which prolonged the pile distances with 42 % but also increased the overall reinforcement ratio with the same value (in this case an advantage as the moment involves the span in square and the reinforcement was increased linear). The floor was poured with handheld laser and bull-floater. Because of the denser reinforcement and the excluded vibration the fibre concrete did not fill the voids under the grid of reinforcement and therefore the concrete probably lacks 20 % of the initially meant concrete strength.

The store manager of project M (13.) that mostly and with exaggeration had seen the clients (L) stores in Germany that was up to the roof loaded with palletized goods (building materials) soon, and probably too soon after the floors were installed, locally filled up the racking and floor areas with 7-16 times the design value. Also the long-distance lorries were driven into the building onto the pile supported floor to speed-up the discharge, according to the shop manager in charge. Both actions were way to much overloading the floor. Shortly after wide and wild cracking could be seen and were developed mainly at yield lines following the dimensioning yield pattern but also other following in near the dilatation joints. The crack openings were 1-5 mm after 3.5 years and in August 2010 this was almost doubled. Also the dilatation joints were opened to 12-20 mm in 2010.

14. From project N, Kungälv (built 2003); no reports have been heard regarding this floor.

15. Client L also built a Do-It-Yourself store in Västerås, project O (built 2003), that with the same solution and almost the same floor plan as in Gothenburg (13) the same year. The difference was a much stiffer but anyway piled sub layer. The floors were loaded at same magnitudes and in the same way which resulted that the floor developed similar yield cracks, circular and straight ones (as expected by the designer). As the sub layer is rather stiff with a limited depth to bedrock the slab rests on the ground. This has been measured through the dilatation joints, during several years as the first author lives in Västerås and frequently visits the store. The joint openings were about 5-10 mm after 3 years but are now in 2012 about 10-20 mm.

16. From the project P (built 2004), a central distribution centre, there is reported problem with cracking. The amount and size of them are not known. Insufficient function and dilatation joint are expected to be the problem as this was observed already to some extent already at construction.

17. At the Contractor P's construction of a ware house for a distributor in Norrköping (built 2004), only minor problem with levelness was reported in 2006. This was further confirmed by Anders Nilsson, Logistic Contractor in a floor seminar held 26-27 October 2010 at Swedish Cement and Concrete Research Institute (CBI) which had no more reports to share.

18. At the project R, in Kålered (built 2004), granolithic surface delamination was observed already at the final inspection that occurred in December 2004. A probable cause was the faulty supplies of concrete with lime stone filler (according to the floor contractor) and evidently too much content of the super plasticiser Carboxylate (double dosage according to concrete supplier). A layer of white powder was found under the granolithic surface. This layer was observed in the end of January 2007 when the first author made an in-situ inspection of the floors and also made sampling which was handed over to Swedish Cement and Concrete Institute (CBI) for analysis. The white powder, between the delaminated granolithic layer and the structural concrete, was tested with x-ray diffraction. The test measures the mineral composition. The granolithic surface has a completely different mineral composition than the aggregates used in Swedish concrete as the material origins from Italy; the sample was shown to be from Swedish bed rock.

Also some cracking was found in the yield lines, straight along the reinforcement and as circular ones above the piles. The segregation of concrete probably caused settlement crack above reinforcement and flotation of fines (from aggregates and cement slurry) which accumulated under the power floated surface. An expected difficulty when pumping fibre concrete may have

triggered the supplier to add too much of super plasticiser causing the segregation. The contractor and the concrete supplier has later in November 2008 agreed in comprise (settlement) before legal actions.

19. The project S (car part retailer) distribution centre (built 2004) in Strängnäs had no reports made before 2006. In several occasions the first author has come back to the facility owner Client E/ Contractor E that has nothing to complain about the floor quality. Later, in 2008, the client came back to Tyréns with a question concerning local strengthening of the floor to install automatic ware handling equipment (Maxi Packer). At that time an in-situ inspection was made with no damages to report.

20. The project T, a warehouse (built 2005) in Sundvall, has reported that the floor suffer of severe cracking and bad flatness tolerances before 2006. Later, in 2007 a second extension was built where the same floor system was inquired for. The floor design calculations were performed by the first author and submitted to the head designer G. No reports have been heard about the extension.

21. In the project U (built 2005), the 2 400 m² pile supported slab on pile for client S central distribution centre for food supplies were built completely restrained. The loadings came from 22 m high racking and automatic cranes and also the structural framing of the building. This forced the slab to take large actions from loads. The floor was about 24×100 m and subdivided by three work joints. The slab was also charged with tightness requirements and therefore cast on a sub layer of friction material and heavily fibre reinforced (50 kg/m³ RC-80/60, C40/50, reinforcement in grid over piles and in other critical sections) No cracks were reported after 1.5 year. No reports have later come to the first author's knowledge.

22. Project V (built 2005). A larger book publishing house (client T) wanted a sorting and distribution centre in Rosersberg and chose a white granolithic floor to save energy costs. Client E/ Contractor E that construct, own and manage properties have a long experience with concrete floors; was the building proprietor of the ware house. The earlier positive experiences of the combined reinforced fibre concrete floors made it their clear choice. After some months settings of ground were reported, after the temperature of the premises was raised, and the building shell completed. One slab had settings of nearly 50 mm in parts where the slab hang out over the piles, here the support consisted of ground only. In some sections, cracks have developed caused by restraining gate framings and columns due to insufficient shrinkage isolation. No reports have later come from this project.

23. Client X made an extension for the store located in Barkarby in 2006. Client X has had some problems with the joint system that has shown a broken rubber seal in aisles where the truck traffic is more frequent. No other reports have been heard about this extension before 2006. In 2010 and 2011 the first author has been involved in another extension beside the previous one. The faulty rubber seal was still a problem and the joints where reconstructed. No other damages on the floor could be found in an in-situ inspection in April 2011.

24. The actors in the project X (built 2006) in Norrköping have not reported any damages.

25. From the project Z (built 2006), a distribution centre in Rosersberg, the floor contractor has reported one crack in total of 19 000 m². The contractor seemed very excited about the floor quality. No reports have later come from this project.

Table 1 – Some Swedish projects designed and constructed as pile supported floors at Tyréns AB, 2001-2006, [1, 6] .

No	Project Name	City	Area in 1000 m ²	Client	Head design/ floor design	Contractor/ Floor contractor	Year
1.	A	Göteborg	0.6	A	A/Tyréns	A/B	2001
2.	–B	Trollhättan	22.0	B	C/Tyréns	C/B	2001- 2002
3.	C	Hallsberg	10.0	C	C/ Tyréns	C/B	2002
4.	D	Jönköping	8.	D	D/Tyréns	D	2001
5.	E	Botkyrka	28.6	E	E/Tyréns	E/B	2002
6.	F	Örebro	3.3	F	F/Tyréns	C/B	2002
7.	G	Malmö	5.0	G	G/Tyréns	C/F	2002
8.	H	Nykvarn	6.0	E	E/Tyréns	E/B	2002
9.	I	Gärtuna	8.0	H	/Tyréns	D/B	2002
10.	J	Haninge	3.0	I	G/Tyréns	F	2002
11.	K	Strömstad	25.0	J	H/Tyréns	D/ B	2003
12.	L	Göteborg	18.0	K	I/Tyréns	G	2003
13	M	Göteborg	10.5	L	G/Tyréns	H/B	2003
14.	N	Kungälv	5.0	M	J/Tyréns	I	2003
15	O	Västerås	10.5	L	G/Tyréns	H/B	2003
16.	P	Mosås	25.0	O	E/Tyréns	C/B	2004
17.	Q	Norrköping	17.0	P	K/ Tyréns	J/ B	2004
18.	R	Kålered	5.0	Q	L/Tyréns	K/ B	2004
19.	S	Strängnäs	10.0	E	E/Tyréns	E/B	2004
20.	T	Sundsvall	17.0	R	G/ Tyréns	H/ L	2005
21.	U	Göteborg	2.4	S	M/Tyréns	M/ B	2005
22.	V	Rosersberg	6.6 of 20.0	T	E/Tyréns	E/B	2005
23.	X	Barkarby	2.5	R	G/ Tyréns	H/ L	2005
24.	Y	Norrköping	4.0	U	D/ Tyréns	M/ B	2006
25.	Z	Rosersberg	19.0 of 36.0	V	E/Tyréns	E/B	2006

Table 2 – Properties and damages for the pile supported slabs in Table 2. The top-reinforcement n and the bottom-reinforcement n' are placed in strips. By using brackets means that the reinforcement has stirrup, otherwise non-existent, \emptyset = round and # = square pile caps.

No	Properties							Damages reported		
	Thick-ness t [mm]	Pile span l [m]	Pile cap [m]	Concrete class	Fibre content [kg/m ³]	Reinforce-ment [$n+n'$, mm]	Service load [kN/m ²]	Year	No of types	Description of damages, notices.
1.	260	4.0	\emptyset 0.6	K35	35	[8+4], Φ 12	15	01-06	2	Restrained columns, cracks at narrow sections.
2.	300	3.0×3.0	\emptyset 0.6	K30	35	3+3, Φ 16	50	06-12	1	Shrinkage cracks in yield lines in unloaded areas.
3.	240	3.5×3.5	\emptyset 0.6	K40	40	5+2, Φ 16	15.3		0	
4.	300	5.7×5.7	\emptyset 0.7	K35	35	[9+9], Φ 12	4.0	06-12	0	None reported in SFC slab, only were used mesh.
5.	270	4.6×5.1	\emptyset 0.6	K35	35	7+3, Φ 16	20	06-12	1	Few restraint shrinkage cracks
6.	250	3.7×3.7	\emptyset 0.6	K35	35	6+3, Φ 16	30		0	
7.	210	5.3×4.9	#0.6	K35	35	5+3, Φ 16	4		0	
8.	250 270	3.9×4.8 4.5×5.1	#0.6	K35	35	5+3	15		0	
9.	400	2.0×2.0 4.55×4.55 6.0×6.0	#0.25 #1.07 #1.07	K35	35	4+2, Φ 16	29.6 23.6 15.1	02-06		Cracking at cross falls of scuppers, and cracking at restrained joints.
10.	215	4.15×4.15	\emptyset 0.6	K35	35	6+3, Φ 16	7			
11.	210 180	4.0×4.0	\emptyset 0.6	K35	35	5+3, Φ 16	10 4			
12.	300	4.9×4.9	\emptyset 0.6	K35	35	13+7, Φ 16	30	03-06	2	Cracks in yield lines, some severe parallel with joints.
13.	200	3.5×3.5	\emptyset 0.6	K35	35	2+2, Φ 16	12	03-06	1	Cracks in yield lines, some severe parallel with joints.
14.	280	3.8×3.8	\emptyset 0.6	K35	35	7+3, Φ 16	30			
15.	200	3.5×3.5	\emptyset 0.6	K35	35	2+2, Φ 16	12	03-06	1	Cracks in yield lines.
16.	220	4.0×4.0	\emptyset 0.6	C28/35	35	2+2, Φ 16	15	04-06	1	Cracking is reported.
17.	230	3.7×3.7	\emptyset 0.6	C28/35	35	8+4, Φ 16	35	04-06	1	Levelness problems.
18.	290	5.0×5.0	\emptyset 0.6	C28/35	35	9+4, Φ 16	20	04-06/07	2	Settlements cracking and surface delamination.
19.	200	3.0×3.0	\emptyset 0.6	C28/35	35	4+2, Φ 16	20			
20.	180 200	4.0×4.0	\emptyset 0.6	C28/35	35	2+2, Φ 16	5 13	05-06	2	Severe cracking and flatness problems.
21.	300	3.0×3.0	\emptyset 0.6	C28/35	35	5+2, Φ 16	29.4			
22.	230	2.8×3.0 3.8×3.9	\emptyset 0.6	C28/35	35	4+2, Φ 16 5+2, Φ 16	32.0 15	05-06	2	Some cracking at restraints. Settlement of foundation.
23.	200	3.0×3.0	\emptyset 0.6	C28/35	35	2+2, Φ 16	15	05-06	1	Problems with joint bridges.
24.	260	3.45×3.45	\emptyset 0.6	C28/35	35	5+2, Φ 16	30			
25.	300	5.5×5.5	\emptyset 0.9	C28/35	35	12+6, Φ 16	20			

3.3 Designing for increased quality

High quality design may be adding features that lead to less disturbance of end user production, less maintenance and perfect surfaces, often in means of low deviation in flatness and levelness. Also features as floor surfaces free of joints, cracks, tracks and truck marks from black tires or light emission add quality. Of special interest is low or excluded wearing down of joints and corner and edge cracking. Proper low cost measures to introduce when increasing the quality may be to:

1. Use well proportionated floor concrete
2. Place concrete only on well compacted and levelled sub layers and ground surface with low tolerance deviation.
3. Be sure of careful measuring of thickness and concrete level at placing, levelling and power floating.
4. If possible, use hard concrete screed in light colour (granolithic concrete).
5. Mark-free screeds (or tires).
6. Careful triple curing.
7. Give feedback to involved actors.

Of the above actions: 1. will result in low deviation in flatness due to less setting of concrete. 2. will result in less compaction of the graded material and even thickness of structural concrete. 3. will if the measuring instruments (lasers) are positioned near and set to low tolerance give a full control of the thickness, levelness and flatness. 4. brings by low cost per m² a compact, impermeable solid enclosure of the surface that is durable, hard and light emitting. The later also bring the features of low cost for illuminating the facility. Up to 95 % light reflecting has been measured in the USA [2]. the fifth issue (5.) gives the floor a non-marking surface at use of any tires, black, grey or white, white screed will result in less maintenance, less energy consuming (environmentally right) and a cleaner look [2]. 6. the easiest way to obtain less cracking, less curling and a harder and stronger concrete in surface and structural concrete is proper curing. By extended triple curing, i.e., use of curing agent (membrane), water and fully taped covering with plastic sheets covering more than 14 days, a proper curing is secured. 7. share experiences and give objective positive and negative feedback to increase involvement and interest of the final product.

4. LESS JOINTS GIVE LESS PROBLEM

Truck traffic over joints in free movement areas and in especially narrow aisles where the joint openings are large gives problems with cumulative damages: i.e., degradation and wear of joint edges and trucks becomes damaged. Avoiding joints is not always easy. When it comes to traditional reinforcement with steel mesh the day-stages are relatively small, about 100-250 m².

Using a combination of steel bars and fibre concrete (combined reinforcement), or steel fibre only, opens up for solutions with large day stages, often about 900 m², or in extreme floors free of joints (jointless floors) larger than about 2500 m². When comparing the reinforcement solutions a significant quality improvement is found in wider subdivision of the floor and therefore the combined reinforcement method is preferable for pile supported floor slabs (and slabs on grade).

The steel fibre only solution for slabs-on-grade always has a need of reinforcement in edges, corners and around columns etc. if optimizing the floor thickness.

4.1 Optimum joint spacing?

A subdivision of joints at $4 \times 4 \text{ m}^2$, gives 8 m joints per panel, increasing the subdivision to $20 \times 20 \text{ m}^2$ gives 40 m joint per panel etc. In a $10\,000 \text{ m}^2$ square floor the total joint length is shown in *Figure 4*, rectangular, anomaly shaped floor plan and larger floors may give other joint lengths.

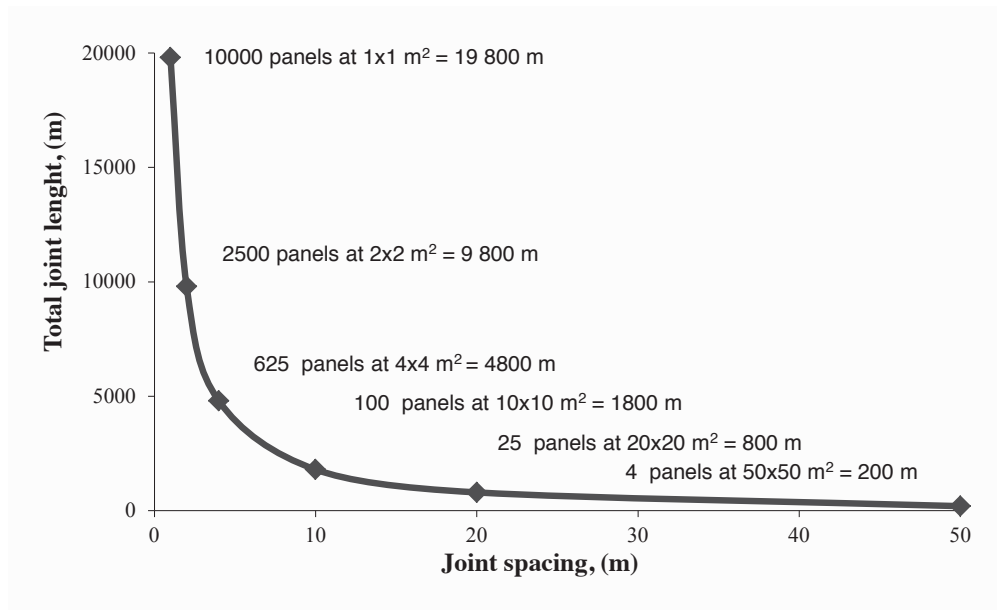


Figure 4 - Relationship between utilised joint spacing and resulting total joint length in a $10\,000 \text{ m}^2$ square slab.

Redesigning from $10 \times 10 \text{ m}^2$ joint division to $40 \times 40 \text{ m}^2$ means using only 17 percentage of the latter joint length and of course an 83 percentage in saving on joint costs.

Avoiding joints is more a question for the floor designer than for the contractor to deal with although the contractor and the client have greatest interest in installation of less joint length. This becomes an important and interesting issue to deal with especially when the designer seldom has the power to decide the final solution.

4.2 Swedish recommendations

In 2004 the Swedish Concrete Association, (SCA) started a committee that should gather the best experts in Sweden on concrete floors.

A small working group has with help of a larger reference group put their work on paper in a report that treat the most common concrete floors. The chapters of the report cover (1) demand identification, demand formulation, and procurement, (2) damages, (3) material selection and material properties, (4) construction, (5) operation and maintenance, (6) slabs on grade, (7) pile-supported slabs, (8) overlays, and (9) research needs and was issued for publication in 2008 [9].

5. CONCLUDING REMARKS

Careful design and construction of concrete floors start in proper choice of material for a correct design solution with appropriate construction method. The steel fibre concrete concept gives in overall accepted quality floors used with modern construction techniques.

Even in case the participant actors try to perform the very best many things can go wrong and lead to faulty floors. Some important aspects to consider are the following:

- The floor owner must have full control over its own situation with expected activities on the floor and future requirements.
- In the design state proper assumptions must be made in co-operation with the owner, the contractor and the material supplier.
- The contractor must understand the owners' and the consultants' intentions and be able to fulfil the stated requirements.

The client's wishes and intentions are often forgotten. He/she has usually a low knowledge base regarding floor so it must be the consultant and the contractors' ambition to guide him to the suitable floor solution.

Of the 25 floors studied, during their present life that varies from 6 to 11 years, 11 of them have cracking in various extents (*1, 2, 5, 9, 12, 13, 15, 16, 18, 20* and *22*). Only two of them have reported problems with levelness (*17* and *20*) and only one has reported problems with joints. It seems to show that there is no problem with joints, however cracks are often following the joints and thereby caused by them.

Of the 25 floors studied, 12 of the floors have no reported damages. This fact does not mean that there is no cracking existing in these floors as owners may value the damages and consequences differently. Only two floors were damaged severely according to the first author, floor no *12* and *13*, this due to overloading which seems to be an unusual situation.

Of the 25 floor studied, the majority of cracking of floors is probably caused by segregation and plastic settlement of concrete (and or subsoil) due to too much super plasticizer and high consistency class of concrete, in purpose of increasing the workability. By the loading of the subsoil the poor pressure increases and the soil may consolidate or collapse. In both cases the reinforcement, placed on piles, is fixed, which sometimes causing to large transversal tensile stresses above the bars. The cracking is probably induced early, power floated over and only visible after some time of shrinking.

ACKNOWLEDGEMENTS

The authors wish to acknowledge the involved companies and foundations for financial contributions and all people supporting the work of reforming the floor building branch.

The Development Fund of the Swedish Construction Industry, (SBUF)

Tyréns AB, Stockholm, Sweden.

Sven Tyréns Foundation, Stockholm, Sweden.

Department of Structural Engineering, Royal Institute of Technology, Stockholm, Sweden.

Bekaert Building Products, Belgium.

Bekaert Svenska AB, Sweden.

Swedish Concrete Association, (SCA), committee on Industrial Concrete Floors.

Swedish Cement and Concrete Research Institute, CBI.

AB Linotolgolv, Kungsör, Sweden.

Kilenkryset AB, Strängnäs, Sweden.

REFERENCES

1. Hedebratt, J., "Integrated Design and Construction of Industrial Floors – Methods to Increase the Quality," Licentiate Thesis, Bulletin 78, Department of Structural Engineering, Royal Institute of Technology, Stockholm, 2004, 221 pp. (Only available in Swedish).
2. Andersson, R., "Bonnier Promotes White Concrete," (Bonnier satsar på vit betong) Tidskriften Betong, nr 2 2006, Swedish Concrete Society, p 28, (In Swedish).
3. Hedebratt, J. & Silfwerbrand, J., "Integrated Design and Construction of Industrial Floors – Instrumented In-Situ Studies on Differential Shrinkage," Proceedings, 6th International Colloquium on Industrial Floors, Ostfildern, Germany, January 21th-23th, 2003, Vol. 1, pp. 1043-1047.
4. Hedebratt J., Silfwerbrand J., "Integrated Design and Construction of Industrial Floors – An Innovative Approach to the Design of Pile Supported SFRC Slabs," Proceedings of the 6th Rilem Symposium on Fibre-Reinforced Concretes, BEFIB 2004 edited by M. di Prisco, R. Felicetti and G. A. Plizzari, Varenna-Leccho, Italy, 20th-22th September, 2004, pp. 945-954.
5. Nord T., Hedebratt J., "The Creation of a Lean Construction Enterprise and the Role of the Change Agent" Article in doctoral course, Lean Construction, Division of Structural Engineering, Luleå University of Technology, Luleå, 2006.
6. Hedebratt J., Silfwerbrand J., "Full-Scale Tests on Pile Supported Floor Slabs – Steel Fibre Reinforced Concrete Only or in a Combination with Steel," Proceedings of the International Symposium on Innovation & Sustainability of Structures in Civil Engineering-Including Seismic Engineering (Volume 1), November 20-22, 2005, Nanjing, China, 2005, pp. 437-448.
7. Hedebratt J., "Integrated Design and Construction of Industrial Floors – New design of Suspended Pile Supported SFRC Slabs – Arch Action in Industrial Floors," Proceedings of the Nordic Mini-Seminar on Fibre-Reinforced Concretes, Design Rules for Steel Fibre Reinforced Concrete, October 6th, 2003, Veidekke ASA, Skøyen, Oslo, Norway.
8. Swedish Concrete Association, "Steel Fibre Reinforced Concrete – Recommendations for Design, Construction, and Testing," (Stålfiberbetong – rekommendationer för konstruktion, utförande och provning), *Concrete Report* No. 4, 2nd Edn, Stockholm, Sweden, 1997. (In Swedish).
9. Swedish Concrete Association, "Industrial Floors – Recommendations for Design, Chose of Material, Construction, Operation and Maintenance," (Industrigolv – rekommendationer för

- projektering, materialval, production, drif och underhåll), *Concrete Report* No. 13, Stockholm, Sweden, 2008. (In Swedish).
10. Hedebratt, J., Silfwerbrand J., "Full Scale Test of a Pile Supported Steel Fibre Concrete Slab," Paper submitted to Rilem – Materials and Structures, 2012.
 11. Hedebratt, J. "Industrial Fibre Concrete Slabs – Experiences and Tests on Pile-Supported Slab," Ph.D. thesis, Bulletin No 113, Department of Structural Engineering, Royal Institute of Technology, Stockholm, Sweden, 2012.

Properties of concretes mixed with Pulverized Fly Ash



Anders Lindvall
M.Sc., Ph.D.
Thomas Concrete Group
Ringögatan 14,
SE 417 07 Göteborg
E-mail: anders.lindvall@tcg.nu

Oskar Esping & Ingemar Löfgren
M.Sc., Ph.D.
Thomas Concrete Group
Ringögatan 14,
SE 417 07 Göteborg
E-mail: oskar.esping@tcg.nu & ingemar.lofgren@tcg.nu



Tang Luping
Professor
Chalmers University of Technology
Div. of Building Technology,
SE 412 96 Göteborg
E-mail: luping.tang@chalmers.se

ABSTRACT

In this paper two investigations made at the Central laboratory of Thomas Concrete Group where the properties of concretes mixed with combinations of fly ash and Portland cement are presented. Some of the results from these investigations are presented and discussed. Generally the results show that concrete with fly ash gets properties that are equivalent to comparable Portland cement concretes. The investigations show that the regulations in the standards EN 206-1 and SS 13 70 03 are in most situations reasonable, but in some situations too conservative.

Key words: Pulverized fly ash, strength durability, frost attack, chloride ingress.

1. INTRODUCTION

1.1 General

There is an increasing interest of using different types of industrial by-products, e.g. Pulverized Fly Ash (PFA) from coal fired power plants, to partly replace cement in the mixing of concrete. In this way the environmental impact, e.g. from CO₂, as well as the production costs are reduced compared to Portland cement (CEM I) concretes. Moreover the performance of the fresh and

hardened concrete compared to CEM I concretes is in many cases also improved with additions of PFA.

PFA can be added to concrete either as a cement (CEM II, where the PFA is added to or inter-ground with Portland cement klinker at the cement factory) or as an addition at the concrete plant, where cement and PFA are mixed in the concrete mixer. The latter provides larger flexibility to choose concrete composition and influence the concrete properties than if a CEM II cement is used. At present (April 2012), however, no CEM II cement with fly ash is available in Sweden. Therefore only PFA added as an addition at the concrete plant is covered in this paper.

The properties of PFA intended to be used as an addition in concrete is regulated in the standard EN 450-1 [1]. In [1] a large number of requirements regarding the chemical and physical properties of fly ash in general are defined. However, in reality it is only fly ash from coal fired power plants that meet these requirements. In this paper only PFA from a coal fired power plant was used.

In Sweden, the usage of PFA in concrete is regulated in the standards EN 206-1 [2] and SS 13 70 03 [3]:

- **EN 206-1.** In [2] the usage of PFA is regulated by either the concept with efficiency factors, k , or with equivalent concrete performance concept (ECPC). The k -factors are used to describe the effects of different binders on the performance of the concrete, where usually the compressive strength is considered. With ECPC a concrete should have equivalent performance (e.g. both strength and durability) compared to a reference concrete. In this study, however, only the concept with k -factors was considered.
- **SS 13 70 03.** The allowed dosages of PFA in concrete are regulated in [3], where the maximum contents that are allowed to mix is dependent on the exposure conditions, where the lowest contents are allowed in severe environments with exposure to chloride and frost, i.e. in exposure classes XS 3, XD 3 and XF 4, as described in [2].

In Sweden concrete for civil engineering structures (and housing structures, but these are not covered in this paper) are also regulated in AMA (General description of material and execution of work) [4], which is a series of handbooks used to make technical descriptions of structures to be built. Most Swedish clients, e.g. Trafikverket (the Swedish Transport Administration), refer to this document when they make technical descriptions. In [4] additional restrictions regarding the usage of PFA are introduced, see further below.

1.2 Usage of fly ash in concrete

In Sweden the usage of PFA is regulated with the concept of k -factors. In [2] and [3] the k -factor is 0.4 for PFA. In some situations higher k -factors are allowed, but this requires validation by extensive laboratory testing. A replacement of cement with up to 33 wt-% (PFA) of CEM I is allowed, where the additions are allowed to be included in the equivalent water-cement ratio $(w/c)_{eq}$. Larger additions are considered inactive and may therefore not be included in $(w/c)_{eq}$. The maximum amount of allowed additions of PFA depends on the exposure conditions:

- X 0 & XA 1. 50 %.
- XC 1-XC 2. 50 %.
- XC 2-XC 4, XS 1-XS 2, XD 1-XD 2, XF 1-XF 3 & XA 2. 50 %.
- XS 3, XD 3 & XF 4. 25 %.

In AMA the additions of PFA are, however, limited to 6 % (in XF 4) and 11 % (in other exposure classes) of the cement weight, in bridge structures. For civil engineering structures in other exposure conditions [4] refers to [3] regarding additions of PFA

The regulations in standards regarding k -factors and additions of PFA often reflect the worst case, i.e. PFA that are just meeting the requirements in the standards [1] is used, which means that the k -factors and allowed additions are conservative (low). If PFA with better quality is used higher values of k -factor and/or amount of allowed additions could be used. At the Central laboratory of Thomas Concrete Group two investigations of the properties of PFA in concrete have been made, (1) to quantify the actual k -factors and (2) to determine if the allowed additions of PFA in [3 & 4] are reasonable.

1.3 Properties of PFA

PFA is a by-product from coal fired power plants which consists of the remaining of the coal after passing the furnace. PFA consists mainly of spherical amorphous particles (60-90 weight-%) and different forms of crystalline particles, [5]. The amorphous particles, which give PFA its puzzolanic properties, are created when the remaining of burnt coal rapidly is cooled down in the exhaust gas (and collected by electrostatic precipitators). There will also be a small part of unburned coal in the PFA. Important factors that are influencing the properties of PFA are its glass content, the amount of unburned coal, fineness and the specific surface.

The quality and efficiency of PFA can be tested in several ways. Generally the results from the investigations show that in reality the efficiency (described with the k -factor) is not constant, but vary depending on several factors, for example: (i) The contents of PFA, (ii) The properties of the PFA, (iii) The properties of the cement, and (iv) The concrete composition, e.g. w/c .

In the investigations presented in this paper the quality of PFA has been determined in terms of loss on ignition (LOI¹), which describes the amount of unburned material in the PFA, and activity index (AI), which describes the efficiency of PFA. In [1] LOI is limited to 5.0 % in the highest quality class (A). The activity index (AI) has been studied according to EN 196-1 and describes the quotient between the strength of a mortar mixed with PFA and Portland cement and that of a mortar mixed with only Portland cement (reference) at the same age. In [1] there is a requirement that the AI must exceed 70 % (after 28 days) and 85 % (after 91 days) if a k -factor equal to 0.4 is to be used for a specific PFA.

Some of the results from the investigation of LOI and AI are presented in Figure 1 and Figure 2 respectively. The PFA comes from BauMineral Werk Rostock in Germany and has been imported to Sweden by Thomas Cement. The AI presented in Figure 2 has been determined for the PFA mixed with different cements available on the Swedish market are presented.

¹ LOI. When the loss on ignition is determined the material sample is heated to +975 °C. The mass of the sample is determined before and after heating and the relative loss of mass is finally determined.

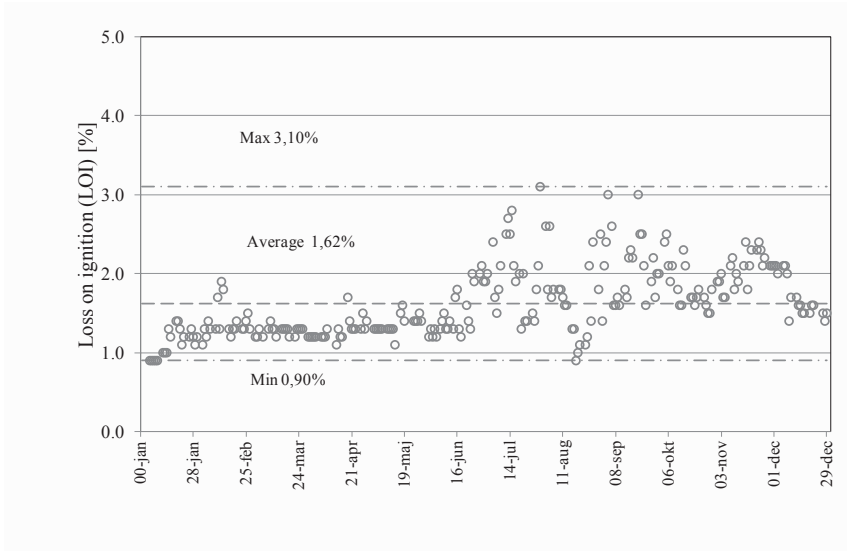


Figure 1 – Loss on ignition over time for PFA from BauMineral Werk Rostock. Data from [6].

The results that are presented in Figure 1 show that the measured LOI both are low (significantly below the maximum allowed 5 % in category A in [1]) and have low variations. Thus the PFA from BauMineral Werk Rostock well fulfils the requirements in [1] (category A, which defines the highest quality).

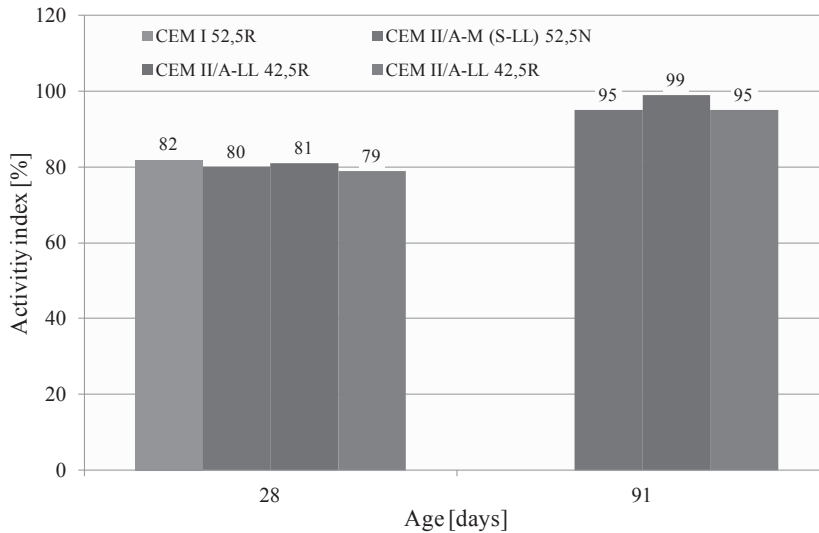


Figure 2 – Activity index (AI) for PFA from BauMineral Werk Rostock and cements available on the Swedish market. Data from [6].

In Figure 2 it can be observed that the AIs are significantly higher than 75 % (at 28 days) and 85 % (at 91 days), which are the minimum requirement in [1], for all tested cement types. This is an

indication that the PFA has high reactivity and that the k -factor that has been used ($k=0.4$) is realistic.

1.4 Properties of concrete mixed with PFA

The performance of concretes mixed with PFA is well documented in the literature for most properties. Many properties are improved when additions of PFA are used compared with the cases if only CEM I is used, for example:

- **General.** When PFA is added to concrete it partly replaces CEM I, which in its turn means that the amount of CEM I can be reduced. This reduction results in less amount of energy needed in the concrete production and, as a consequence, less environmental impact. Additionally the expenditures for the concrete can also be reduced, since PFA usually is cheaper than CEM I.
- **Fresh concrete,** where the workability is improved when additions of PFA are used in the concrete. Concrete with additions of PFA also has less bleeding problem.
- **Young concrete,** where heat development is lower whilst strength development is slower. This is beneficial in some structures, e.g. in massive cross-sections where there is risk of temperature cracking.
- **Hardened concrete,** where strength development is slower up to an age of 28 days, but larger after 28 days, compared to CEM I concrete. Furthermore, the durability is improved for many deterioration processes compared to CEM I concrete, e.g. in structures subjected to chloride or sulphate attacks, cf. [7-11]. However, for other types of attacks, e.g. frost attack, there are fears that the performance of concrete with additions of PFA is slightly worse than for CEM I concrete.

From the list above it is obvious that concretes with additions of PFA get not only improved properties, but also reductions in environmental impact and energy use, compared to CEM I concretes. In many cases the properties are improved with increasing amounts of PFA (up to what is allowed in [3]). However in some cases there are fears that the performance gets worse with additions of PFA, e.g. in concrete subjected to frost attack. Therefore there is a need to investigate and clarify how the additions of PFA influence the properties of concrete and if properties comparable with the ones for CEM I concrete can be achieved (with special focus on frost attack).

In the following chapters some results from two investigations of properties of concrete with additions of PFA, made at the central laboratory of Thomas Concrete Group, are presented. The first investigation has been made in collaboration with Chalmers University of Technology as a Master Thesis project [12] and the second project has been made with support from the Development Fund of the Swedish Construction Industry (SBUF) [16]. Special focus in both investigations has been on concrete in exposure class XF 4, i.e. frost attack with high water saturation and de-icing agents present. According to [3] a concrete exposed in these conditions must have $(w/c)_{eq} < 0.45$ and the maximum allowed addition of PFA is 25 wt-% of CEM I and $k=0.4$. However in order to investigate how the frost resistance is influenced with larger additions of PFA than what is allowed in [3], concretes with additions of PFA up to 33 wt-% of CEM I have been tested. An addition of 33 wt-% PFA of CEM I is the maximum allowed in [3] if the PFA is to be included in the equivalent water-cement ratio $(w/c)_{eq}$.

2. INVESTIGATIONS BY KNUTSSON (2010)

Thomas Concrete Group has in collaboration with Chalmers University of Technology participated in a Master Thesis project, where the aim was to investigate the durability of concretes with PFA, with special focus on frost durability. In the following sections a short review of the project is made. A full presentation of the results is given in [12].

2.1 Concrete compositions and performed test

The concrete mixes tested by [12] were proportioned so as to fulfil the requirements specified in [3] for exposure class XF4, i.e. $(w/c)_{eq}=0.45$. In total four different mixes were included in the investigation (with different additions of PFA and k -factors):

- Mix 1. 20 wt-% PFA of CEM I and $k=0.4$.
- Mix 2. 20 wt-% PFA of CEM I and $k=1.0$.
- Mix 3. No PFA (reference mix).
- Mix 4. 6 wt-% PFA of CEM I and $k=0.4$.

Cementa Anläggningscement (CEM I 42.5 N MH/SR/LA) and PFA from BauMineral Werk Rostock (Warnow Füller, which fulfils the requirements in category A in [1]) were used in all concrete mixes. The workability and air content of the concrete was adjusted by additions of superplasticizer (VR, SIKA Sikament 56/50, which is polycarboxylate based) and an air entraining agent (AEA, SIKA SikaAer-S, which is a synthetic tenside). Both the AEA and the VR were added with the mixing water. The concrete has been mixed for two minutes in a Zyklos Rotating Pan Mixer before casting.

The dosages of the admixtures were regulated so the air content in the fresh concrete was kept at the level of 4.5 ± 0.5 %. The required dosage of AEA varied between the different mixes, where the mixes with 20 % PFA required higher dosages of AEA than the reference mix (up to approximately four times more). Another interesting observation was that the AEA had to be combined with VR to reach the requested air content with reasonable dosages of the AEA. This will be further discussed in chapter 4.

2.2 Results

Several tests were performed on the properties of both the fresh concrete, e.g. slump and air content, and hardened concrete, e.g. compressive strength, resistance against chloride ingress and frost attack. The properties of the air pore system have also been investigated on four of the mixes, by means of microscopic analysis of thin sections. In this paper only the results from testing of the compressive strength, resistance against chloride ingress and frost attack will be presented. A complete presentation of the results is given in [12].

Compressive strength

The compressive strength was determined on cubes ($150\times 150\times 150$ mm³) after 7, 28, 56 or 90 days curing in water. The testing was in accordance with EN 12390-3 [13]. The results are presented in Figure 3.

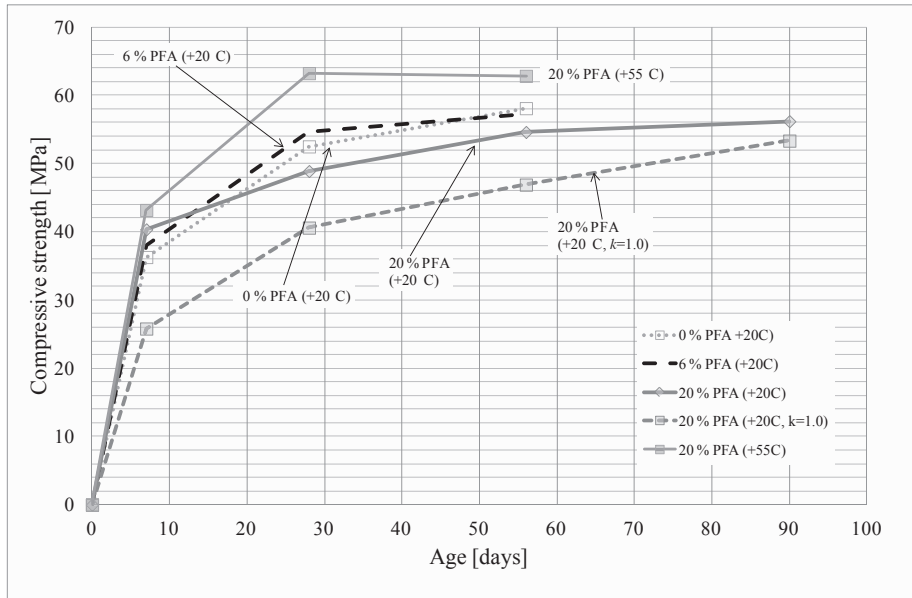


Figure 3 – Compressive strength determined on concrete with 0-20 % PFA of CEM I with different curing conditions and k -factors. Testing according to [13] Data from [12].

The results in Figure 3 show that the curing conditions and the value of the k -factors have significant influence on the compressive strength. Curing in higher temperature has, as expected, a positive effect on the strength development where the strength after 28 days is approximately 10 MPa higher for the specimens cured in +55°C compared to the ones cured in +20°C. This is explained by the fact that the samples cured at higher temperature also have higher degree of maturity. The influence of the k -factor for the concrete mixes with PFA is clear, where $k=0.4$ gives almost similar strength as for the concrete mixes without PFA, while $k=1.0$ gives significantly lower strength.

Resistance against chloride ingress - D_{RCM}

The resistance against chloride ingress was determined in terms of a rapid chloride migration coefficient, D_{RCM} , according to the method described in NT Build 492 [14]. The results from the tests are presented in Figure 4, where D_{RCM} for all tested concrete mixes are shown.

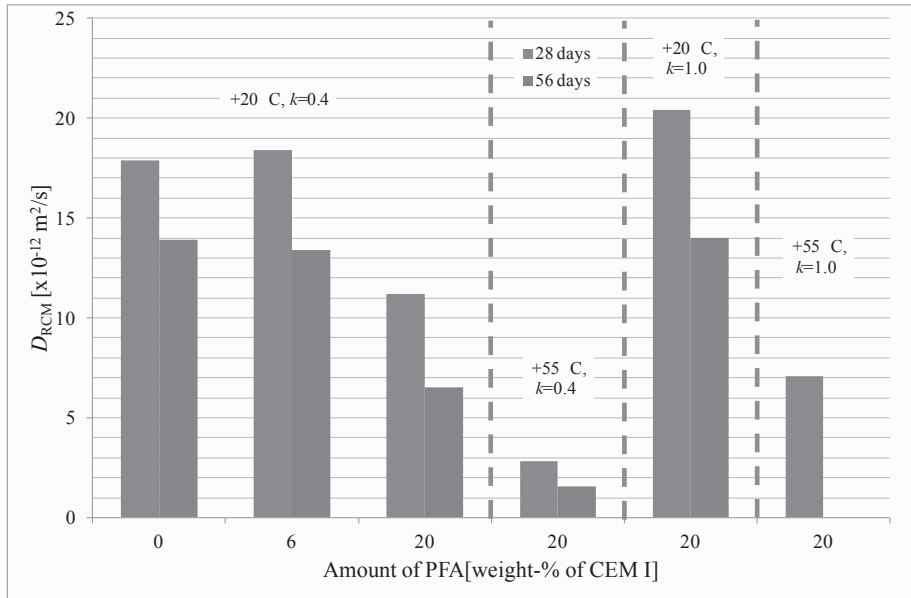


Figure 4 – Resistance against chloride ingress determined as D_{RCM} for concrete with 0-20 % PFA of CEM I with different curing conditions and k -factors. Testing according to [14]. Data from [12].

The results presented in Figure 4 show that additions of PFA have positive effect on the resistance against chloride ingress, where D_{RCM} decreases with increasing additions. Compared with the mix with only CEM I D_{RCM} for the mix with 20 wt-% PFA of CEM I is approximately halved for 56 days curing. Prolonged curing or curing at higher temperature decreases D_{RCM} , also for concrete without additions of PFA. These results correspond with what is reported in the literature, where additions of up to 50 wt-% PFA (of the cement) increase the resistance against chloride ingress, see e.g. [7-10].

Frost resistance

The frost resistance was determined according to the method described in the Swedish standard SS 13 72 44 [15], procedure IA (i.e. sawed surface from a cube exposed to 3.0 % NaCl-solution). In Figure 5 the results from all investigated concrete mixes are shown (with scaling measured after 28, 56 and 112 freeze/thaw cycles). The acceptance criteria for very good frost resistance (maximum accumulated amount of scaled material after 56 freeze/thaw cycles 0.10 kg/m^2) and good frost resistance (maximum accumulated amount of scaled material after 112 freeze/thaw cycles 0.50 kg/m^2) have been added to the figure. The indexes of x -axis indicate age of the concrete when the testing started (28-90 days of curing) and the curing temperature (+20°C or +55°C)

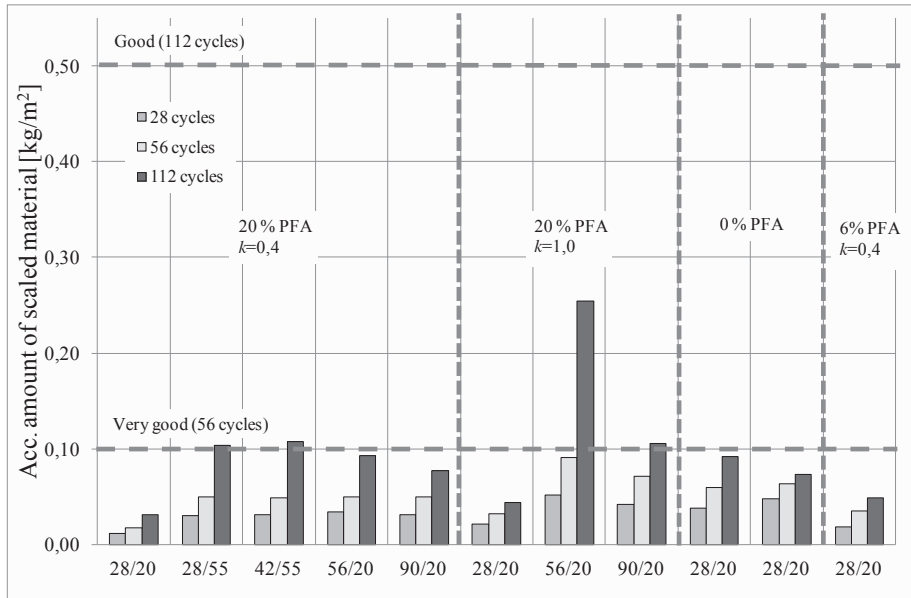


Figure 5 – Frost resistance for concrete with 0-20 wt-% PFA of CEM I with different curing conditions and k -factors. Testing according to [15]. Data from [12].

The results presented in Figure 5 show that all mixes have very good frost resistance, i.e. the accumulated amount of scaled material is less than 0.10 kg/m^2 after 56 freeze/thaw cycles. The results show that a concrete with up to 20 wt-% PFA of CEM I has very good frost resistance as long as a good air pore system has been created (i.e. with a certain air content and spacing factor). All tested concrete mixes had extra air ($4.5 \pm 0.5 \%$) by addition of AEA.

The effect of different k -factors has been studied. When a higher k -factor is used it will result in a lower amount of binder, which in its turn results in a less dense pore structure and lower strength. As a consequence on one hand the hydraulic pressures get lower, which reduces the risk of frost damage, but on the other hand the amount of freezable water increases and the strength of the concrete decreases, which worsens the frost resistance. Based on the results in Figure 5 it seems that the latter is slightly more dominant and that the frost resistance is slightly decreased when $k=1.0$ compared to $k=0.4$, but still it is good enough.

An interesting observation in Figure 5 is the effect of prolonged curing. For all concretes with additions of PFA prolonged curing seemed to slightly increase the scaling, but anyhow the frost resistance is very good. One possible explanation to this observation is that curing at higher temperature (i.e. at $+55^\circ\text{C}$) may result in micro cracking, which in its turn may adversely influence the frost resistance. This can, however, not explain the increased scaling after prolonged curing (i.e. 56 or 90 days of curing before start of testing). An additional explanation is therefore that the structure of the concrete gets denser after prolonged curing or curing at higher temperature. The size of or the distance between the air pores will not be influenced, but the capillary pores connecting the air pores will become finer. As a consequence the hydraulic pressures, which occur when water is transported during freezing, may increase, resulting in a higher risk of damage of the pore structure.

2.3 Final comments – Knutsson (2010)

The general conclusion from the investigations by [12] is that concrete with additions of PFA (up to 20 wt-% of CEM I and that fulfils the requirements in [1]), $k=0.4$, gets properties that are equivalent to comparable CEM I concretes. If $k=1.0$ the performance is somewhat reduced compared to comparable CEM I concretes. The effects from prolonged curing or curing at higher temperatures on the properties of concrete with PFA are varying.

The results from the concretes with low additions of PFA (6 wt-% of CEM I) show that there are only small differences in properties compared to Portland cement concretes and thus low additions of PFA would have no noticeable effect on the concrete properties.

3. INVESTIGATIONS BY LINDVALL (2011)

Thomas Concrete Group has with support from the Development Fund of the Swedish Construction Industry (SBUF), made an investigation where the aim was to investigate the durability of concretes with PFA. Special focus was on the frost resistance of concrete with PFA (up to 33 wt-% of CEM I). In the following sections a short review of the project is made. A full presentation of the results is given in [16].

3.1 Concrete compositions and performed test

The concrete mixes tested by Lindvall (2011) have been proportioned so as to fulfil the requirements specified in [3] for exposure classes XD3 and XF4, i.e. $(w/c)_{eq}=0.40$ & 0.45 . In total 15 different mixes were included in the investigation (with different additions of PFA, where $k=0.4$ has been used, mixed with both CEM I and CEM II cements):

- $(w/c)_{eq}=0.40$. 0-25 wt-% PFA of CEM I. Mixed with CEM I. Three mixes.
- $(w/c)_{eq}=0.45$. 0-33 wt-% PFA of CEM I. Mixed with CEM I. Six mixes.
- $(w/c)_{eq}=0.50$. 0-25 wt-% PFA of CEM I. Mixed with CEM I. Three mixes.
- $(w/c)_{eq}=0.45$. 0-25 wt-% PFA of CEM I. Mixed with CEM II. Three mixes.

The cements used were Cementa Anläggningscement (CEM I 42.5 N MH/SR/LA) and Cementa Byggcement (CEM II/A-LL 42.5 R). The PFA used in all mixes was PFA from BauMineral Werk Rostock (Warnow Füller, which fulfils the requirements in category A in [1]). The workability and air content of the concrete was adjusted by additions of VR (SIKA Sikament 56/50, which is polycarboxylate based) and AEA (SIKA SikaAer-S, which is a synthetic tenside). Both the AEA and the VR were added with the mixing water. The concrete has been mixed for two minutes in a Zyklos Rotating Pan Mixer before casting.

The dosages of the admixtures were regulated so the air content in the fresh concrete was kept at 5.5 ± 0.5 %, slightly higher than that studied by Knutsson [12]. The required dosage of AEA varied between the different mixes, where the dosages of AEA had to be increased with increasing addition of PFA (the dosage of AEA is up to three times higher in the mixes with PFA). Similar to [12], another interesting observation was that the AEA had to be combined with VR to reach the requested air content with reasonable dosages of the AEA. This will be further discussed in chapter 4.

3.2 Results

Several tests were performed on the properties of both the fresh concrete, e.g. slump and air content, and hardened concrete, e.g. compressive strength, resistance against chloride ingress and frost attack. In this paper only the results from testing of the compressive strength, resistance against chloride ingress and frost attack will be presented. A complete presentation of the results is given in [16].

Compressive strength

The compressive strength was determined on cubes ($150 \times 150 \times 150 \text{ mm}^3$) after 7, 28 or 56 curing in water ($+20^\circ\text{C}$). The testing was in accordance with [13]. The results from the mixes with CEM I, $(w/c)_{eq}$ and with up to 33 wt-% PFA of CEM I are presented in Figure 6.

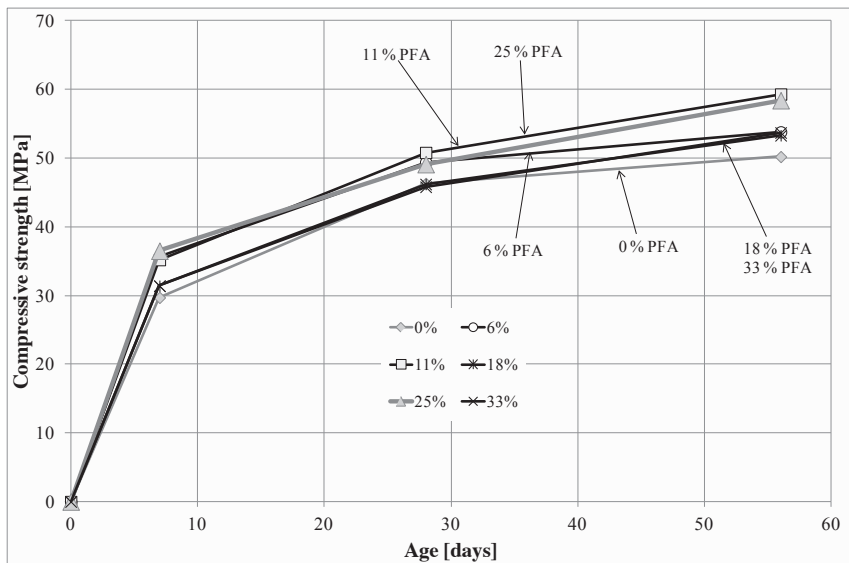


Figure 6 – Compressive strength determined on concrete with 0 %-33 % PFA mixed with CEM I with different curing times. $(w/c)_{eq}=0.45$. Testing according to [13]. Data from [16].

In Figure 6 it can be seen that the compressive strength after 28 days varies between 46.2 MPa and 50.8 MPa. The highest and lowest strengths were measured on the mixes with 11 wt-% PFA of CEM I and 0 % PFA, respectively. The differences in strength between the different mixes are somewhat large and cannot solely be explained by the influence from PFA. Other factors that may influence are variations in air content and/or moisture in the aggregates between the mixes.

The effect from the curing time can be observed in Figure 6, where the strength increases with increasing curing time for all mixes. The increase of strength is more pronounced for the mixes with more than 11 % PFA, where the strength continues to increase also between 28 days and 56 days. This is mainly a result of the fact that the pozzolanic reactions of the PFA are slower than the reactions of CEM I.

Resistance against chloride ingress - D_{RCM}

The resistance against chloride ingress was determined in terms of a rapid chloride migration coefficient, D_{RCM} , according to the method described in [14]. The results from some of the tests are presented in Figure 7, where D_{RCM} for the concrete mixes with up to 33 wt-% PFA of CEM I and mixed with CEM I.

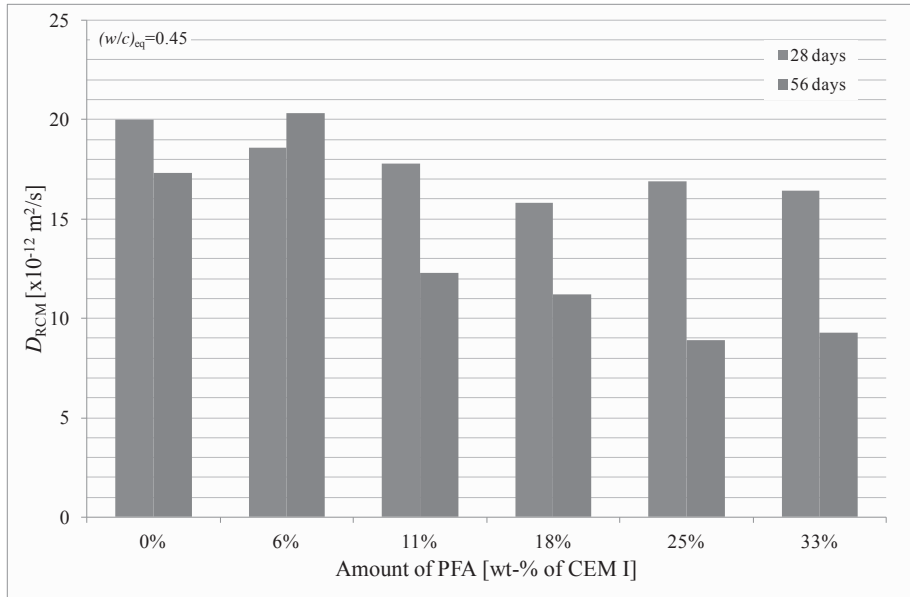


Figure 7 – Resistance against chloride ingress determined as D_{RCM} for concrete with 0-33 % PFA of CEM I mixed with CEM I after 28 days and 56 days of curing. $(w/c)_{eq}=0.45$. Testing according to [14]. Data from [16].

In Figure 7 it is clear that additions of PFA and prolonged curing decrease D_{RCM} , which means that the resistance against chloride ingress increases. The effect of prolonged curing is especially clear for the mixes with large additions of PFA (25 and 33 wt-% of CEM I). The difference between D_{RCM} measured after 28 days and 56 days is up to approximately 45 % for the mixes with large additions of PFA. Compared with the mix with only CEM I cement D_{RCM} for the mix with 25 % and 33 % PFA is approximately halved for 56 days curing. This is mainly a result of the pozzolanic reactions of the PFA, which proceed slower than the reactions of Portland cement.

A somewhat strange result is that D_{RCM} for the mix with 6 % PFA increases between 28 days and 56 days. The reason for this is not known.

Frost resistance

The frost resistance was determined according to the method described in the Swedish standard SS 13 72 44 [15], procedure IA (i.e. sawed surface from a cube exposed to 3.0 % NaCl-solution). In Figures 8 and 9 the results from all investigated concrete mixes are shown (with scaling measured after 28, 56 and 112 freeze/thaw cycles) after curing for 28 and 56 days, respectively. The acceptance criteria for very good frost resistance (maximum accumulated

amount of scaled material after 56 freeze/thaw cycles 0.10 kg/m^2) and good frost resistance (maximum accumulated amount of scaled material after 112 freeze/thaw cycles 0.50 kg/m^2) have been added to the figure. The indexes of the x -axis indicate $(w/c)_{\text{eq}}$ and the amount of PFA added to the mix.

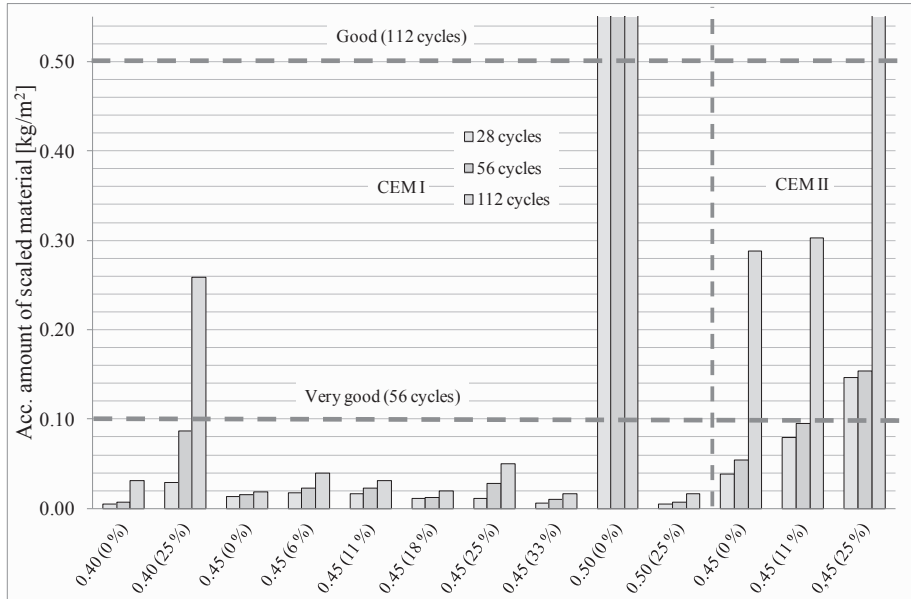


Figure 8 – Frost resistance for concrete with 0-33 wt-% PFA of CEM I mixed with CEM I or CEM II cement and cured for 28 days before testing. Testing according to [15]. Data from [16].

The results in Figure 8 show that all mixes, except two, have very good frost resistance, i.e. the accumulated amount of scaled material is less than 0.10 kg/m^2 after 56 freeze/thaw cycles. The frost resistance for the mix with 0 % PFA and $(w/c)_{\text{eq}}=0.50$ is not acceptable and this is most probably caused by a bad air pore system even though the air content in the fresh concrete was sufficiently high (5.5 %). However, the properties of the air pore system have not been further investigated, e.g. by means of microscopic analysis. The mix with CEM II, 25 % PFA has acceptable frost resistance, i.e. the accumulated amount of scaled material is less than 1.00 kg/m^2 after 112 freeze/thaw cycles.

In Figure 8 the results from the mixes with 11 % PFA, $(w/c)_{\text{eq}}=0.40$ and $(w/c)_{\text{eq}}=0.50$, are missing. Due to a mistake the testing was started after 56 days instead of 28 days. The frost resistance for these mixes is, however, probably very good, c.f. the results presented in Figure 9 where the testing has been started after 56 days of curing.

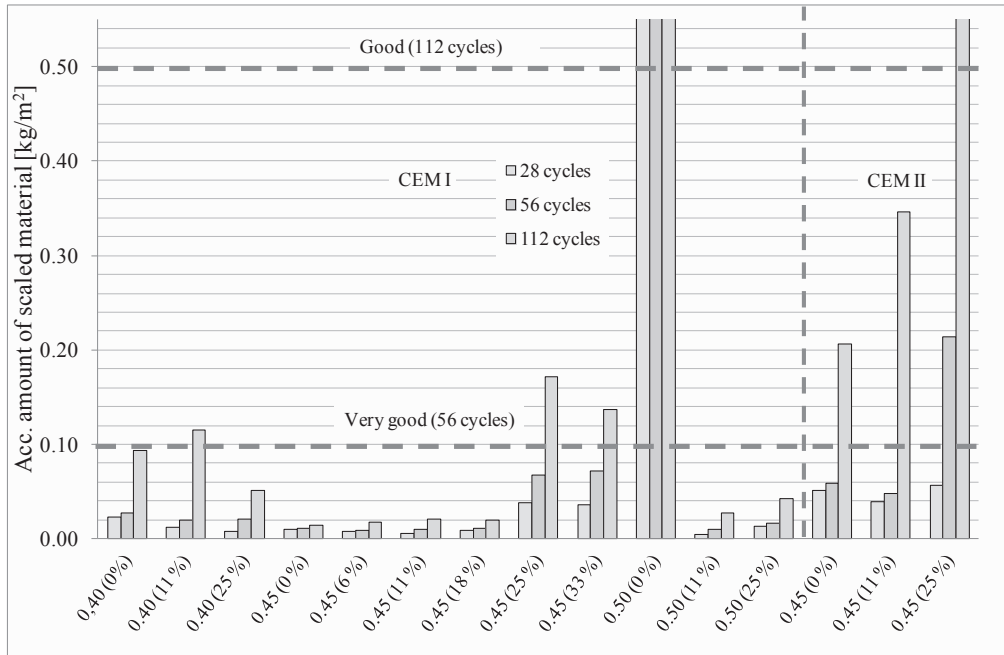


Figure 9 – Frost resistance for concrete with 0-33 wt-% PFA of CEM I mixed with CEM I or CEM II cement and cured for 56 days before testing. Testing according to [15]. Data from [16].

The results in Figure 9 show that all mixes, except two, have very good frost resistance, i.e. the accumulated amount of scaled material is less than 0.10 kg/m^2 after 56 freeze/thaw cycles. The same mix that failed at testing after 28 days of curing also failed after 56 days of curing. Similarly, the mix with CEM II and 25 % PFA, $(w/c)_{\text{eq}}=0.45$ has acceptable frost resistance, i.e. the accumulated amount of scaled material is less than 1.00 kg/m^2 after 112 freeze/thaw cycles.

When comparing the results in Figures 8 and 9 it can be observed that prolonged curing does not improve the frost resistance. Instead the frost resistance is slightly decreased for some of the mixes, similar to what observed in the study by Knutsson [12]. Furthermore the mixes with CEM II show generally somewhat lower frost resistance than the mixes with CEM I, especially with additions of 25 wt-% PFA of CEM I, and this can be explained the fact that it is harder to create a good air pore system in concrete mixed with the CEM II that has been used. These observations are further discussed and explained in chapter 4.

The results presented in Figures 8 and 9 show that the most important factor to create a frost resistant concrete is to create a good air pore system in the concrete (i.e. a pore system with a sufficient air content and spacing factor). Additions of PFA have no negative influence on the frost resistance, at least for additions of up to 33 wt-% PFA of CEM I, as long as the air pore system is good. The experiences from the investigation in [16] also show that the dosage of AEA has to be increased, when PFA is added to the concrete (the dosage of AEA is up to three times higher in the mixes with PFA), possibly due to an absorption of the AEA (AEA) on the PFA particles. The AEA had to be combined with VR to achieve reasonable dosages of the AEA (within the recommended limits from the manufacturer).

3.3 Final comments – Lindvall (2011)

The general conclusion from the investigations by Lindvall (2011) is that concrete with additions of PFA (up to 33 wt-% of CEM I and that fulfils the requirements in [1]), $k=0.4$, gets properties that are equivalent to comparable Portland cement concretes. The effects from prolonged curing (56 days) are unclear for concrete with PFA, where the results show that the performance is both improved and impaired.

4. DISCUSSION

The aim of the investigations presented in this paper was to investigate whether concrete with PFA gets properties that are equivalent to comparable Portland cement concretes. The results show that this is the case (at least for additions of up to 33 wt-% PFA of CEM I and with a PFA that fulfils the requirements in [1]). For some properties the performance is also improved compared to CEM I concrete.

4.1 Strength

The measurements of compressive strength show that there are differences between the concrete mixes, both in terms of strength and strength development. Additions of PFA influence the strength development, since the reactions of PFA are slower than from Portland cement (the pozzolanic reactions of the PFA require calcium hydroxide from the cement to proceed). As a consequence the strength development up to 28 days is slower for concrete with PFA but it continues also after 56 days. Additionally the contribution from PFA on the strength is less than Portland cement, which means that the amount of PFA that is added to a concrete must be larger than the amount of Portland cement it replaces, to achieve comparable strengths. The additions of PFA are regulated with the k -factor, where $k=0.4$ (which also is prescribed in [2]) has been used in the investigations presented in this paper. The concrete strength results show that this k value is reasonable for concrete production in combination with the Cementa Anläggningcement (CEM I 42.5 N MH/SR/LA).

4.2 Resistance against chloride ingress - D_{RCM}

The measured D_{RCM} show that the concretes with PFA get significantly higher resistance against chloride ingress than comparable Portland cement concretes, especially with prolonged curing time. With additions of PFA that exceeds 10-15 wt-% of CEM I D_{RCM} is decreased with approximately 20 % (after 28 days of curing) and 50 % (after 56 days of curing) compared to Portland cement concretes. The largest reduction of D_{RCM} was observed for the concrete with 33 wt-% PFA of CEM I. This is a result of the pozzolanic reactions of the PFA and that the total amount of binder is larger in concrete with PFA (since $k=0.4$, which means that the amount of PFA is larger than the amount of Portland cement it replaces). This also means that $k=0.4$ is probably too low when the resistance against chloride ingress is considered.

D_{RCM} decreases with increasing age of the concrete, which is a result of that both Portland cement and PFA continues to react also after 28 days. As a result the structure of the concrete gets denser which increases the resistance against penetration of harmful substances, e.g. chlorides. As expected the effect is clearer for concrete with PFA since the reactions of the PFA

continues in larger extent than the reactions of the Portland cement after 28 days of age. Furthermore pore blocking may occur in concrete with PFA, where the pore system gets discontinuous, which results in a less permeable concrete.

4.3 Frost resistance

The frost resistance, which has been in focus in the investigations presented in this paper, is very good for all investigated concrete mixes (according to the requirements in [15]), also for concrete with PFA (at least up to 33 wt-% of CEM I, where the PFA fulfils the requirements in [1]). The prerequisite to achieve good frost resistance is that a good air pore system has been created in the concrete, irrespective if PFA is added to the concrete or not (i.e. a pore system with sufficient air content and spacing factor). All investigated concrete mixes have sufficiently entrained air, by addition of AEA, so the air pore systems are acceptable (with respect to air contents and spacing factors). The frost resistance of two of the investigated concrete mixes was less good, which could be attributed to the fact that the air pore system was relatively poor, which can occur in both concretes with and without PFA. One of the concrete mixes, $(w/c)_{eq}=0.50$, no PFA mixed with CEM I, got not acceptable frost resistance, while the other concrete mix $((w/c)_{eq}=0.45$, 25 % PFA mixed with CEM II) got good frost resistance.

The dosages of AEA vary between the concrete mixes, where the dosages had to be increased to achieve sufficiently high air content when PFA is added to the concrete. A super plasticizer had also to be added to the concrete to achieve reasonable dosages of the AEA (within the limits recommended by the manufacturer). Similar observations are reported in the literature, cf. [17], where higher dosages of AEAs were required in concretes with PFA compared to Portland cement concretes. An explanation is that the air entrain agent is absorbed by the PFA particles, where especially unburned carbon particles influence the number of “absorption sites”. Another interesting observation was that, to achieve the requested air content in the fresh concrete, with reasonable dosages of the AEA, both superplasticizer and AEA have to be added to the mix. If no superplasticizer was added the dosage of AEA had to be increased to a level significantly above the recommended levels from the manufacturer. A probable explanation can be that the superplasticizer blocks or occupies the “adsorption sites”, which results in less adsorption of the AEA that instead is available to entrain air in the concrete. Additionally there is a synthesis between the AEA and the superplasticizer (polycarboxylate based), which results in lower dosages of the AEA to achieve the requested air content in the concrete with PFA.

The influence of curing with prolonged age or at a higher temperature was studied, where the frost resistance was slightly decreased for concrete with PFA. Prolonged curing age and/or curing at higher temperature have some contradicting effect on the properties of concrete. On one hand the maturity and the strength of the concrete get higher, which lead to reduced porosity and water adsorption (which should improve the frost resistance), whilst on the other hand the capillary pore structure of the concrete gets finer which may lead to higher hydraulic pressures under freezing. As a consequence, there seems to be an increased risk of frost damage. The latter effect might be more dominant in the investigations presented in this paper and therefore the frost resistance is slightly reduced. This has also been confirmed by microscopic analysis of thin sections of some of the concrete mixes.

The influence of k -factor on the frost resistance was investigated, where the frost resistance for concrete with $k=1.0$ is slightly decreased compared to that with $k=0.4$. A higher k -factor means that the total amount of binder decreases in the concrete. This implies on one hand that the

strength of the concretes is lower, which decreases the frost resistance, whilst on the other hand the capillary pores are getting coarser, which should result in reduced hydraulic pressures and a lower risk for frost damage. The reduced strength of the concrete might be more dominant in this case and consequently the frost resistance is lower.

There is a difference in frost resistance between concrete mixed with CEM I and CEM II, the latter has lower frost resistance also for mixes without PFA. The AEA that has been used is in first hand developed for the Swedish CEM I (since this cement normally is used for structures in exposure class XF4). There are also differences in chemical composition and physical properties between the CEM I and CEM II, which influence the performance of the AEA. Additionally the CEM II contains porous limestone powder, which may improve the water saturation and consequently result in an increased risk of frost damage.

5. FINAL COMMENTS AND RECOMMENDATIONS

The results from the investigations presented in this paper show that concrete with additions of PFA (which fulfils the requirements in [1] and with dosages that are prescribed in [3]) has properties that are at least similar to comparable Portland cement concretes. For some properties additions of PFA also improves the performance compared to Portland cement concretes.

5.1 Final comments

The following final comments can be given based on the results from the investigations presented in this paper:

- **Compressive strength**, where the strength at 28 days is approximately the same for all investigated concrete mixes with Cementa Anl ggningscement (CEM I 42.5 N MH/SR/LA) if $k=0.4$ (i.e. what is prescribed in [2]). The strength development is usually slower for concrete with PFA up to an age of 28 days, but continues faster after 28 days, due to the pozzolanic reactions of the PFA, which are slower than Portland cement.
- **Resistance against chloride (D_{RCM})**, where the resistance generally is higher for concretes with PFA than for comparable Portland cement concretes. The results show that the resistance increases with increasing addition of PFA (at least up to 33 wt-% PFA of CEM I).
- **Frost resistance**, where concrete with PFA gets similar resistance as Portland cement concrete if the requirements [2] and [3] are fulfilled (maximum addition of PFA 25 wt-% of CEM I and $(w/c)_{eq}=0.45$). The most important factor to create a frost resistant concrete, irrespective the additions of PFA, is to create a good air pore system (i.e. sufficient air content and spacing factor). A good air pore system is created by additions of AEA with regulated dosage and with combination of superplasticizer.

5.2 Recommendations

Additions of PFA have been used for a long time to alter and in some situations improve the properties of concrete. With the increasing requirements of durable structures with reduced environmental impact the interest of using PFA in concrete has increased. However, the standards that regulate the addition of PFA in concrete should reflect the worst case, i.e. PFA

that are just meeting the requirements in the standards [1] are used, which means that the k -factors and additions are conservative with regard to the durability of concrete. In the investigations presented in this paper concrete mixed with high quality PFA was used and the results indicate that the regulations in the standards are too conservative. Therefore it is suggested that the standards should be reviewed with respect to k -factors and additions of PFA, to allow higher k -factors and additions also in rough environments.

REFERENCES

- 1 EN 450-1, Fly ash for concrete – Part 1: Definitions, specifications and conformity criteria, *Standard EN 450-1*, SIS – Swedish standards institute, Stockholm, 2005.
- 2 EN 206-1, Concrete – Part 1: Specification, performance, production and conformity, *Standard EN 206-1*, SIS – Swedish standards institute, Stockholm, 2005.
- 3 SS 13 70 03, Concrete – Application of EN 206-1 in Sweden, Swedish Standards Institute, Stockholm, 2008.
- 4 AMA Anläggning, AMA Anläggning 10 – Allmän material- och arbetsbeskrivning för anläggningsarbete (General description of material and execution of civil engineering work), Svensk Byggtjänst, Stockholm, 2011.
- 5 ACI, Use of Fly Ash in Concrete, ACI 232.2R-96, reported by ACI committee 232, American Concrete Institute, Farmington Hills, 1996.
- 6 Thomas Cement, Unpublished data regarding properties of fly ash “Warnow Füller” from Werk Rostock – factory production control according to EN 450-1, 2011.
- 7 Dhir, R.K. & Jones, M.R., Development of chloride-resisting concrete using fly ash, *Fuel*, Vol. 78, pp. 137-142, 1999.
- 8 Schiessl, P., Wiens, U., Schröder, P., Müller, C., Neue Erkenntnisse über die Leistungsfähigkeit von Beton mit Steinkohlenflugasche (New knowledge about the durability of concrete with fly ash), *Beton*, Vol. 1-2, 2001. (in German)
- 9 Thomas, M.D.A., Matthews, J.D., Durability of pfa concrete, *BRE Report*, Building Research Establishment (BRE), Watford, 2004.
- 10 Thomas, M.D.A., Matthews, J.D., Performance of pfa concrete in a marine environment – 10-years results, *Cement and Concrete Composites*, Vol. 26, pp. 5-20, 2004.
- 11 BRE, Concrete in aggressive ground, *BRE Special Digest*, Vol 1:2005, Building Research Establishment (BRE), Watford, 2005.
- 12 Knutsson, A., Freeze/Thaw Durability of Concrete with Fly Ash, *Master's Thesis 2010:154*, Department of Civil and Environmental Engineering, Division of Building Technology/Building Materials, Chalmers University of Technology, Göteborg, 2010.
- 13 EN 12390-3, Testing hardened concrete – Part 3: Compressive strength of test specimens, Swedish Standards Institute, Stockholm, 2009.
- 14 Nordtest, Concrete, mortar and cement-based repair materials: Chloride migration coefficient from non-steady-state migration experiments, NT Build 492, Nordtest, 1999.
- 15 SS 13 72 44, Concrete testing – Hardened concrete – Scaling at freezing, Swedish Standards Institute, Stockholm, 2005.
- 16 Lindvall, A., Beständighetsegenskaper hos anläggningsbetong med stenkol-flygaska (Durability of concrete with fly ash), Final report from SBUF project 12382, SBUF (The Development Fund of the Swedish Construction Industry), Stockholm, 2011. (in Swedish)
- 17 Bortz, B.S., Salt-scaling durability of fly ash concrete, Master Thesis, Department of Civil Engineering, College of Engineering, Kansas State University, Manhattan, Kansas, 2010.

Critical Conditions for Depassivation of Steel in Concrete: Interface Chloride Profiles and Steel Surface Condition



Nelson Silva
M.Sc., Ph.D. Student
Division of Building Technology
Chalmers University of Technology
SE-412 96 Gothenburg, Sweden
nelson.silva@chalmers.se



Dimitrios Boubitsas
Lic.Eng., Ph.D. Student
Materials Group
CBI Swedish Cement and Concrete Research Institute
Box 857, SE-501 15 Borås, Sweden
dimitrios.boubitsas@cbi.se



Tang Luping
Ph.D., Professor
Division of Building Technology
Chalmers University of Technology
SE-412 96 Gothenburg, Sweden
tang.luping@chalmers.se



Jan Erik Lindqvist
Ph.D., Senior Researcher
Materials Group
CBI Swedish Cement and Concrete Research Institute
Box 857, SE-501 15 Borås, Sweden
janerik.lindqvist@cbi.se

ABSTRACT

The composition and macrostructure of the concrete-steel interface and the surface finish of the steel are fundamental for the chloride induced corrosion initiation in reinforced concrete, with direct influence in the chloride threshold values (C_{th}). In this paper these characteristics were examined for vertically cast samples immersed in salt solution. After depassivation, the specimens were open for visual examination. Corrosion always initiated at the front side and surface defects were found to influence the corrosion onset. Chloride, calcium and iron profiles along the interface were drawn by means of laser ablation inductively coupled plasma mass spectrometry (LA-ICP-MS) and higher chloride contents were measured around active corroding areas.

Key words: Steel-concrete interface, steel surface condition, chloride threshold values, elemental distributions, LA-ICP-MS.

1. INTRODUCTION

Chloride induced corrosion is a major cause of degradation of reinforced concrete structures. The penetration of chlorides, both from marine environments or from de-icing salts, and their accumulation at the level of the reinforcement, lead to the destruction of the rebar passive layer once the chloride concentration reaches the threshold value (C_{th}).

A number of literature reviews [1-4] on the topic has shown that C_{th} values can vary over two orders of magnitude due to both conceptual and practice related reasons. Under laboratory conditions, the C_{th} can be defined as the chloride content required for depassivation of steel [4] best expressed in % per weight of cement or binder [1]. However, a consensual test setup is still lacking [5] because a great number of experimental parameters influence the outcome of the C_{th} measurement. These include: binder type and exposure conditions [6-8]; type of steel and rebar surface conditions [9-11]; depassivation detection techniques [12,13] and specimen size [14,15], among others.

Moreover, mix design, execution, curing and pre-conditioning prior to the test must also be considered. In particular, the casting direction and compaction procedures play a significant role on the measured C_{th} since it affects the quality of the steel-concrete interface and therefore, the susceptibility of steel to depassivation. Mohammed and Hamada [11] defined C_{th} as the “chloride ion concentration that caused the initiation of active corrosion of steel bars in concrete, provided that there are no voids/damages at the steel-concrete interface”.

The microstructure and composition of the steel-concrete interface influences the corrosion initiation and the C_{th} by physically and chemically interacting with the aggressive species. The porosity, homogeneous distribution of the cement hydration products at the steel surface

Under a microscopic point of view, the main characteristics of the steel-concrete interface that influence the corrosion initiation and the C_{th} are 1) the pH buffering capacity of a segregated calcium hydroxide layer at the steel surface [16-19] in the case of chloride ingress accompanied by hydroxyl leaching and 2) the porosity, dependent on the homogeneous distribution of the cement hydration products around the steel which are capable of screening the chloride ions from reaching it. This is most relevant in the case of horizontal bars where the underside, due to collection of bleeding water, is expected to present higher porosity and lower calcium hydroxide content when compared to the upper side [20]. Similar characteristics could also be observed between the lower and upper side of the ribs in vertically casted bars. Horne et al. [20] reported larger amounts of calcium hydroxide and higher porosity at the interface when compared to the bulk cement paste. On the other hand, Glass et al. [21] observed that the cement hydration products formed at the interface with steel were similar to those in the bulk cement matrix. Therefore, the authors in [21] suggested that the capacity of the pore solution to resist leaching of hydroxyl ions and their consumption in the anodic reactions is buffered by all solids with pH dependant dissolution characteristics.

Macroscopic defects may also play a major role on the corrosion initiation. Sandberg [6] studied the influence of interface defects by adhering filter paper on the steel surface. A negative effect was found for field exposed concrete in submerged and splash zones and for laboratory concrete exposed to wetting/drying cycles but not for submerged laboratory concrete. Variations on the moisture and temperature conditions at the depth of reinforcement caused by wetting/drying resulted in significantly lower C_{th} .

Recently Angst et al. [22] evaluated the influence of the casting direction and surface defects at the steel-concrete interface on the corrosion initiation of ribbed “as-received” bars. SEM observations demonstrated the presence of entrapped air voids and gaps on the underside of the rebars with respect to casting direction as a result of bleeding, plastic settlement and segregation. These observations are in agreement with previous findings by Horne et al. [20] and by Soylev and François [23]. In the study by Angst et al. [22], corrosion always initiated on the underside of the rebars with respect to casting direction, regardless of the direction of the chloride penetration. However, contrarily to what was observed by Hartt and Nam [7] or by Ryou and Ann [24], the corrosion initiation sites never coincided with the location of macroscopic defects such as air voids, because of the moisture content below saturation resulting from the wet-dry cycles exposure regime. Implications of the casting direction on the determination of C_{th} are that it is not necessarily the chloride content at the depth of the front side that is decisive. This may be true for horizontal rebars but it’s rather unlikely for vertical casting, as the study also demonstrated.

A number of studies have qualitatively shown the influence of the steel-concrete interface on the initiation of corrosion. However, very little quantitative information exists as to what concerns the chloride distributions at the initiation sites. The available sampling procedures for chloride analysis provide average values of the chloride content, at the cover depth level but away from the interface where pitting occurs. Experimental studies by Hartt and Nam [7], Yu and Hartt [25] and Yu et al. [26], showed that the chloride content at the top of the rebar can be twice as high as that at the same depth away from the rebar due to reinforcement obstruction effect and spatial distribution of coarse aggregate. Nevertheless, under a practical point of view, the current practice seems adequate.

However, Yu et al. [27], measured non-uniform chloride distribution along the interface, with higher chloride contents at corrosion active sites when compared to passive locations along the bar, while SEM observations such as those reported by Glasser and Sagoe-Crentsil [28] and Poupard et al. [29], suggest that the accumulation of chlorides at the interface.

Therefore, more information on the chloride content variations at a micro and meso scale, in particular, the distribution of chlorides along the steel-concrete interface, is required and useful for a better understanding of the pitting corrosion process and the initiation mechanisms. This paper deals with the study of the chloride profiles along the interface by means of LA-ICP-MS.

2. EXPERIMENTAL

2.1 Materials

The specimens used in this work are part of a larger project aiming the development of a test method for the determination of the C_{th} where T-shaped corrosion cells (see Figure 1) were developed based on the procedure described by Nygaard and Geiker [30]. The mixture proportions of the concrete used in the experiments is presented in Table 1. Eight smooth cool-drawn carbon steel bars ($\varnothing 10$ mm) with traces of mill-scale were cast at four different cover depths (10, 15, 20 and 25 mm). At the age of 35 days, the specimens were exposed to sodium chloride solution (6 wt%), with the level of solution reaching 130 mm from the bottom of the specimen. Further details regarding specimen preparation, pre-conditioning, electrochemical monitoring and C_{th} calculation is described by Boubitsas and Tang [31].

It is however worth to mention that bars #1 to #4 were monitored under open circuit conditions while bars #5 to #8 were kept under potentiostatic control. This paper is focused only on the study of bars #1 to #4.

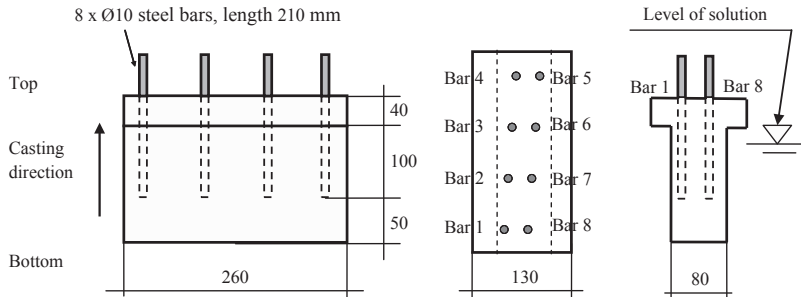


Figure 1 – Geometry of the corrosion cell (dimensions in mm) [31].

Table 1 – Concrete mix proportion.

CEM I 42.5 N (kg/m ³)	Aggregates 0-10 mm (kg/m ³)	Water (kg/m ³)	Superplasticiser (wt% CEM)	Slump (mm)	Air (%)	Compressive Strength @ 28 days (MPa)
380	1817	190	0.5	180	3	58

In this study, all the bars were opened at the end of the exposure period (329 days) with exception of bar #1 (138 days). The section of the cell containing the corroding bar was cut-out and opened by cutting two grooves along the steel in order to allow removal of the bar with minimum interference in the interface. At these ages, macro-scale chloride profiles were measured according to conventional powder sampling procedure followed by potentiometric titration according to AASHTO-T260 1997 [32] the results of which can be found in [31].

2.2 Laser ablation inductively coupled plasma mass spectrometry (LA-ICP-MS)

In order to study the chloride distributions along the concrete-steel interface, LA-ICP-MS was employed. This is a suitable technique for the characterization of solid samples in materials science, enabling multi-element spatial identification and quantification at very low concentration levels and at a micro scale. For calibration, a set of 5 pellets of CEM I concrete powder was used as reference material with the chloride and calcium contents determined by potentiometric titration [32] and given in Table 2. These were chosen so that the chlorine detection is guaranteed and within a range that represents both the restrictions imposed by EN 206-1 [33] and the chloride threshold levels recently reviewed by Angst et al. [4].

Table 2 – Composition of the pellets used for calibration.

Cl (wt% of sample)	0.04	0.08	0.12	0.22	0.33
Cl (wt% of CEM)	0.19	0.41	0.64	1.29	1.93

The equipment used was a CETAC LSX-200 laser ablation system coupled to a Perkin Elmer Sciex Elan 6000 quadrupole ICP-MS. The laser, with beam diameter of 300 μm , was operated at a pulse rate of 20 Hz (7.5 mJ/pulse) while moving the sample at 100 $\mu\text{m/s}$. The measured element isotopes were ³⁵Cl, ⁴⁴Ca and ⁵⁶Fe. Argon was used as carrier gas. The experimental conditions were optimized for chloride detection.

3. RESULTS AND DISCUSSION

3.1 Calibration and detection limits

For each pellet, approximately 1 minute of data, with the laser blocked, was acquired in order to obtain the background signal. The laser was then triggered and the gross ablation signal collected. The length of each scan line was 6 mm. Element intensities were observed to correlate quite well, following very similar distribution patterns and thus indicating homogeneous pellet preparation. Nevertheless, simultaneous fluctuations observed in the element signals can be attributed to inhomogeneous ablation as a result of surface topography, small fluctuations in the output laser energy, chloride/calcium distribution in the sample and possibly chloride binding capacity of the cement hydration products.

Quantitative determinations were only possible for chloride since in the given range of calcium concentrations, linearity was not observed and no quantitative information for iron, in the reference samples, was available. Calibration was performed prior to the analysis of each specimen. For each scan line, the average of the background signal was subtracted from the gross ablation signal to obtain the net intensity. The average of the net intensity was then plotted against the chloride content to obtain a calibration curve as the one shown in Figure 2, with the error bars indicating the standard deviation. The relative standard deviation (i.e., standard deviation divided by the average and expressed in %) showed to be independent of pellet composition, varying between 18-30%. These results are in agreement with the findings reported by others [34,35] while using different analytical techniques. Curve fitting generated good linear correlations, with regression values (R^2) varying between 0.981 and 0.992. The limit of detection (LOD) was calculated from the mass spectrum of the blank argon gas by the following equation:

$$\text{LOD} = \frac{3s_b - a}{m} \quad (1)$$

where, s_b is the standard deviation of three independent measurements of the blank in counts per second (cps), a is the y-intercept parameter of the calibration curve in cps and m is the slope of the calibration curve in cps/wt%. In this study, the limits of detection varied between 0.010 and 0.030 wt%, similar to the repeatability (0.0135 wt%) of a classical test method recommended by RILEM TC 178-TMC [36]. Chloride concentrations of the investigated pellets were always above the limit of detection.

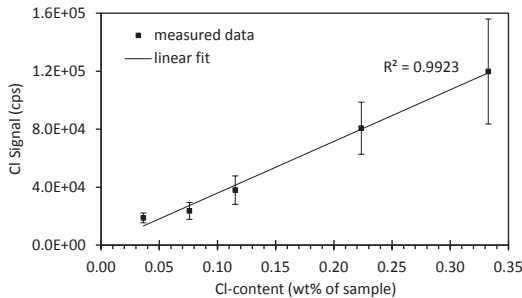


Figure 2 – Correlation between the chloride content in the pellets and the chlorine signal (example of calibration plot valid for bar 4). Error bars represent 1 standard deviation.

3.2 Elemental distributions

Figures 3 and 4 are the results from the LA-ICP-MS scan lines showing the chlorine, calcium and iron distributions along the interface. Two or three parallel line scans with a minimum spatial resolution of 300 μm and distancing from approximately 500 μm were ablated so as to investigate the reproducibility of the analysis. Although point-to-point vertical reproducibility is affected by variations in the microstructure, very good agreement was found and the differences in analytical results shown between scan lines match the differences in microstructure shown in the micrograph, indicating that the observed trends are reproducible.

The overall observed tendency was for the analysed elements to follow similar distribution patterns, especially along passive areas of the interface. Because the level of exposure solution reached 130 mm from the bottom of the specimen, very low chloride signals were detected at the top section and the intensities increased towards the bottom of the specimens. Besides the exposure conditions, the casting direction may also play a role here. As the specimens were cast up-side-down it is possible that some segregation as occurred. However, this seems not to be the dominant factor, as higher concentrations were often measured at the middle section.

Because the spatial distribution of aggregates at the front trace of the reinforcement may influence the chloride ingress, it is possible that, at the depth of the reinforcement, the chloride distribution is not homogeneous. For example, using embedded chloride ion selective electrodes, Angst et al. [38] measured a considerable scatter in the chloride ion activity in the concrete pore solution at a constant depth. Yu and co-workers [25,26], measured coarse aggregate gradients along the top trace of the rebar and reported that not only corrosion initiated at the locations with lower aggregate contents but also the chloride concentration was higher at the active sites. Moreover, the ranges between which both the aggregate and the chloride content varied were found to decrease with increasing cover thickness [37]. In the present study, the effect of the cover thickness has been considered, as the distance between the formwork and the reinforcement varied between 35 and 50 mm (see Figure 1), while limiting the maximum aggregate particle size to 10 mm. Nevertheless, taken in consideration that smooth bars were used in this study, a large number of interface defects, mainly air voids, was observed. In vertical cast conditions, such as in this study, these are the result of ascending air entrapped between aggregate particles and the reinforcement.

When concrete is exposed to chloride ingress, calcium hydroxide dissolution occurs so as to compensate for a local fall in the pH and calcium ions are redistributed [16]. This can partially account for the fact that some of the profiles obtained in this study, indicate a decrease in the calcium intensity for higher chloride concentrations, particularly in areas of active corrosion. However, considering the heterogeneity of concrete, the composition and microstructure along the steel-concrete interface is expected to vary as a result of the pore solution phase chemistry and early age development of the interface microstructure [39]. A range of cement hydration products with different chloride binding capacity and pH dissolution characteristics is therefore present at the interface. A combination of these factors may explain why, in this study, high calcium intensities were registered in both passive and active areas of the interface. It is however difficult to ascribe the specific reason as the method cannot distinguish between free and bound chlorides.

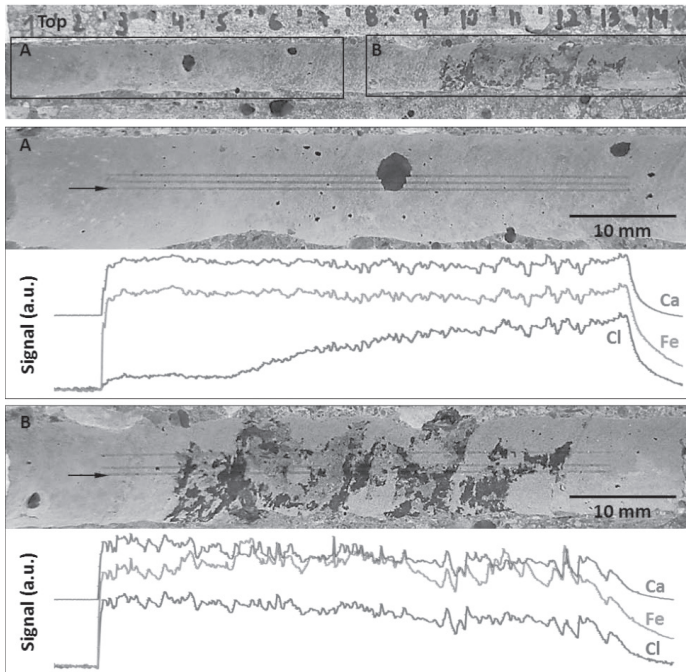


Figure 3 – Element distributions along the interface with bar #3 (20 mm cover depth) obtained for the scan lines indicated by the arrows.

An interesting feature is present in the distributions obtained at the interface with bar #4 (Figure 4) where the topography of the interface is clearly influenced by the surface finish of the steel. Due to the thickness of the cover depth, very low chloride signals were measured. However, the profiles in Figure 4 show disturbances in the calcium and iron contents coupled, in some cases, with peaks in the chloride distributions probably resulting from surface crevices and discontinuities in the steel mill-scale. These metallographic features, caused for example from cooling and drawn procedures, influence the corrosion initiation by promoting the establishment of microgalvanic cells between adjacent areas covered with and free from mill scale [10]. In addition, Horne et al. [20] demonstrated that wire-brush steel surfaces can lead to higher levels of calcium hydroxide at the interface when compared to uncleaned rebars and therefore a more homogeneous microstructure. The screening effect of the adherent hydration products at the steel surface influences the pitting susceptibility of the metal by limiting the rate at which chlorides reach the passive film and promote its dissolution.

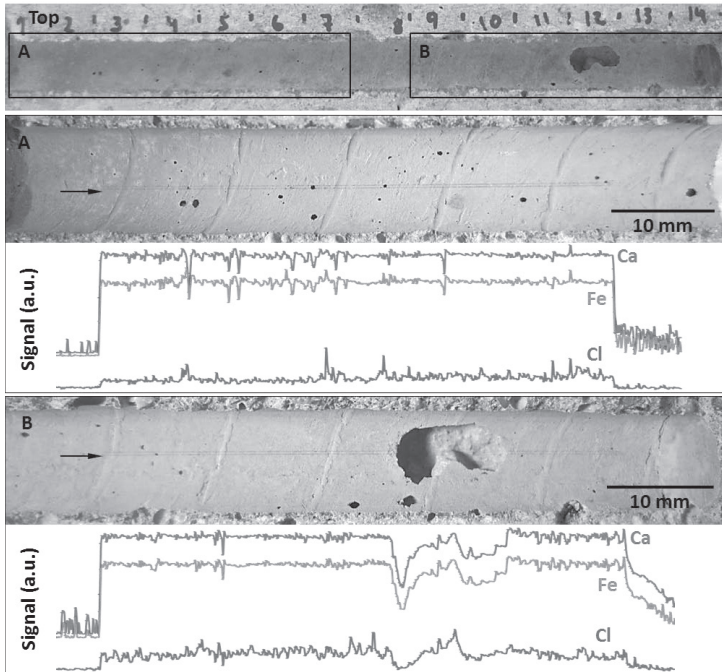


Figure 4 – Element distributions along the interface with bar #4 (25 mm cover depth) obtained for the scan lines indicated by the arrows.

3.3 Chloride content and corrosion initiation

From visual examination of the split specimens, a number of air voids, sometimes of large dimensions (up to 10 mm), was present at the concrete-steel interface. The homogeneity of the interface is often appointed as one of the reasons why laboratory specimens show higher C_{th} when compared to site concrete [39]. However, as it can be seen in this study, even for vertically cast, high slump, vibrated specimens, large interface defects were found.

Figures 5 and 6 present the average chloride content distribution (black line) along the interface for bars #1 and #2. As expected, an increase in the chloride content is measured from the top to the bottom of the specimen, opposite to the casting direction. Generally, for specimens that showed corrosion, higher chloride contents were measured around the active areas. These observations are in agreement with previous reported findings [25-27]. The specimens in the present study were open sometime after the corrosion onset and therefore, the uncertainty regarding the chloride content at the interface, at the time of initiation, is large. Nevertheless, the results are comparable to those presented by Boubitsas and Tang [31]: the C_{th} values for the present specimens are between 1 and 1.6% chloride by weight of cement. Finally, although these values are consistent with the fact that in laboratory specimens C_{th} values above 1% are often found [39], they are in line with the results presented by Tang and Utgenannt [40] relevant for field exposure where on-going corrosion was visible by destructive visual examination.

In this study the simultaneous influence of the interface macrostructure and of the steel surface finish on the initiation of corrosion was observed. For rebar #1 (Figure 5), two active spots were

identified, one of which coinciding with a visible surface defect. In this case, it is likely that corrosion initiated at one of the locations followed by repassivation to later initiate at another site. The repassivation mechanism is not yet well understood however it has been suggested that when a pit is formed, a cap of porous corrosion products acts as a barrier ceasing the corrosion by limiting the exchange of local and bulk electrolytes [41] or due to the pH neutralization capacity of the cement hydration products in the vicinity of the pit. Nevertheless it is interesting to see that comparable chloride levels were measured at both locations, showing higher contents in the vicinity of active regions. As no macroscopic defects are associated with the corrosion location, the initiation is likely to have resulted from a metallurgical characteristic at the steel surface, e.g., discontinuity in the mill-scale.

Regarding rebar #2 (Figure 6), corrosion appears associated to an air void. It is also clear that the middle section of the interface, where corrosion initiated, registers higher chloride levels. On the other hand, at the bottom end of the specimen, a large number of surface defects were also found, but chloride distribution was low and no corrosion was detected. It is unclear why chloride content in this part of concrete was low. As discussed in the introduction, in order for corrosion to start associated to large air voids, these must be in the saturated condition, which can be assumed from the exposure conditions in this study. As the chloride content seems not to be uniformly distributed along the interface, it may be concluded that a combination of surface defect and high chloride content was required to initiate corrosion. A similar interpretation may apply to bar #3 (Figure 3), although here, due to the large deposition of corrosion products, it is very difficult to determine the pitting location.

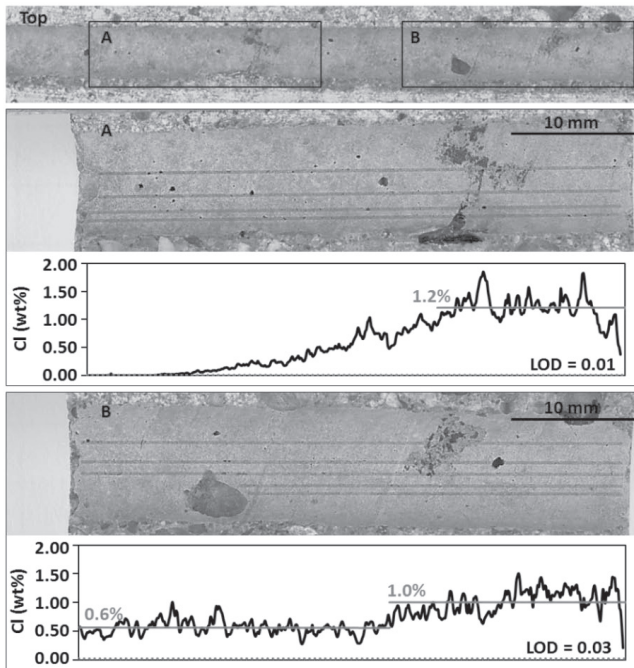


Figure 5 – Average chloride content and chloride profiles along the interface with bar #1 (10 mm cover depth). The black line indicates the average of all scan lines. Limit of detection (LOD) is represented by a red dotted line.

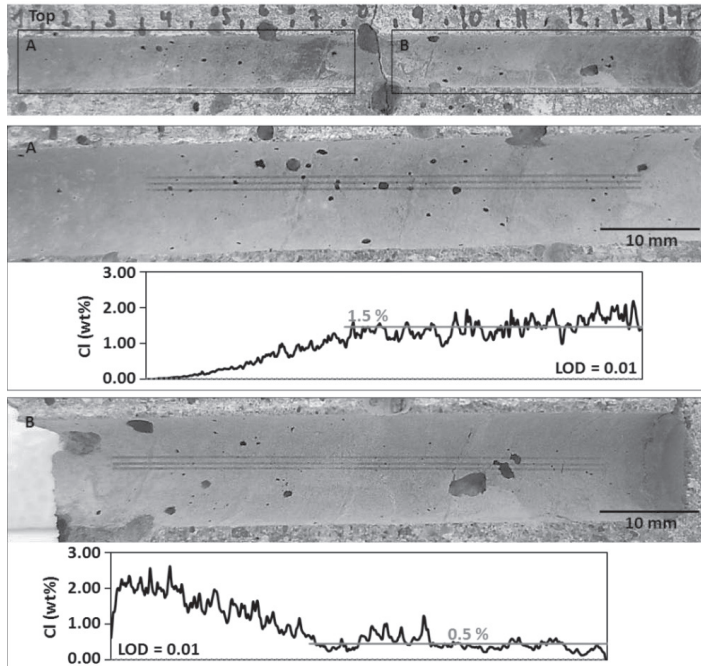


Figure 6 – Average chloride content and chloride profiles along the interface with bar #2 (15 mm cover depth). The black line indicates the average of all scan lines. Limit of detection (LOD) is represented by a red dotted line.

4. CONCLUSIONS

The steel-concrete interface micro and macrostructures and the surface finish of the steel play a significant role in the depassivation of steel embedded in concrete by the action of chlorides.

LA-ICP-MS was used to study the chloride distributions along the steel-concrete interface. The method has been calibrated using concrete powder pellets with a limit of detection of 0.010-0.030 wt%. Within a resolution range smaller than 300 μm , linear calibration curves with correlation coefficients between 0.98-0.99 were obtained. Calcium and iron distributions were also qualitatively investigated.

Element profiles did not indicate signs of aggregate blocking effect to chloride ingress. Calcium levels were observed to decrease as a result of chloride ingress and corrosion initiation, but portlandite leaching from the interface did not seem significant. The surface condition of the steel influenced the topography and the elemental distribution at the interface.

A large number of air voids were observed. These were often found to influence the location where corrosion initiated and usually associated with higher chloride contents. A range of chloride levels along the concrete-steel interface could be detected, showing good reproducibility within a resolution of 300 μm . Non-uniform chloride distribution along the interface was observed with higher chloride levels around corroded areas, thus reinforcing the necessity for the evaluation of the conditions at the interface and their influence in the C_{th}

measured at macro-scale. It was shown that LA-ICP-MS technique can be used to measure chlorides in concrete. Its main advantages are spatial resolution and time of analysis, in particular when compared to depth chloride profiling by means of standard chemical analysis due to an easier sample preparation and speed of analysis.

Surface defects and steel surface condition play a significant role in the corrosion initiation with major impact on the C_{th} . Therefore a more systematic study is needed to characterize the steel surface condition and the air void size distribution so as to evaluate their effect on the chloride distributions at the interface and consequent pitting positions.

ACKNOWLEDGEMENTS

The support of the Swedish Research Council (FORMAS project No. 243-2007-1512) is acknowledged.

REFERENCES

1. Glass, G.K. and Buenfeld, N.R., "The presentation of the chloride threshold level for corrosion of steel in concrete", *Corrosion Science* 39-5 (1997) 1001-1013.
2. Ann, K.Y., and Song, H-W., "Chloride threshold level for corrosion of steel in concrete", *Corrosion Science* 49-11 (2007) 4113-4133.
3. Alonso, M.C. and Sanchez, M., "Analysis of the variability of chloride threshold values in the literature", *Materials and Corrosion* 60-8 (2009) 631-637.
4. Angst, U., Elsener, B., Larsen, C.K., and Vennesland, Ø., "Critical chloride content in reinforced concrete – A review", *Cement and Concrete Research* 39-12 (2009) 1122-1138.
5. Frederiksen, J.M., "On the need for more precise threshold values for chloride initiated corrosion", *Materials and Corrosion* 60-8 (2009) 597-601.
6. Sandberg, P., "The effect of defects at the steel- concrete interface exposure regime and cement type on pitting corrosion in concrete", Report TVBM-3081, Lund Institute of Technology, Division of Building Materials, Sweden, 1998.
7. Hartt, W.H. and Nam, J., "Effect of cement alkalinity on chloride threshold and time-to-corrosion of reinforcing steel in concrete", *Corrosion* 64-8 (2008) 671-680.
8. Manera, M., Vennesland, Ø. And Bertolini, L., "Chloride threshold for rebar corrosion in concrete with addition of silica fume" *Corrosion Science* 50-2 (2008) 554-560.
9. Mammoliti, L.T., Brown, L.C., Hansson, C.M., and Hope, B.B., "The influence of surface finish of reinforcing steel and pH of test solution on the chloride threshold concentration for corrosion initiation in synthetic pore solutions", *Cement and Concrete Research*, 26-4 (1996) 545-550.
10. Pillai, R.G. and Trejo, D., "Surface condition effects on critical chloride threshold of steel reinforcement", *ACI Materials Journal* 102-2 (2005) 103-109.
11. Mohammed, T.U., Hamada, H., A discussion of the paper "Chloride threshold values to depassivate reinforcing bars embedded in a standardized OPC mortar" by C. Alonso, C. Andrade, M. Castellote, and P. Castro, *Cement and Concrete Research* 31-5 (2001) 835-838.
12. Alonso, C., Castellote, M., and Andrade, C., "Chloride threshold dependence of pitting potential of reinforcement", *Electrochimica Acta* 47-21 (2002) 3469-3481.

13. Xu, J., Jiang, L. and Wang, J., "Influence of detection methods on chloride threshold value for the corrosion of steel reinforcement", *Construction and Building Materials* 23-5 (2009) 1902-1908.
14. Li, L. and Sagüés, A.A., "Chloride corrosion threshold of reinforcing steel in alkaline solutions – effect of specimen size", *Corrosion* 60-2 (2004) 195-202.
15. Angst, U., Rønquist, A., Elsener, B., Larsen, C.K., and Vennesland, Ø., "Probabilistic considerations on the effect of the specimen size on the critical chloride content in reinforced concrete", *Corrosion Science* 53-1 (2011) 177-187.
16. Page, C.L., "Mechanism of corrosion protection in reinforced concrete marine structures", *Nature* 258 (1975) 514-515.
17. Al Khalaf, M.N. and Page, C.L., "Steel/mortar interfaces: microstructural features and modes of failure", *Cement and Concrete Research* 9-2 (1979) 197-208.
18. Monteiro, P.J.M., Gjorv, O.E. and Mehta, P.K., "Microstructure of the steel-cement paste interface in the presence of chloride", *Cement and Concrete Research* 15-5 (1985) 781-784.
19. Yonezawa, T., Ashworth, V. and Procter, R.P.M., "Pore solution composition and chloride effect on the corrosion of steel in concrete", *Corrosion* 44-7 (1988) 489-499.
20. Horne, A.T., Richardson, I.G. and Brydson, R.M.D., "Quantitative analysis of the microstructure of interfaces in steel reinforced concrete", *Cement and Concrete Research* 37-12 (2007) 1613-1623.
21. Glass, G.K., Yang, R., Dickhaus, T. and Buenfeld, N.R., "Backscattered electron image of the steel-concrete interface", *Corrosion Science* 43-4 (2001) 605-610.
22. Angst, U., Elsener, B., Larsen, C.K., and Vennesland, Ø., "Defects at the steel/concrete interface and their influence on chloride induced reinforcement corrosion", *Cement and Concrete Research* (submitted).
23. Soylev, T.A. and François, R., "Quality of steel-concrete interface and corrosion of reinforcing steel", *Cement and Concrete Research* 33-9 (2003) 1407-1415.
24. Ryou, J.S. and Ann, K.Y., "Variation in the chloride threshold level for steel corrosion in concrete arising from different chloride sources", *Magazine of Concrete Research* 60-3 (2008) 177-187.
25. Yu, H., and Hartt, W.H., "Effects of reinforcement and coarse aggregates on chloride ingress into concrete and time-to-corrosion: Part 1 - Spatial chloride distribution and implications", *Corrosion* 63-9 (2007) 843-849.
26. Yu, H., Himiob, R.J. and Hartt, W.H., "Effects of reinforcement and coarse aggregates on chloride ingress into concrete and time-to-corrosion: Part 2 - Spatial distribution of coarse aggregates", *Corrosion* 63-10 (2007) 924-931.
27. Yu, H., Shi, X., Hartt, W.H. and Lu, B., "Laboratory investigation of reinforcement corrosion initiation and chloride threshold content for self-compacting concrete", *Cement and Concrete Research* 40-10 (2010) 1507-1516.
28. Glasser, F.P. and Sagoe-Crentsil, K.K., "Steel in concrete: Part II. Electron microscopy analysis", *Magazine of Concrete Research* 41-149 (1989) 213-220.
29. Poupard, O., Ait-Mokhtar, A. and Dumargue, P., "Corrosion by chlorides in reinforced concrete: determination of chloride concentration threshold by impedance spectroscopy", *Cement and Concrete Research* 34-6 (2004) 991-1000.
30. Nygaard, P.V. and Geiker, M.R., "A method for measuring the chloride threshold level required to initiate reinforcement corrosion in concrete", *Materials and Structures* 38-4 (2005) 489-494.
31. Boubitsas, D. and Tang, L., "The influence of reinforcement steel surface condition on chloride induced corrosion", (to be submitted).

32. AASHTO-T260, "Standard method of test for sampling and testing for chloride ion in concrete and concrete raw materials", American Association of State Highway and Transportation Officials, 1997.
33. European Standard EN206-1, "Concrete – Part 1: Specification, performance, production and conformity", European Committee for Standardization, 2000.
34. Wilsch, G., Weritz, F., Schaurich, D. and Wiggemhauser, H., "Determination of chloride content in concrete structures with laser-induced breakdown spectroscopy", *Construction and Building Materials* 19-10 (2005) 724-730.
35. Mori, D., Yamada, K., Hosokawa, Y. and Yamamoto, M., "Applications of electron probe microanalyzer for measurement of Cl concentration profile in concrete", *Journal of Advanced Concrete Technology* 4-3 (2006) 369-383.
36. RILEM TC 178-TMC, "Analysis of total chloride content in concrete – Recommendation", *Materials and Structures*, 35-11 (2002) 583-585.
37. Yu, H., and Hartt, W.H., "Modelling corrosion initiation of reinforcing steel in concrete: Effect of non-diffusive coarse aggregate", *Journal of Composite Materials* 45-2 (2011) 153-169.
38. Angst, U., Elsener, B., Larsen, C.K., and Vennesland, Ø., "Chloride induced reinforcement corrosion: Electrochemical monitoring of initiation stage and chloride threshold values", *Corrosion Science* 53-4 (2011) 1451-1464.
39. Page, C.L., "Initiation of chloride-induced corrosion of steel in concrete: role of the interfacial zone", *Materials and Corrosion* 60-8 (2009) 586-592.
40. Tang, L. and Utgenannt, P., "A field study of critical chloride content in reinforced concrete with blended binder", *Materials and Corrosion* 60-8 (2009) 617-622.
41. McCafferty, E., "Introduction to corrosion science", 1st ed., 2010, Springer.

Research Council and Editorial Board for Nordic Concrete Research

Prof. Dr. Olafur H. Wallevik, Chairman for the Research Committee

Dr. Dirch H. Bager, Editor of Nordic Concrete Research

**Danish
Concrete
Association**

Dr. Dirch H. Bager
DHB-Consult
Lavendelparken 5
DK - 9310 Vodskov
Tel: +45 98292412
Mobile: +45 2049 7324
E-mail: dirch.bager@bbnpost.dk

Mr. Claus Pade
Concrete Centre,
Danish Technological Institute
Gregersensvej
DK - 2630 Taastrup
Tel: + 45 7220 2183
E-mail: cpa@teknologisk.dk

**Finnish
Concrete
Association**

Mr. Juha Valjus
Concrete Association of Finland
Unioninkatu 14 PL 381
FI - 00131 Helsinki
Tel: +358 41 533 6020
Mobile: +358
E-mail: juha.valjus@betoniyhdistys.fi

Lic.Sc.Tech. Klaus Juvas
Consolis Technology
Box 72
FI - 21291 Rusko
Mobile: +358 40 5160 316
E-mail: klaus.juvas@consolis.com

**Icelandic
Concrete
Association**

Prof., Dr. Borge Johannes Wigum
Mannvit
Grensásvegur 1
IS - 108 Reykjavik
Tel: +354 422 3030
Mobile: +354 896-0756
E-mail: wigum@mannvit.is

Prof. Dr. Olafur H. Wallevik
Innovation Center Iceland
IS - 112 Keldnaholti
Tel: +354 522 9000
Mobile: +354
E-mail: wallevik@ru.is

**Norwegian
Concrete
Association**

Dr. Terje F. Ronning
Norcem, FoU Department
P.O.Box 38
N - 3991 Brevik
Tel.: +47 3557 2347
Mobile: +47 9157 6046
E-mail: terje.ronning@norcem.no

Dr. Ing. Helge Brå
Norwegian Public Road Authority
Abelsgate 5
N - 7030 Trondheim
Mobile: +47 9709 5277
E-mail: helge.braa@vegvesen.no

**Swedish
Concrete
Association**

Adjunct. Prof., Tekn.Dr. Mikael Hallgren
Tyréns AB
Peter Myndes Backe 16
SE - 118 86 Stockholm
Tel: +46 104 522 351
Mobile: +46 70 661 05 33
E-mail: Mikael.Hallgren@tyrens.se

Tekn. Dr. Peter Utgenannt
CBI Swedish Cement and Concrete Research
Institute
P.O. Box 857
SE - 501 15 Borås
Tel: +46 105 166 870
Mobile: +46 706 452 008
E-mail: peter.utgenannt@cbi.se

Active reviewers for Nordic Concrete Research as per June 2012**DENMARK**

Dr. Dirch H. Bager
 Prof., Dr. Lars Damkilde
 Dr. Mette Glavind
 Prof., Dr. Per Goltermann
 Mr. Oscar Klinghoffer
 Prof., Dr. John Forbes Olesen
 Mr. Claus Pade
 Prof., Dr. Eigil V. Sørensen
 Prof., Dr. Jens Peder Ulfkjær

FINLAND

Dr. Klaus Juvas
 Dr. Matti V. Leskala
 Prof., Dr. Jussi Mattila
 Mr. Erik Nordenswan
 Dr. Jouni Punkki
 Mr. Juha Valjus

ICELAND

Mr. Einar Einarsson
 Mr. Haukur J. Eiriksson
 Dr. Gisli Gudmundsson
 Mr. Karsten Iversen
 Mr. Torfi G. Sigurdsson
 Mr. Sveinbjörn Sveinbjörnsson
 Dr. Jon E. Wallevik
 Prof., Dr. Ólafur H. Wallevik
 Prof., Dr. Børge J. Wigum

NORWAY

Dr. Helge Brå
 Ms. Danielle Bosnjak
 Mr. Anton Gjørven
 Mr. Steinar Helland
 Dr. Bernt Jacobsen
 Prof., Dr. Terje Kanstad
 Dr. Terje F. Rønning
 Mr. Tor Kristian Sandaker
 Mr. Sverre Smeplass
 Mr. Hans Stemland

SWEDEN

Prof., Dr. Anders Ansell
 Dr. Thomas Blanksvärd
 Prof. Lennart Elfgren
 Prof., Dr. Mats Emborg
 Prof., Dr. Kent Gylltoft
 Prof., Dr. Mikael Hallgren
 Prof., Dr. Jan-Erik Jonasson
 Prof., Dr. Björn Lagerblad
 Prof., Dr. Karin Lundgren
 Prof., Dr. Tang Luping
 Prof., Dr. Per-Erik Petersson
 Prof., Dr. Johan Silfwerbrand
 Dr. Peter Simonsson
 Dr. Peter Utgenannt